KINETICS OF VACUUM DRYING AND REHYDRATION OF ILLINOIS #6 COAL SAMPLES. IMPLICATIONS FOR PORE STRUCTURE*

Karl S. Vorres**, Roger Kolman and Timothy Griswold
Chemistry Division, Building 211
Argonne National Laboratory
Argonne, Illinois 60439

*Work performed under the auspices of the Office of Basic Energy Sciences, Division of Chemical Sciences, U. S. Department of Energy, under contract number W-31-109-ENG-38.

**To whom correspondence should be addressed.

ABSTRACT

The kinetics of vacuum dehydration and rehydration in nitrogen near room temperature have been studied with Argonne Premium Coal Samples. A block, -20 mesh and -100 mesh material were used. Three types of kinetic behavior were observed in dehydration and rehydration. These included a first order mass change, a combination of some or all of an initial linear, parabolic and final linear (LPL) segments, and a behavior which can be plotted to appear similar to an adsorption isotherm. The mechanisms involved in the linear-parabolic-linear sequence are tentatively assumed to be loss from macro pores, bulk diffusion, and loss of "bonded water" respectively. The rates are higher for dehydration in vacuum than for rehydration in nitrogen. The rates increase as the external surface increases from the block through the -20 mesh to the -100 mesh material.

INTRODUCTION

Studies of oxidation of coal at ambient conditions by measurements of weight change are complicated by the mass changes due to loss of moisture. As an initial step in determining the rate of oxidation, the kinetics of moisture loss at room temperature were measured.

Drying is also one of the oldest chemical engineering unit operations. The process involves a complex interaction of heat and mass transfer (1). If the heat transfer effects are held constant in a series of experiments, then an understanding of the mass transfer effects may be gained. In the experiments to be described the experimental arrangement was maintained in order to focus on the mass transfer involved in the dehydration and rehydration.

Moisture is believed to reside in pores in the coal structure. These pores occur with a range of diameters. The diffusion from these pores would be expected to affect the drying behavior. Gan, Nandi and Walker (2) have studied coal samples with a range of ranks and observed variation in pore sizes and volumes. The rate of diffusion in and out of these pores could provide a more complete understanding of the pore and internal structure of coal, and later lead to better understanding of the kinetics of heterogeneous reactions for coal conversion.

APPARATUS, MATERIAL AND PROCEDURE

The kinetic studies were made by placing the samples into a quartz pan, and suspending the pan inside of a quartz envelope under an Ainsworth thermobalance. The thermobalance provided electrical signals to a Bristol recorder which provided a continuous record of weight as a function of time (1" = 1 mg). The temperature was kept constant with a water bath which surrounded the sample. A weight switching mechanism provided a dynamic range of 400 mg weight change. Sample weights were in the range of 0.1 to 1 gram.

The coal samples were Illinois #6 material taken from the Argonne Premium Coal Sample Program -100 and -20 mesh material. The one-gram block was picked from a supply of material kept in chunk form, and collected at the same time and place that the Premium Sample was collected. This sample is a high volatile bituminous C rank coal with the following partial analysis:

moisture:	7.97 %
ash:	15.48 % (dry)
volatile matter:	40.05 % (dry)
carbon :	77.67 % (maf)
hydrogen:	5.00 % (maf)

In a typical run the sample was quickly weighed, transferred to the thermobalance, and the quartz envelope placed around the sample. The recorder was started, and balance released to get an initial weight reading. The vacuum pump was used to reduce the pressure to about 200 microns inside of the envelope. A buoyancy effect was observed and correction was later made for it. The weight loss was recorded, and later reduced to a table of weight and time for computer analysis using Lotus 1-2-3 or a non-linear least squares program to provide for plots, and least squares fits for these plots. After a period of time the weight loss for the sample was extremely slow, and the dehydration was halted. Rehydration was done by stopping the vacuum pump, backfilling the envelope with dry nitrogen, removing the quartz envelope, and dropping an ice cube into it. After replacing the envelope, the apparatus was evacuated, and backfilled with nitrogen to avoid contact with oxygen. The ice cube was melted, and a water bath placed around the sample for the rehydration experiment. These experiments were also allowed to continue for up to several days. For experiments involving several cycles of dehydration and rehydration, the process was started again by removing the quartz envelope, pouring out the water, drying with acetone, blowing with dry nitrogen, and replacing the envelope as quickly as possible.

RESULTS

The shape of the curve of mass loss or gain with time indicated a relatively rapid initial change which progressively became slower. Figures 1 and 2 indicate the weight change for the block on several cycles of dehydration and rehydration. The results of curve fitting efforts are also shown in the figures.

Similarly the changes and curve fitting for the -20 mesh material are indicated in Figures 3 and 4, while the results for the -100 mesh material are indicated in Figures 5 and 6.

DISCUSSION

Three types of curves were observed when the mass was plotted as a function of time. Each of these involved a rapid initial loss which gradually slowed. While the overall shape of the curves was similar, the data from these experiments fit different equations, indicating differences in the rate determining steps.

The equilibrium Langmuir adsorption isotherm has a characteristic shape. The fraction of the available surface is plotted against a concentration variable such as partial pressure. This type of curve was also seen in these kinetic studies when the fraction of the moisture adsorbed was plotted against time. The amount of moisture adsorbed is proportional to the available sites. The effect of time may be seen if the time to adsorb one half of the total moisture is used as a unit. The shape of the adsorption isotherm would indicate that if the concentration of the adsorbed gas was doubled, then the amount adsorbed would increase from 1/2 to 2/3. If it were tripled then the amount adsorbed would be increased to 3/4 etc. In a similar way if the time for half sorption were doubled then the amount of sorbed gas would be increased to 2/3. The effect of doubling the time is similar to the effect of doubling the concentration. The label "adsorption" has been applied in the data analysis of data which fit this type of curve.

For a unimolecular reaction of a gaseous reactant on the surface of a solid, the rate is proportional to the fraction of the surface covered by the gas. At the beginning of the adsorption the water molecules are adsorbed on the bare surface and the rate is a maximum, governed by the vapor pressure of the water and the external surface accessible to the gas. However the equation applies over a time long enough to adsorb or desorb most of the water which implies a rapid transfer of moisture from the external surface to the interior. The rate is reduced and can be characterized by a time to reach a reduction by one half. The label "first order" has been applied to data which fit this type of curve.

The analysis of the data also indicated a behavior in which the mass change was resolved into three distinct regimes of weight loss. The initial one involved a linear weight loss with time. The second regime involved a parabolic weight loss with time, and the third regime was another linear loss with time, but with a much smaller slope than the first linear one. This was seen in the second dehydration of the -20 mesh material. The label "linear-parabolic-linear" or "LPL" has been applied to data which fit this type of curve. In some cases, such as rehydration of the block, the initial and final linear segments were very short or absent.

The 1.0 gram block was obtained from a 5-gallon storage container kept under nitrogen. The conditions of collection and storage permitted some drying of the sample during the oxygen removal,

and transfer between containers. The initial dehydration was followed by a dehydration, and the cycle was repeated. The sample was then left under nitrogen in contact with saturated water vapor for three weeks. The subsequent (third) dehydration indicated that the sample had acquired a substantially larger amount of water than it possessed during either of the earlier experiments. A second cycle followed the dehydration. The arrows on Figure 1 indicate the relationship between the pairs of dehydration cycles.

The data analysis for the four cycles gave these results:

Cycle	Dehydration	Rehydration
First:	Adsorption	Parabolic
Second:	Adsorption	Parabolic
Third:	Adsorption	Parabolic
Fourth:	Adsorption	Not Done

The data analysis for the dehydration indicated that the fit was better for the adsorption type curve than either of the first order or a combination of the LPL curves. The initial portion of the adsorption curve frequently is linear on the chart paper, and is believed to involve transfer of moisture from the external surface or pores. The weight change required for a monolayer of moisture as typically determined by nitrogen adsorption is about one half milligram per gram of coal. The actual loss is larger than this by an order of magnitude, indicating that the surface moisture is replenished by large open pores. The further loss of moisture is assumed to involve a "bulk diffusion" mechanism. For a solid with a consistent set of pores or defects for diffusion a parabola is observed in a plot of weight change with time. The lack of a fit to a parabolic curve and more rapid decrease in rate than predicted from a parabolic fit is believed to be due to either to diffusion from progressively smaller pores with smaller diffusion constants or to blockage of pores. The data also indicate that the rate is dependent upon the amount of water which is available in the particle. This was especially noticeable after the extended rehydration between the second and third dehydration. The pores were not irreversibly collapsed but were able to accumulate a larger moisture content than was present at the beginning of the experiment. This amount exceeded the ASTM moisture determination.

The analysis for rehydration indicated a better fit for the parabolic equation. The rate for rehydration is significantly less than for dehydration. The minimal amount of linear contribution to the initial mass change indicates that the external surface was quickly covered and subsequent reaction was limited by diffusion through a growing interface layer. This layer may have been a set of blocked pores. The external surface is a minimum for a sample which is a single particle.

The -20 mesh sample was 0.100 grams of a supply kept in a plastic bottle filled from incompletely sealed ampoules. The material had been exposed to the drier atmosphere in the laboratory. The initial dehydration did not remove much moisture since much of it had already been lost. The rehydration restored a considerable amount of the moisture content, and led to a higher rate and a modified curve shape (LPL) for the second and third dehydrations.

The rehydration rates showed a very similar set of curve shapes, and a gradually diminishing rate due to progressive internal changes. Although the curve shapes for the rehydration were similar, the agreement with the adsorption type curve was clearly better than first order for the first two curves, and somewhat better for first order for the third curve.

The data analysis gave the following results:

Cycle	Dehydration	Rehydration
First:	First order	Adsorption
Second:	Linear-Parabolic-Linear	Adsorption
Third:	Linear-Parabolic-Linear	First order

The three regimes in the second and third dehydration indicate that three mechanisms of water loss were occurring during the dehydration. The initial linear loss is believed to be due to the loss of surface water from the external surfaces and macro pores. The parabolic weight loss is believed to be due to bulk diffusion from the coal of "dissolved" water. This water is believed to be caught in very small cavities or imperfections in the packing structure of the coal. These cavities can provide a temporary site for molecules as they diffuse from the bulk to some surface accessible to the external pores. The dynamic motion of the coal "molecules" may permit the opportunity for the water molecules to migrate from one site to another on the way to the external surface. The third regime, involving the second linear portion is believed to be due to the release of water from sites involving "bonded water". The low temperature provides relatively little thermal energy to permit release of the water, but enough to permit a measurement.

Assuming that the pores are filled with water, one can obtain a measure of the macro pore volume by calculating the moisture loss per gram of coal, and using the density of water. Similarly, one can obtain a measure of the "dissolved" water" by noting the weight of the water lost during the parabolic part of the total weight loss curve, and calculating the loss per gram of coal. Again, in a similar way, one could make the calculation for the "bonded water". This portion would represent the water tied to functional groups, or hydrogen bonded.

The first type of water should be "freezable" while the latter two should not have the properties to permit observation of freezing behavior. Freezing is a bulk property, and would require a number of molecules to demonstrate the existence of a solid crystalline material. Individual molecules, separated from other similar molecules would not be able to demonstrate this behavior.

The -100 mesh material was a 0.239 gram sample which had been equilibrated with water for at least 5 days at room temperature. The two dehydration runs fit the adsorption type curve. The two rehydration runs initially followed this type of curve, but later exhibited a more rapid rate and departure from the curve. This behavior is indicative of multilayer formation in the type IV adsorption isotherm, and may indicate a similar phenomenon here. The rates for the second dehydration or rehydration are lower than those for the first run in the cycles. The incremental

change in weight with time toward the end of the run is greater for the second run indicating a tendency to continue and possibly achieve a similar weight gain or loss over a very extended time. For these samples the initial dehydration proceeded with a higher rate than the second. The sample did not take up as much water during the rehydration as it lost during the initial dehydration.

The data analysis gave the following results:

Cycle	Dehydration	Rehydration
First:	Adsorption	Adsorption + multilayer?
Second:	Adsorption	Adsorption + multilayer?

CONCLUSIONS

The rates of dehydration and rehydration near room temperature are complex. The specific form of the equation describing the rates varies depending on the particle size and history of the sample. Several rate equations can be used to provide a "best fit" to all of the data. Blocks of vacuum dried coal will continue to absorb significant amounts of water over a period of weeks at room temperature. The pores in the block were not irreversibly collapsed in a manner that prevented restoration of the moisture content.

The rate of dehydration in vacuum for a given sample is faster than the rate of rehydration in nitrogen. The presence of nitrogen apparently interferes with the rehydration.

The vacuum dehydration of the block of coal followed a first order curve. This is consistent with loss of moisture from the equivalent of a surface with all of the moisture initially upon it. The rehydration of the block follows a parabolic curve, which is consistent with a diffusion controlled process . This would be observed if the moisture diffused into the block through a layer which consisted of swollen pores, and the pores continued to swell as the moisture continued to diffuse. The behavior of the block is believed to represent the behavior of an independent particle. The -20 mesh vacuum dehydration followed a first order curve for most of the vacuum dehydration and one rehydration in nitrogen. The initial two rehydrations followed the adsorption type curve. This behavior is consistent with the limitation on moisture loss due to a transfer from a surface with all of the moisture initially on it, or surface sites equally accessible during rehydration. The appearance of the LPL sequence indicates that the rehydration put enough moisture back into the sample to allow some differentiation of the several mechanisms that were operative. Rehydration initially indicates adsorption to saturate the surface,and may be augmented by particle-particle interaction. The behavior of this sample is believed to reflect the behavior of a sample consisting of many small particles, and which has been exposed to some drying and atmospheric oxidation. The -100 mesh samples had been equilibrated with moisture, and showed an adsorption type of curve on both dehydration and rehydration. The initial steep part of the curve is attributed to the saturation of the surface with moisture. The moisture may be going to junctions between particles. The rehydration curves show evidence for multilayer adsorption as part of their shape.

The behavior of this sample is believed to reflect the behavior of a sample which consists of small particles, has been protected from oxidation and has been given an opportunity to adsorb moisture to achieve near equilibrium at the experimental temperature.

The use of several equations to give a fit to the data prevents a direct comparison of rates. However, one can rank the rates for the different particle sizes by establishing the time required to lose or gain half of the moisture over a reasonably long period of the experiments to be compared. If it is assumed that the -20 or -100 mesh particles would behave in the same manner whether 0.1 or 1 gram were used, then the rates are dependent on particle size, and increase from the block through -20 mesh to -100 mesh. This behavior indicates that the external surface area is important in the overall rates for both dehydration and rehydration.

FUTURE WORK

It is intended to extend this work to the full set of the Argonne Premium Coals over a range of temperature to establish the similarity in behavior, effects of rank, and observe any special behavior that may be found for the low rank coals due to gel structure that may be present in them. In addition it is intended to observe the weight changes following vacuum drying upon introduction of other gases including those which are normally used to establish the surface area.

ACKNOWLEDGMENTS

The authors gratefully acknowledge the support of the Office of Basic Energy Sciences, Chemical Sciences Division, and the Argonne National Laboratory Division of Educational Programs. The glassblowing by Joe Gregar is particularly appreciated. Useful discussions with Anthony Fraioli are also acknowledged.

REFERENCES

1. Marshall, Jr., W. R. in Reaction Kinetics and Unit Operations, Chem. Engr. Progress Symp. Ser. 55, (1959), pp. 213, American Inst. of Chem. Engrs., N.Y.

2. Gan, H., Nandi, S. P., and Walker, Jr., P. L., Fuel, 51, 272(1972).

FIGURE CAPTIONS

These are as indicated. Weight change in milligrams is plotted on the vertical axis, and time in minutes on the horizontal axis. Symbols indicate observed points. Lines indicate calculated values for the curves indicated in the text. The numbers adjacent to the curves indicate the cycle.

Figure 1. Vacuum Dehydration of IL #6 Coal Block

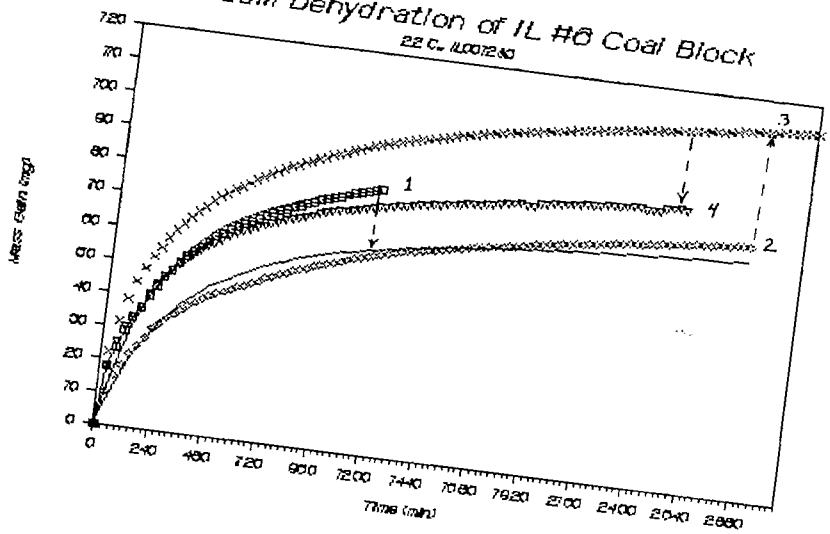

Figure 2. Rehydration of IL #6 Coal Chunk

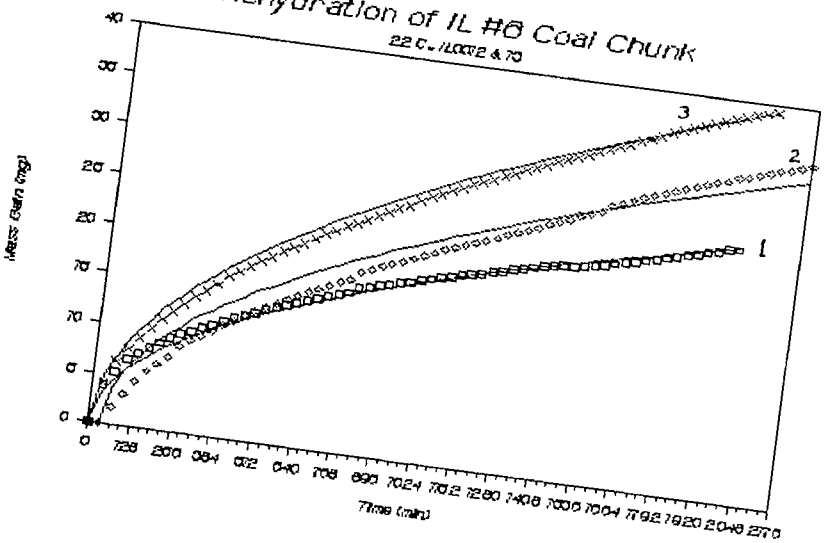

Figure 3. Vac. Dehydration IL#6, -20 Mesh

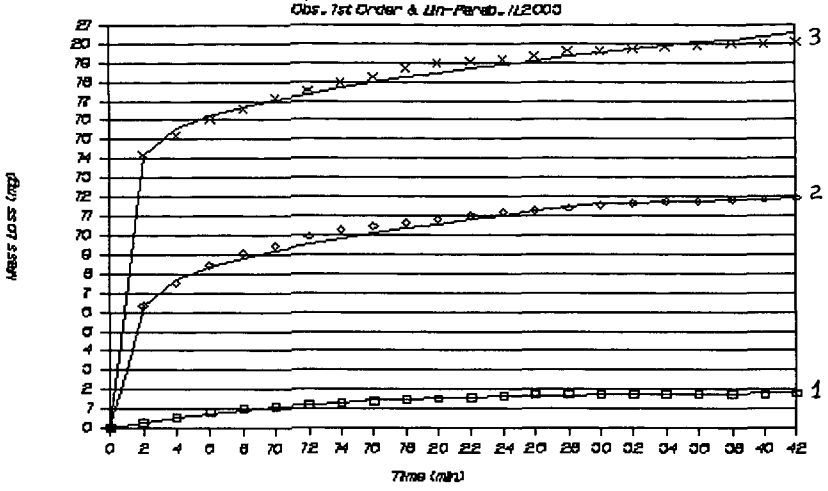

Figure 4. Rehydration of IL#6 in N2, -20 Mesh

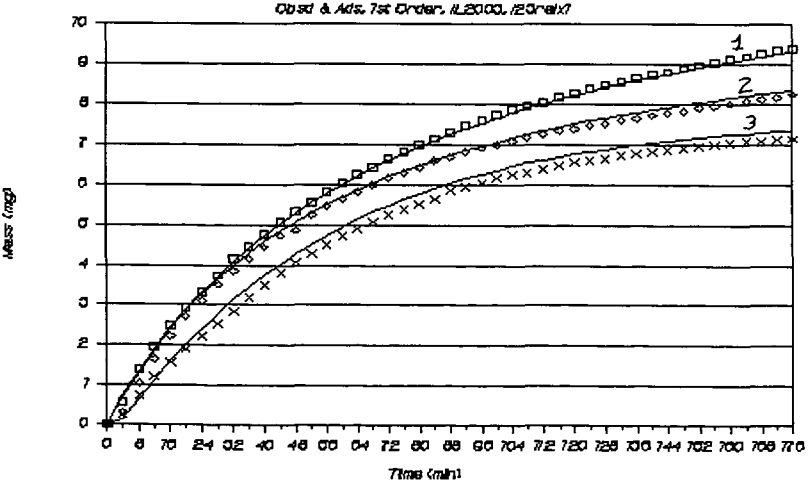

Figure 5. Vac Dehydration of IL #6 −100 Mesh

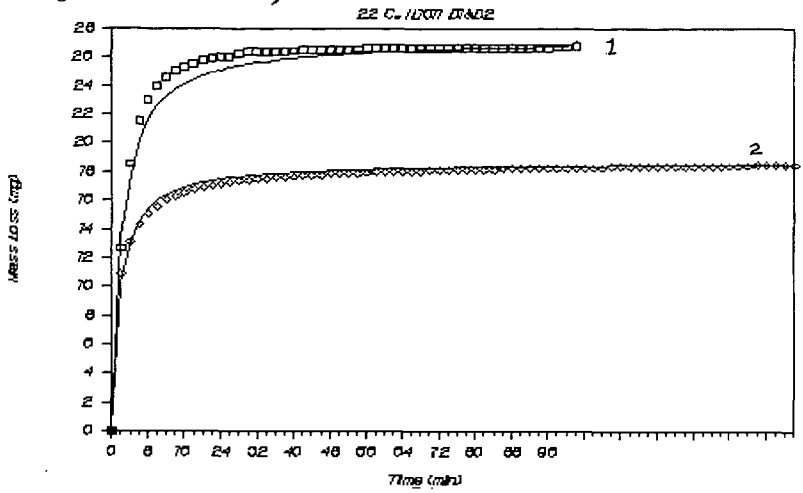

Figure 6. Rehydration of IL #6 −100 Mesh In N2

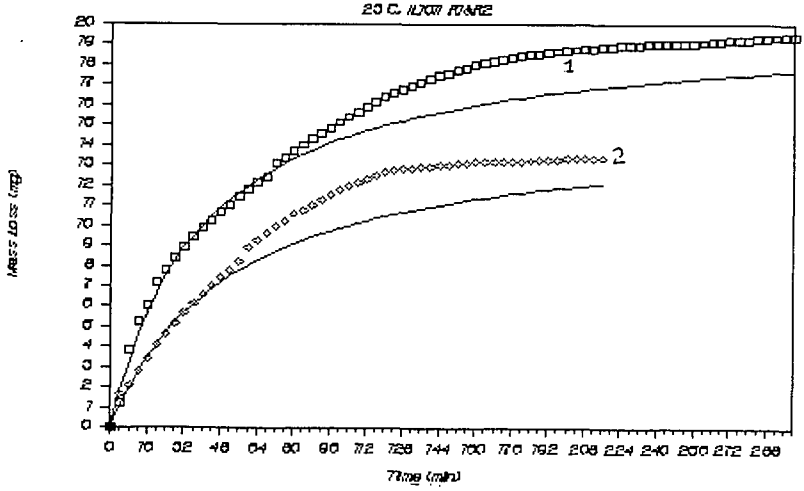

Macromolecular and Chemical Changes Induced by Air-Oxidation of a Medium Volatile Bituminous Coal

Donald Schwartz[1], Peter J. Hall[2] and Harry Marsh,

Northern Carbon Research Laboratories,
School of Chemistry, Bedson Building,
University of Newcastle upon Tyne,
Newcastle upon Tyne, NE1 7RU, U.K.

[1]University of Colorado at Colorado Springs,
Department of Chemistry,
Colorado Springs, Colorado 80907, U.S.A.

[2]Division of Engineering,
Brown University,
Providence, Rhode Island, U.S.A.

INTRODUCTION

The heterogeneity of coal, together with its complex macromolecular nature, has been responsible for much of the difficulties in elucidating its structure and chemical characterization. Most methods of investigation of the chemical structure and physical properties involve breaking macromolecules into smaller fragments by depolymerization, oxidation, reduction, dehydrogenation, acetylation, etc., which, for the most part, solubilizes a major fraction of the coal while trying to preserve as much of its original structure as possible. Depending upon the rank of coal and the solvent used, more than 80% of some coals have been solubilized.

Efforts have been made to study the macromolecular structure of coal as a complete entity with special emphasis on cross-linkages. Techniques are limited but swelling and Differential Mechanical Thermal Analysis (DMTA) have proved to be powerful tools in this important area. Although analyses of chemical fragments and macromolecular studies can give complementary information, neither approach alone can lead to final conclusions. No attempt is reported in the literature to simultaneously undertake both solubilization and macromolecular analyses. This paper reports the results of such an attempt. Air oxidation was chosen to modify the coal structure for several reasons.

Elliott (1) reviews the contributions made to the understanding of coal chemistry by researchers using destructive oxidation to reduce the macromolecular structure of coal to entities that can be explored with available instrumentation and known analytical procedures. Since air causes the natural oxidation of coal and because there is little chance that any atoms other than oxygen can be introduced into the coal molecule when it is used as the oxidant, only air was used for the oxidations in this study. The experiments were carried out at 200°C because no weight loss was observable upon heating in nitrogen at or below that temperature.

There have been many studies undertaken to determine the extent of cross-linking in the coal structure (2, 3). Most investigators believe that the more highly cross-linked the coal structure is, the less it will swell when contacted with an organic solvent. Liotta (4), using tetrahydrofuran on weathered coal, showed that swelling decreased as the time of weathering increased. However, if the nature of the cross-links are such that hydrogen bonds are responsible for much of the cross-linking, then work by Hall, et al., (2) suggests that attack by

a basic solvent may result in an increase in swelling.

The problem of understanding the structure of coal is a complex one. It must be remembered that different coals react differently to reagents. The results that are reported in this paper may be applicable to other coals of similar rank and even coals of different ranks, but no such assumption is made in this study.

It is the purpose of this paper to not only provide researchers with additional insight into the macromolecular structure of coal and its chemical characterization, but also to demonstrate that a concerted effort using a variety of techniques on coal and its oxidation products, can make an important contribution to coal science.

EXPERIMENTAL

Coal Characteristics

The coal sample used in this investigation was a Cortonwood coal from the Silkstone seam furnished by British Coal (NCB Coal Rank Code 501, ISO Classification 634) ground to μm size. Important characteristics of the coal are summarized in Table 1.

Coal Oxidation

The coal was oxidized in air for one, two, four and six day periods at 200°C in a forced circulation oven.

Humic Acid Preparations

Water-insoluble samples of the oxidized coal were extracted with 0.1 M NaOH and precipitated with 0.1 M HCl. Centrifugation at 3500 rpm was used along with filtration to speed the recovery of the humic acids. Considerable washing with distilled water removes any NaCl or HCl absorbed on the humic acids. The humic acids were dried at 105°C.

Infrared Spectra of Coals

All spectra were recorded on a Nicolet 205 SXB FTIR spectrometer using KBr pellets. All samples submitted were dried at 105°C.

Volumetric Swelling Technique

The technique perfected by Green, et al., (5) of the procedure developed by Liotta, et al., (4) for measuring swelling was used. In this technique, μm coal samples were centrifuged at 3500 rpm in 6 mm tubes to ensure tight packing. The height of the coal column was measured to ±0.01 mm using a cathetometer. Excess solvent was added. The ground glass stoppered tubes were shaken every 12 hours until equilibrium was reached. Constant height readings of the coal column indicated equilibrium. After equilibrium, the tubes were again centrifuged and the height of the coal column measured. The swelling ratio, Q, is equal to the height of the swollen coal divided by the height of the unswollen coal. Reproducibility was found to be ±0.05 which is in agreement with that of Green (5) and Hall (2). To examine the structure of the coal hydrogen bonding and how it changes on oxidation, swelling was carried out in a set of sterically similar substituted pyridines of differing basicity. Hall, et al., (2) have shown that the weaker bases swell coals by dissociating weak hydrogen bonds from the macromolecular network while the stronger bases swell coals by dissociating stronger

bonds from the structure. A plot of coal swelling (Q) against the pKb of the solvents gives an indication of the hydrogen bond energy distribution of the coal.

Thermal Gravimetric Analyses

A Stanton Redcroft STA-780 Series Thermal Analyser was used for thermal gravimetric analyses. Sample masses of 12-26 mg was used, with heating rates of approximately 6°C to 20°C min^{-1} in nitrogen at temperatures from room temperature to 1000°C.

Petrographic Techniques

Reflectance was measured at 546 nm using oil immersion objectives (n=1.518 at 23°C) on a Leitz MPV3 Microscope Photometer. The photocathode was an EMI S-11. The samples were mounted in epoxy resins and were ground and polished according to the procedures prescribed by Stach, et al., (6). Twenty-five measurements were recorded for each sample in polarized light.

Results and Discussional
Humic Acid Formation

A series of experiments were carried out to determine the rate of oxidation in terms of humic acid formation as a function of time of oxidation. Table 2 and Figure 1 shows the yields of humic acid formation versus time of oxidation while Figure 2 shows a plot of the rate of humic acid production versus time of oxidation. From Figure 2, the maximum rate of humic acid formation should occur at 2.33 days. Of the four periods of oxidation used in these experiments, oxidation for two days showed the maximum yield.

The nature of the humic acids obtained from each of the samples oxidized for various lengths of time showed no functional group differences--as evidenced by infrared analyses. The spectra were characterized by the very broad bands covering C–H and O–H stretching frequencies at the 2500 cm^{-1} to 3500 cm^{-1} region; the COO^- absorption at 1709 cm^{-1}; aromatic and/or hydrogen bonded carbonyls at 1604 and 1216 cm^{-1}; and the shoulder at 1376 cm^{-1} usually assigned to phenolic O–H.

Upon petrographic examination, the humic acids appeared to be isotropic with a random orientation as evidenced when inserted in cross polars with a full wave length retarder plate. The colours were invariant purple during rotation of the stage. The reflectivity did not change on stage rotation using plane polarized light. No pyrite was visible in the humic acids. Large curved cracks from swelling and shrinking were evident. The surface was rather soft, probably due to the sample being polished with relief. The reflectivity was lower than the coal, in the 0.85 range. No visible fluorescence was noticed under ultra violet excitation. To the naked eye, the humic acids appeared to be a black, crystalline solid.

Because of the relative non-volatility of the coal as well as the humic acids, mass spectrometry did not provide useful data in this investigation. Instrument limitations prevented analyses beyond 300°C and thermal gravimetric analyses demonstrated that there was little or no weight loss of the coal below 400°C.

The oxidized coal residue, resulting after the humic acids were extracted, emitted a yellow-brown fluorescence under ultraviolet and blue wavelength excitation during observations made when using fluorescence microscopy indicating the presence of aliphatic hydrocarbons. A considerable amount of pyrite was visible when

viewed under polarized light in various states of preservation, ranging from pristine to a severely oxidized orange state. It appeared that 25-30% of the residue of the sample that was oxidized for six days was pyrite. Byers (7) presents an in-depth discussion of the problems caused by pyrites in coal during furnace operation. Although washing and float and sink methods have had some success in removing pyrites from many coals, small particles usually get into the furnace resulting in high sulphur emissions, slagging and furnace problems. Air oxidation at relatively low temperature followed by an alkaline wash may enhance pyrite removal from coal.

Swelling as a Result of Oxidation

In the experiments carried out in this study, evidence is presented to indicate that basic organic solvents can effect cross-linkages caused by oxidation because of the formation and destruction of hydrogen bonds.

The effect of oxidation on the hydrogen bond structure can be interpreted from Figure 3. There is an initial increase in swelling from the fresh coal to the one day oxidized coal suggesting an initial increase in all strengths of hydrogen bonding. Oxidation from one to two days reduces swelling in the weaker bases (pKb<8) but increases swelling in the strongest base. This suggests that weak hydrogen bonds are being eliminated from the structure and hydrogen bonds are being formed that are not susceptible to attack by pyridine. Further oxidation does not change the density of weak hydrogen bonds to any great extent but swelling in the two strongest bases increases, which implies an increase in the density of strong hydrogen bonds in the structure.

When this data is coupled with the increase of humic acid yield on oxidation the implication is that initial oxidation (up to two days) attacks the alkane and cycloalkane groups, changing these into hydrogen bond crosslinks which are relatively weak and can be broken by the weaker bases. Further oxidation (after two days) is associated with significant production of humic acids. Humic acids have large concentrations of carboxylic acid groups and such groups may lead to strong hydrogen bonding in the coal matrix.

Infrared studies appear to support the data obtained from swelling studies. The oxidation of the coal to form humic acids appears to be due in part to the oxidation of aliphatic groups. The intensity of the alkyl group band at 2900 cm^{-1} is diminished considerably after one day of oxidation. Under petrographic study, increases in the vitrinite reflectance along with increased reflectance of the exinite may be due to increased aromaticity as the coal is progressively oxidized for one and two days. After two days, further oxidation decreases the reflectance indicating the possible attack on aromatic structure. Table 3 shows the reflectance data for the unoxidized and oxidized coals and Figure 4 shows the plot of the data. Figure 5 shows the histograms. Thus it appears that initial oxidation attacks both the alkane and cycloalkane structure of the coal, some of which act as cross-linkages to aromatic clusters. The Cortonwood coal has a relatively high H/C ratio when compared to most medium volatile bituminous coals. The strong hydrogen bonds appear to be associated with the high density of carboxylic acids that are present in the humic acids. The infrared spectra of the unoxidized and oxidized coals show a strong band formed at 3418 cm^{-1} and another strong band at approximately 1700 cm^{-1} appearing after oxidation for one day indicating humic acid formation. The 3418 cm^{-1} band is characteristic of strongly hydrogen bonded OH groups (8) and the 1700 cm^{-1} peak is characteristic of COO^{-} formation (9, 10, 11, 12). The intensity of the alkyl band at 2900 cm^{-1} present in the spectra of the original coal is diminished considerably after one day of oxidation.

Using thermal gravimetric analyses, it can be demonstrated that the weight loss upon heating the unoxidized Cortonwood coal in nitrogen from 105°C to 200°C and maintaining the sample at 200°C for five minutes resulted in no weight loss. It is interesting to note that no appreciable weight loss occurred when pyrolysing the coal under nitrogen until over 400°C. Only about 32% of the coal is ever volatilized at temperatures up to 950°C. Figure 6 shows the results of the thermal gravimetric analyses of the unoxidized coal. The sample lost less then 1.9% moisture upon heating from room temperature to 105°C.

SUMMARY

Air oxidation of a medium volatile bituminous coal at 200°C for six days yields 85% by weight humic acids. The rate of oxidation increases to a maximum at 2.33 days and decreases in a Gausian distribution. The humic acids are characterized by their infrared spectra showing a strong band at 1709 cm^{-1} for the COO^- group, the strong band at 1604 and 1216 cm^{-1} indicative of aromatic and/or hydrogen bonded carbonyl, and a shoulder at 1376 cm^{-1} usually assigned to phenolic OH. Oxidation of coal results in the formation and destruction of hydrogen bonds. Hydrogen bonds form as humic acids are produced from the oxidation of alkyl and alicyclic cross-linkages in the macromolecular structure. Weak hydrogen bonds, already existing in the coal and formed during the oxidation are attacked by pyridine and lead to swelling. Substituted pyridines having pK_b values higher than pyridine are able to break stronger hydrogen bonds in the oxidized coals. Petrographic studies and thermal gravimetric analyses support the information generated by the data gathered from swelling experiments and infrared absorption investigation.

ACKNOWLEDGEMENTS

The authors wish to thank Miss Nina Skorupska, Mr. Stephen Bend, Miss Lynda Jones and Mrs. Christine Morris for their assistance with the petrographic studies. Also, they wish to thank Mr. Oean Field for his assistance in the thermal gravimetric analyses.

REFERENCES

1. Elliott, M.A., "Chemistry of Coal Utilization", John Wiley & Sons, 1981, p. 455-469.
2. Hall, P.J., Marsh, H. and Thomas, M.K., submitted to Fuel.
3. Korov, N.Y., O'Shea, J.M. and Sergeant, G.D., Fuel, 1967, 46, 415.
4. Liotta, R., Brown, G. and Isaacs, J., Fuel, 1984, 63, 935.
5. Green, T.K., Kovac, J. and Larson, J.W., Fuel, 1984, 63, 935.
6. Stack, E., Mackowsky, M-Th., Teichmuller, N., Taylor, G.H., Chandra, D., and Teichmuller, R., "Stack's Textbook of Coal Petrology", Gebruder Borutraeger, 1982, p. 295.
7. Byers, R.W., "The Physical and Chemical Characteristics of Pyrites and Their Influence on Fireside Problems in Steam Generators", ASME Paper No. 75-WA/CD-2, 1975.
8. Silverstein, R.M., Bossler, G.C., and Morrill, T.C., "Spectrometric Identification of Organic Compounds", 3rd Edition, John Wiley & Sons, 1974, p. 91.
9. Painter, P.C., Snyder, R.W., Pearson, D.E. and Kwong, J., Fuel, 1980, 59, 282.
10. Chang, K.K., Flagan, R.C., Gavalas, G.R. and Sharma, P.K., Fuel 1986, 65, 75.
11. Rhoads, C.A., Senftle, J.T., Coleman, M.M., Davis, A. and Painter, P.C., Fuel, 1983, 62, 1387.
12. Starsinic, M., Otake, Y., Walker, P.L. and Painter, P.C., Fuel, 1984, 63, 1003.

Table 1
Characteristics of Cortonwood Coal

Proximate Analysis (as determined)	wt.%
Moisture	1.0
Ash	2.2
Volatile Matter	34.7
Fixed Carbon	62.1
Ultimate Analysis (dry mineral matter free basis)	
Carbon	87.20
Hydrogen	5.60
Oxygen (diff.)	3.9
Nitrogen	1.70
Sulphur	0.70

Table 2
Yield of Humic Acids

Time of Oxidation (days)	Yield of Humic Acids (%)
1	3.4
2	18.8
4	78.7
6	85.8

Table 3
Reflectance of Unoxidized and Oxidized Cortonwood Coal

Time of Oxidation (days)	Reflectance (% R_{mean})	Standard of Deviation
0	0.91	0.07
1	1.15	0.09
2	1.27	0.07
4	1.19	0.08
6	1.10	0.08

Figure 2. Rate of Humic Acid Production vs. Time

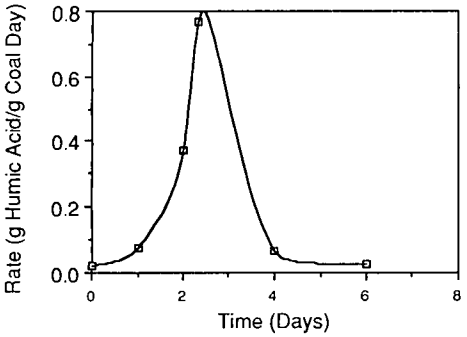

Figure 1. % Humic Acid Production vs. Time

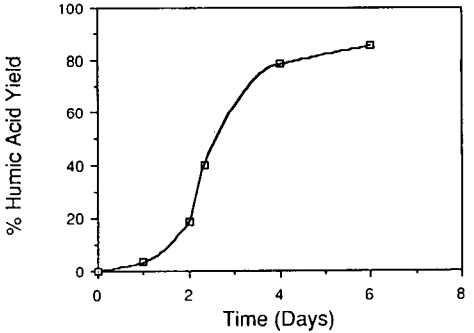

Figure 3. The Effect of Oxidation on Cortonwood Swelling

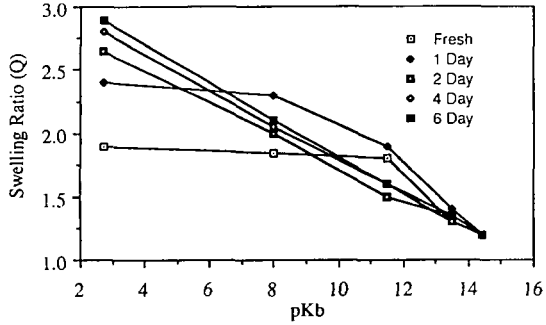

Figure 4. Reflectance vs. Time of Oxidation

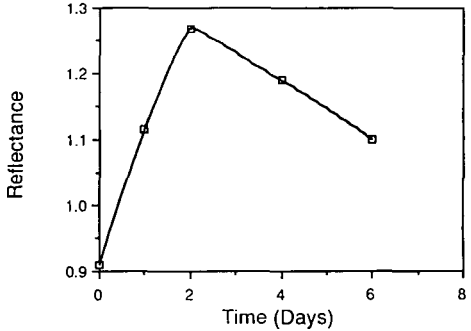

Figure 6. TGA of Cortonwood in Nitrogen

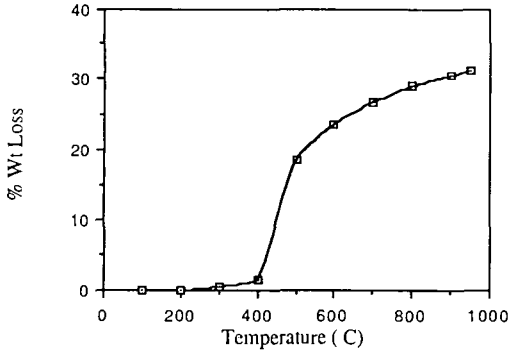

Figure 5. Reflectance Histogram of Unoxidized and Oxidized Cortonwood Coal

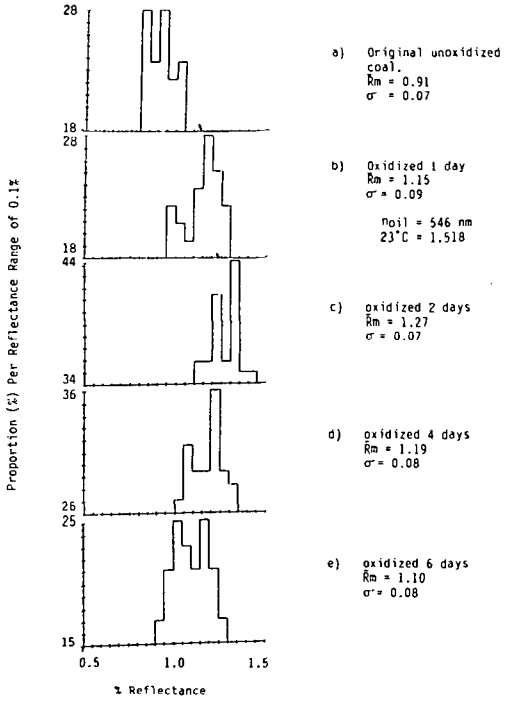

BENEFICIATION OF A BITUMINOUS COAL AND A LIGNITE COAL BY AGGLOMERATION USING NOVEL BINDING OILS.

R.C. Timpe, C.L. Knudson, P. Mack,

University of North Dakota Energy and Mineral Research Center
P. O. Box 8213, University Station
Grand Forks, ND 58202

ABSTRACT

Illinois #6 and both as received and hot water dried Zap (IndianHead) North Dakota lignite were agglomerated with Mandan refinery decant oil containing either p-xylene or deodorized rectisol naphtha from the Great Plains Gasification Plant. The effectiveness of each of the binding oils on agglomeration was determined from ash reduction and organic recovery as a function of mixing speed, mixing time, particle size, and oil-to-coal ratio. Results indicated that, although the ash reduction was significant in the Mandan decant/rectisol naphtha binder for both coals, greater reduction was achieved with the Mandan decant/p-xylene. Higher mixing speeds, longer mixing times, smaller particle size, and binder to coal ratio of 0.35 gave the greatest ash reductions. Agglomeration time was shortened substantially when either p-xylene or rectisol naphtha was added to the Mandan decant in place of using Mandan decant alone as binder.

INTRODUCTION

With the recent effort to educate the world's population on the wise use of the dwindling petroleum reserves and the associated emphasis on coal utilization, the world's supply of high quality, easily mined, low ash coal has also begun to dwindle.(1) Finding new, more efficient methods of beneficiation of higher ash coals has become a priority in coal research. Among the most widely used methods of fine coal beneficiation at present is froth flotation. Although the technique works quite well with higher rank coals and fines with larger particle sizes and low ash, it does have some drawbacks, among them comparatively low yield and high moisture content of product when fines are <76 μm and have high ash content. In addition, the lower rank, more readily mined coals and oxidized coal surfaces are not amenable to beneficiation by flotation. A promising complementary and possibly alternative technique is oil agglomeration.(2)

Agglomeration studies of lignite and subbituminous (low-rank) coals have not met with a great deal of success primarily because the experiments have centered around the successful techniques used to agglomerate bituminous coal. Since agglomeration is a surface phenomenon, the binding oil selected to form the aggregates of fines must be compatible with the surface functional groups on the fines. Most oils used for this purpose are oleophilic and as a result are readily adsorbed to the surface of the coal particles provided they have minimal polar groups exposed. This is characteristic of the bituminous coals but not of the lower rank coals. The subbituminous and lignite coals contain large amounts of surface oxygen making their surfaces more oleophobic than the bituminous. Since the theory of agglomeration assumes mineral material is considerably more hydrophilic and oleophobic than the organic coal matrix, the mineral material will dissolve or form a suspension in an aqueous medium and the organic matter will form aggregates and separate from that phase. Again, this is true for the coals of higher rank but not for the lower rank coals with their more polar, hydrophilic surfaces. The focus of this study was to investigate the agglomeration of a well behaved bituminous coal and a lignite coal when light organic compounds and lower value streams from a petroleum refinery and coal gasification plant are used as

binding oils. The reduction in ash content in the coal was studied as a function of particle size, mixing conditions, and oil characteristics.

In a successful agglomeration, the mineral content of the coal will be reduced significantly as the coal forms aggregates of organic rich material and the minerals are suspended in the aqueous phase. The degree to which a coal can be beneficiated by agglomeration is limited by several factors. The first is the particle size. The finer the particle size the more liquid solid surface contact and, consequently, the better are the chances of the carbonaceous material liberating its associated minerals thus lowering the ash content (3). Although fine grind enhances inorganics removal, it creates problems in handling the cleaned product and provides more area for undesireable surface reactions with oxygen. Effective agglomeration following ash reduction helps to solve these problems.

The second factor to be considered is the composition of the oil used as a binder. Light agglomerating oils (density < 0.90 g/cc) have been shown to give ash reductions in bituminous coals within 10 to 20 percent of those obtained with the Stoddard solvent (4). These oils, however, do not wet the surface of low rank coals well, and are not useful as binding oils for these coals. If heavier oils such as coke oven tars, pitches, and petroleum crudes are used, low-rank coals can be agglomerated, but these oils are more difficult to recover for reuse (4).

pH is a third consideration when carrying out agglomeration. Removal of most mineral material can be done with pH adjustment. However, with elements such as pyritic sulfur which is best removed at a pH between 7-11 the coal becomes more hydrophilic and agglomeration is less effective, requiring multiple pH adjustments to get maximum ash removal and agglomerate size and to reduce agglomeration time (1). Table 1 shows the ash content of the coal used in this study.

TABLE 1.
Agglomeration Test Coals

Sample	Mesh(70 wt %)	Ash mf(wt %)
Illinois #6	200	12.75
Illinois #6	325	24.85
Indian Head (AR)	325	14.63

The size of the agglomerates produced is a function of such processing variables as mixing speed, mixing time, mixer design, and solvent to coal ratio. Physical impact forces result in reduced agglomerate sizes with increased mixing speed and mixing time and contact with surfaces of smaller surface areas such as blade edges.(5) To minimize these impacts a blunt stir bar providing maximum contact area between agglomerates and bar is recommended. Thorough agitation may increase the yield but not necessarily the size of the agglomerates. Increasing the ratio of binding oil to coal tends to increase agglomerate size, making binding oil recovery an economically important aspect of this method of beneficiation (6). Recovery of 40 to 50% of the binding oil by thermal treatment under reduced pressure maintains the calorific value of the product, decreases the moisture content, increases mechanical stability, and results in reduction of selfignition hazards.

EXPERIMENTAL

Agglomeration tests were carried out on as-received Illinois #6 bituminous coal and an as-received and a hot water dried North Dakota lignite from the Indian Head mine. The coals were ground to 70 wt% 200 mesh (75 μm) and 325 mesh (45 μm).

The percent ash values on a moisture free basis are shown in Table 1.

Screening tests were carried on nine different liquids to determine the most suitable binding oil for agglomerating the test coals. The oils tested included Lummus Arabian and Lloydminster petroleum resids, North Slope ATB, Mandan Decant oil, Mayan crude, rectisol naphtha, JP4 aviation fuel, 1 octanol, and p-xylene. The Mandan crude exhibited better agglomerating results than the other oils for both the bituminous and the lignite coals. The binding oils selected for this study were Mandan Decant oil (MDO) from the Amoco refinery at Mandan,North Dakota, and mixtures of MDO with p-xylene (MDO/XY) or rectisol naphtha (MDO/RN) from the Great Plains Gasification Plant at Beulah, North Dakota. The solvent mixtures were 50 wt % Mandan Decant oil in either p-xylene or rectisol naphtha.

The laboratory experiments were carried out in both large and small scale mixers. The small scale experiments (called micro agglomeration) consisted of stirring 0.50 g coal, 0.15 to 0.35 g of oil, and 10 g H20 at 10,000 to 21,000 revolutions per minute (rpm) in a micro-agglomeration cell for measured time periods.

A variable speed blender with a fabricated bar propeller stirring rod was used to carry out the larger scale experiments. Five hundred ml of deionized water was poured into a stainless steel mixing cup. The weighed binding oil was poured into the cup and the oil and water mixture was stirred at 10,000-20,000 rpm for several minutes prior to introducing the weighed coal sample into the unstirred mixture. The water, oil, and coal was stirred at the above rate for from 1 to 6 minutes.

Following the stirring, the inherent pH of the slurry was measured using pH paper. (The effect of pH adjustment on the agglomeration was not included as part of the study reported here but instead is included in the work currently underway.) The slurry was then poured over a 100 mesh screen to collect the agglomerates. 500 ml of deionized water was used to rinse the agglomerates and then they were extracted with 100 ml tetrahydrofuran (THF), filtered under vacuum, and air dried over night. Moisture and ash content were then determined.

RESULTS AND DISCUSSION

The initial experiments were carried out with Mandan decant oil pxylene on the Illinois #6 bituminous coal since previous agglomeration work has been successful with this coal rank. Micro- and large-scale agglomeration experiments produced agglomerates which differed in size and texture with different solvent to coal ratios, mixing speeds and mixing times. A satisfactory solvent to coal ratio for agglomeration of the bituminous coal with Mandan decant oil was determined by first investigating the agglomerating properties of the oil itself and then by comparing those properties with those of dilutions of decant oil with p-xylene. Rectisol naphtha, a light oil stream obtained from the commercial coal gasification plant at Beulah, North Dakota, was substituted for the p-xylene in some of the later experiments. The ash content of the agglomerates formed in this solvent was determined and compared with that of agglomerates formed at the same conditions using the MDO p-xylene.

The characteristics of the agglomerates apparent to the eye are described in terms of size and texture. Micro-agglomerates or flocs are the smallest, discrete are "medium sized", and amalgams are the large coal-in-oil pastes. The texture is either firm or loose. Tables 2 and 3 show the characteristics of agglomeratesformed at a variety of conditions for both the bituminous and the lignite coal. The series of experiments carried out with Mandan Decant oil to determine its agglomerating ability gave the desired firm amalgam at a minimum solvent to coal ratio of 0.6 when allowed to stand overnight. Sun and McMorris

reported that high specific gravity oils do not disperse well enough in coal slurry to wet the coal (1). Since MDO has a specific gravity of 1.0202 (considered high), accounting for the slow formation of agglomerates, lower specific gravity organic liquids were added to reduce it to the medium range. A 50 wt % MDO in p-xylene gave a medium range specific gravity of 0.9400 and this binding oil agglomerated the 325 mesh bituminous coal sample within minutes at a solvent to coal ratio of 0.7 when stirred for 3 minutes at 10000 rpm. The larger 200 mesh particles formed firm agglomerates at a solvent to coal ratio of 0.5 under the same stirring conditions.

TABLE 2.

MICROAGGLOMERATION RESULTS FOR 325 MESH ILLINOIS #6 BITUMINOUS "COAL, AS RECEIVED

Binding Oil	Solvent/Coal Ratio	Speed (rpm)	Mixing Time(min) Solvent	Mixing Time(min) Slurry	Agglomerates Type	Agglomerates Texture
Illinois #6 Bituminous						
MDO	0.4	10,000	1	3	floc	loose
MDO	0.5	10,000	1	3	floc	loose
MDO	0.6*	10,000	1	3	amal	firm
MDO	0.7	10,000	1	3	disc	loose
MDO/XY	0.5	10,000	1	3	disc.	firm
MDO/XY	0.6	10,000	1	3	disc.	firm
MDO/XY	0.7	10,000	1	3	amal.	firm
MDO/XY	0.5	10,000	2	3	amal.	firm
MDO/XY	0.6	10,000	2	3	amal.	firm
MDO/XY	0.7	10,000	2	3	amal.	firm
MDO/XY	0.8	10,000	2	3	none	--
India Head Lignite						
MDO/XY	0.30	10,000	2	3	floc	firm
MDO/XY	0.40	10,000	2	3	disc.	firm
MDO/XY	0.50	10,000	2	3	disc.	firm
MDO/XY	0.60	10,000	2	3	disc.	firm
MDO/XY	0.70	10,000	2	3	disc.	firm
Hot Water Dried Indian Head Lignite						
MDO/XY	0.30	10,000	2	3	disc.	firm
MDO/XY	0.40	10,000	2	3	amal.	firm
MDO/XY	0.50	10,000	2	3	amal.	firm
MDO/XY	0.30	20,000	2	3	disc.	firm
MDO/XY	0.40	20,000	2	3	disc.	firm
MDO/XY	0.50	20,000	2	3	amal.	firm

MDO/XY = 50 wt % MDO in XY
MDO = Mandan Decant Oil
XY = p-xylene
floc = micro-agglomerates
disc = discrete agglomerates
amal=amalgams
*agglomerates formed overnight

Table 4 shows the results in terms of product ash content of experiments carried out on the larger unit. Simple calculation from this table shows the ash reduction of the 325 mesh bituminous coal was greater than that of the 200 mesh samples. This is not unexpected in light of the fact that the smaller particles have more surface contact with the oil. Experiments with the 200 mesh bituminous

coal on the larger scale unit showed that firm amalgams could be formed at a ratio of as low as 0.3 when stirred for 6 minutes at 13,000 rpm resulting in an ash reduction of 8%. Although these particles are more easily handled physically, Table 4 shows that greater ash reduction is accomplished in forming the smaller particles.

TABLE 3.

MICROAGGLOMERATION RESULTS FOR 70 wt % 200 MESH IILLINOIS BITUMINOUS COAL, AS RECEIVED

Binding Oil	Solvent/Coal Ratio	Speed (rpm)	Time(min) Solvent	Mixing Time(min) Slurry	Agglomerates Type	Texture
MDO/XY	0.5	10,000	2	3	amal.	firm
MDO/XY	0.6	10,000	2	3	amal.	firm
MDO/XY	0.7	10,000	2	3	amal.	firm

The same solvent as in the experiments with the bituminous coal was used in the experiments with the Indian Head lignite. In the micro agglomeration tests with 325 mesh asreceived lignite at solvent to coal ratios of 0.250.70 and stirring rates of 10,000 rpm for 3 minutes no firm amalgams were formed. However, under identical conditions hot water dried lignite formed firm amalgams at solvent to coal ratios of 0.40, and at similar conditions but with a stirring rate of 20,000 rpm, amalgams formed in a solvent to coal ratio of 0.50. In large scale tests, the as received lignite formed only firm discrete agglomerates. With hot water dried lignite firm amalgams were formed in the MDO p-xylene when mixing at 10,000 rpm for 3 minutes in a solvent to coal ratio of 0.25 and resulted in a 21% reduction in ash content. Firm amalgams were also formed at ratios of 0.30, 0.35, and 0.40 at the same mixing speed and time conditions with nominally 8% reduction in ash. Increasing the mixing speed to 20,000 rpm resulted in firm amalgams at a ratio of 0.30 with a 14% reduction in ash. Substitution of the rectisol naphtha for the p-xylene in the solvent mixture was found to yield only firm discrete particles and the most satisfactory solvent to coal ratio was 0.40. The ash reduction was 13% as compared with a reduction of 17% with the MDO p-xylene at the same mixing conditions.

The pH was determined to be ~6 for the slurries included in this study. Current work getting underway includes a study of the effect of adjusting the pH to enhance agglomeration and ash reduction.

CONCLUSIONS

The following conclusions are suggested by the data:

- Mandan Decant Oil, a high density oil, will agglomerate the studied coal types only after standing for extended periods of time, while a 50 wt % mixture of MDO in either p-xylene or rectisol naphtha, which forms a medium density oil, will agglomerate these coals within several minutes.
- Hot water drying of lignite enhances its agglomerating properties.
- Agglomerates which are flocculate or discrete in form generally gave higher ash reductions than amalgam agglomerates.
- Higher mixing speeds and longer mixing times although not giving large agglomerates, generally gave higher ash reductions with both coals studied.

- The MDO/XY binder caused greater reduction of the ash content of the 325 mesh as received lignite (17%) than the MDO/RN (13%).
- Agglomerate formation is dependent on the design of the stirrer.
- When using the MDO/XY solvent, the ash content of the 325 mesh bituminous coal was reduced more than that of the 200 mesh coal, showing reductions of 17% and 14% respectively. A 14% reduction in ash was realized for the 325 mesh hot water dried lignite as compared to 12% for the as received lignite.

TABLE 4.

AGGLOMERATION RESULTS FOR A 50 WT % MANDAN DECANT OIL IN P-XYLENE OR RECTISOL NAPHTHA.

Solvent/Coal Ratio	Speed (rpm)	Time(min) Solvent	Time(min) Slurry	Agglomerates Type	Texture	Product % Ash *
200 Mesh Illinois #6 Bituminous, as received						
0.30	13,000	2	3	disc.	firm	11.75
0.35	13,000	2	3	disc.	firm	10.91
0.40	13,000	2	3	amal.	loose	11.05
0.25	13,000	2	6	disc.	firm	11.97
0.30	13,000	2	6	amal.	firm	11.69
0.35	13,000	2	6	amal.	firm	11.37
0.25	16,000	2	6	disc.	firm	11.25
0.30	16,000	2	6	disc.	firm	11.07
0.35	16,000	2	6	disc.	firm	10.96
325 Mesh Illinois #6 Bituminous, as received						
0.25	16,000	2	6	floc	firm	21.83
0.30	16,000	2	6	floc	firm	20.99
0.35	16,000	2	6	disc.	firm	20.55
325 Mesh Indian Head Lignite, as received						
0.40 MDO/XY	15,000	2	6	disc.	firm	12.09
0.40 MDO/RN	15,000	2	6	disc.	firm	12.72
325 Mesh Hot Water Dried Indian Head Lignite						
0.25	10,000	2	3	amal.	firm	8.73
0.30	10,000	2	3	amal.	firm	10.29
0.35	10,000	2	3	amal.	firm	10.12
0.40	10,000	2	3	amal.	firm	10.27
0.30	20,000	2	3	amal.	firm	9.49
0.35	20,000	2	3	disc.	firm	9.44
0.40	20,000	2	3	disc.	firm	9.58

*Moisture free basis.
MDO/XY = 50 wt % Mandan Decant Oil in p-xylene
MDO/RN = 50 wt % Mandan Decant Oil in rectisol naphtha

REFERENCES

1. Sarkar, G.G., B.B.Konar, J. of Mines, Metals, and Fuels, 28, No. 5, 103, (1980).

2. Bandopadhyay, P., Urja, 15, No.5, 377, (1984).

3. Bhattacharyya, R.N., A.K. Muza, and G.G. Sarkar, "Role of Operating Variables in Oil Agglomeration of Coal", Agglomeration Seventy Seven, 2, 931938, (1977).

4. Liu, Y.A., Editor, Physical Cleaning of Coal, Chapter 6, Marcell Dekker, New York, (1982).

5. Hazra, S.K., T.C. Rao, G.G. Sarkar, "Effects of Process Variables on Size Distribution of Oil Agglomerates of Fine Coal", Coal Preparation, 3, 7787, (1986).

6. Masologites, G.P., "Process for Agglomerating Coal", Patent No. US 4355999, Atlantic Richfield Co., 1978.

ACKNOWLEDGEMENT

Financial support for this project was provided by the U.S.Department of Energy through the Pittsburgh Energy Technology Center under contract no. DEFC2186MC10637.

THE COMPARISON OF A LIGNITE CHAR, SUBBITUMINOUS COAL CHAR, AND A BITUMINOUS COAL CHAR USED IN THE REACTION WITH STEAM TO PRODUCE HYDROGEN.

R.C. Timpe and R.E. Sears

University of North Dakota Energy and Minerals
Research Center, Grand Forks, North Dakota 58201

ABSTRACT

The use of coal as a carbon source in the char-steam reaction to produce hydrogen gas over the temperature range 700°-800°C (973-1073 K) at atmospheric pressure has been studied in detail. Velva lignite has properties which give its char superior reactivity over those of the other coals tested. Catalysis with alkali carbonates enhanced the reactivity of Velva char substantially, whereas demineralization reduced the reactivity to a relatively constant value over the temperature range studied by removing inorganic material and altering the surface characteristics of the coal. Char produced from a Wyodak subbituminous coal and River King bituminous coal were much less reactive than Velva in the absence of catalyst but responded positively to the addition of alkali carbonates. Upon demineralization, these coals also showed reduced reactivity and altered surface features. This paper discusses the results of the experiments in terms of the reactivity data, SEM photos and elemental mapping, organic properties as determined from ^{13}C NMR and ESCA spectroscopy, and inorganic content of the substrates.

INTRODUCTION

The bench-scale production of hydrogen at atmospheric pressure and moderate temperatures (700°-800°C) from the uncatalyzed and catalyzed reaction of low-rank coal char and steam has been studied extensively at the University of North Dakota Energy and Mineral Research Center (UNDEMRC). The gasification process focuses on utilizing the gasification and the water-gas shift reactions at these conditions to optimize hydrogen production. The limiting step in the process at these conditions is the char-steam reaction (1).

Although the low-rank coals that have been tested exhibit somewhat different reactivities from one another, they are generally more reactive than those of higher rank.(2) The reasons for the differences in reactivity within a rank remain controversial. However, surface area as it relates to turnover number, and the presence of specific catalytic inorganic materials, are certain to play a role in enhancing or retarding reaction rate. Similarly, the decrease in reactivity with increasing rank may be the result of one or both of these, along with the increasing aromatic nature of the coal. This study examined some of the similarities and differences in the chemical properties between representatives of the three ranks, that is, lignite, subbituminous and bituminous coals.

The selection of test coals for this study was based on previous gasification performance as determined from the char reactivity data base at UNDEMRC. One of the test coals that was known to gasify readily was a lignite from the Velva, North Dakota, coal mine. This coal has been extensively studied at UNDEMRC as a feedstock for the hydrogen production process. These studies indicate that this coal is an excellent candidate for use in the gasification process and is

currently being used as a basis for comparing other candidate coals. The subbituminous coal selectd was likewise a much-studied Wyodak coal from Wyoming. Although Wyodak reacts more slowly in the bench-scale tests than the Velva lignite, its reactivity is greatly enhanced when the reaction is catalyzed by an alkali catalyst. The bituminous coal was the unwashed high-ash Illinois #6 coal.

EXPERIMENTAL

The reactions between the coal chars and steam were studied with two different Thermogravimetric Analysis (TGA) systems. The kinetic study of weight change of carbon with time for the char-steam reaction was carried out on a DuPont 951 Thermogravimetric Analyzer (TGA) interfaced with a DuPont 1090 Thermal Analyzer.

Approximately 30 mg samples of -100 x +140 mesh as-received or demineralized coal, or as-received coal containing K_2CO_3 catalyst, were devolatilized under argon flowing at 160 cc/min. The resulting char was then reacted with steam ($p_{(H2O)}$=0.1) for a period not exceeding 180 minutes. Weight, time, and temperature data were recorded for the duration of the experiment. Total gas (product gas plus carrier gas) samples were collected over the duration of the run and were analyzed by gas chromatography (GC).

Selected experiments were duplicated on an UNDEMRC-built large TGA (1) so that large gas samples could be collected, ensuring a more accurate gas analysis. Reactivity parameters, (k), were calculated at each of three temperatures (T) and Arrhenius plots of ln k vs 1/T were constructed for calculating energy of activation (E_a) and frequency factor, (A), as previously described.(3)
Char analyzed by spectroscopic techniques was prepared as in the char-steam reaction experiments, but was cooled to room temperature under argon. These samples were analyzed by Electron Spectroscopy for Chemical Analysis (ESCA) and 50 MHz solid ^{13}C Nuclear Magnetic Resonance Spectrometry (NMR). The NMR technique used on the samples was an adaptation of the Bloch Decay technique in which no cross-polarization with hydrogen and no proton decoupling was used (4). Instead, the ^{13}C spins were polarized directly rather than from rapidly relaxing hydrogen nucleii, thus removing the question of the quantitative nature of cross-polarization in hydrogen deficient species.(5) All spectra were obtained using the same pulsing parameters and TOSS was used to eliminate spinning sidebands. Samples of each char were examined by Scanning Electron Microscopy (SEM) to determine surface elemental distribution and to obtain photographs of the char surface. The field was scanned and representative particles were photographed and mapped to determine the elemental distribution.

RESULTS AND DISCUSSION

There are several significant similarities and differences between the coals used in this study. Two of the basic differences in the coals used in this study were their rank and their geographical origins. The Velva lignite is a northern Great Plains lignite from a mine near Velva, North Dakota. The Wyodak subbituminous coal was from the Green River Basin in Wyoming. The Illinois #6 was a bituminous coal obtained from the River King mine in southern Illinois.

Proximate and ultimate analyses of the three coals are listed in

Table 1. The Velva lignite sample was higher in moisture and ash content than the Wyodak sample. The River King bituminous was lower in moisture but much higher in mineral matter than either of the other two. The three coals have equal quantities of MAF volatile matter and of fixed carbon by weight.

TABLE 1

PROXIMATE AND ULTIMATE ANALYSES

Proximate Analyses	Velva	Wyodak	River King
Moisture %	29.3	13.7	5.8
Ash, wt % mf	13.5	8.1	35.8
Volatile Matter, wt % mf	39.3	42.7	29.2
Volatile Matter, wt % maf	45.4	46.4	45.6
Fixed Carbon, wt % mf	47.2	49.3	35.0
Fixed Carbon, wt % maf	54.6	53.6	54.4
Heating Value, Btu/lb AR	7185	8057	9477
Ultimate Analyses, mf, wt %			
Hydrogen	3.84	4.76	2.61
Carbon	59.93	66.64	44.81
Nitrogen	0.94	0.91	0.40
Sulfur	0.53	0.51	5.16
Oxygen (Diff)	21.26	19.10	6.56

A third difference was in the reactivities of the coal chars in uncatalyzed char-steam reactions as illustrated by Figure 1. The Wyodak subbituminous coal char reacted more slowly than the lignite char but the slowest reaction was that involving the River King char. The reactions of all three chars were enhanced by the presence of alkali catalyst. The River King char reacted the slowest of the three, and therefore the uncatalyzed and catalyzed reaction of that char were only followed through < 25% carbon conversion.

The reactivities of the test coals, the coals containing K_2CO_3 catalyst, and the demineralized coals are shown in Table 2. Note that the bituminous coal char and the demineralized coal chars reacted with steam very slowly at all three temperatures resulting in the termination of each experiment before 50% conversion could be accomplished. The Velva lignite char had reactivities that were 1.5-2 times those of the other coals at each temperature. Catalysis of the reaction at the lower two temperatures increased the reactivity of the Wyodak to values exceeding those of the Velva coal char. However, at 800°C, the reactivity of the Velva was increased to ~2.5 times that of the Wyodak. The reactivity of the River King is greater over the first 0-15 wt % carbon conversion than over the remainder of the conversion as shown in Figure 1. This is attributed to the higher state of oxidation on the char surface particle compared to the subsurface layers, making the surface carbon functionalities more hydrophilic than those beneath the surface. The reactivity of the River King char is lower than that of the other two coal chars even when comparing its highest k value (15% carbon conversion) with 50% carbon conversion for each of the other two. In addition, of the forms tested for this River King, none was greatly responsive to changes in temperatures within the studied temperature range.

TABLE 2.

CHAR-STEAM REACTIVITIES FOR THREE COALS AT 700°, 750°, and 800°C.

	Coal		
	Velva	Wyodak	River King
Conversion, wt % C	50	50*	15
Temperature (°C)	k	k	k
700	1.35	0.84	1.10
750	2.10	0.94	1.23
800	3.56	2.23	1.52
		Coal w/ 10 wt % K2CO3	
700	4.06	9.87	5.00
750	8.17	11.13	5.81
800	34.81	13.07	8.41
		Demineralized Coal	
700	1.06	1.51	1.49
750	1.40	3.25	3.06
800	1.15	8.33	3.13

* k calculated for 10% conversion of demineralized Wyodak char carbon.

The inherent inorganic contents of the ash for the three test coals are shown in Table 3. The aluminum, silicon, and iron concentration of the River King was much higher than in the other two coals. The potassium concentration was also higher in the bituminous coal than in the other two but apparently not in sufficient quantity to enhance the rate of reaction to a level near those of the lower rank coals. The sodium and calcium concentrations, two other elements known to be good catalysts, were much higher in the lower rank coals than in the River King. An effect related to a change in total inorganic content was noted. It was observed that on demineralizing the River King coal, the char reactivity was enhanced over that of the raw coal. Demineralization of the other two test coals left their chars less reactive than the those of the parent coal.

TABLE 3.

RESULTS OF ASH ANALYSES BY XRFA OF THREE COALS IN MOLES OF ELEMENT PER 10000 GRAMS OF COAL.

ELEMENT	VELVA	WYODAK	RIVER KING
Aluminum	3.02	2.38	10.81
Silicon	3.43	3.95	26.77
Sodium	1.06	0.27	0.00
Potassium	0.04	0.05	1.49
Calcium	8.32	3.38	2.34
Magnesium	2.87	1.20	1.16
Iron	0.94	0.70	9.43
Titanium	0.14	0.13	0.38
Phosphorus	0.10	0.14	0.04
Sulfur	1.41	1.02	1.64

The SEM photographs in Figure 2 show the surface effect that results from charring the test coals containing K_2CO_3 catalyst. The ragged, irregular surface and lack of apparent pores in the uncatalyzed char was in contrast to the rounded, nodular surface on the alkali catalyzed char. The degree to which the surface of the coal changed on charring with the addition of catalyst differed among the coals. The Velva char surface was remarkably porous and contained uniform, evenly spaced nodules of approximately 0.05 μm x 0.10 μm in size. The nodules on the surface of the catalyzed Wyodak and River King coal chars were rounded and numerous but not uniform in either size or distribution. The demineralized Wyodak and River King chars had a good deal of surface relief in the form of a few nodules and concavities whereas the surface of the demineralized Velva was relatively smooth. The differences in the surface relief appear to parallel the differences in reactivity and is probably due to changes in available active sites. SEM mapping of the surface for inorganic element distribution showed that the inorganic matter was not distributed uniformly over the surface of the chars except for the potassium. The uniform distribution of the potassium in even the low moisture coals imply a fluid dissemination of the catalyst.

Carbon-13 Nuclear Magnetic Resonance (^{13}C NMR) spectra of chars prepared at temperatures of 750°C shown in Figure 3 indicated the loss of most of the aliphatic carbon on charring. Aromatic carbonyl groups were present in the demineralized Velva and Wyodak chars whereas they appeared to be absent in the other chars. Integration of the demineralized Velva char spectrum indicated the presence of more aliphatic carbon than in the raw Velva char. The opposite was observed for the Wyodak chars, in which the raw Wyodak char had more aliphatic carbon than its demineralized counterpart. The aliphatic content of the two River King chars did not differ significantly.

Table 4 shows the ratio of carbon to the other elements found by ESCA on the surface of the char particles. The carbon-to-oxygen ratio of the lignite was about the same on the surface of the raw char as it was on the demineralized char. However, the ratio increased by factors of 5 and 3 on the demineralized chars over the raw chars of Wyodak and River King, respectively. In the latter two cases, the demineralization appears to remove oxygen along with the mineral matter and/or remove C-O functionalities leaving less

TABLE 4.

SURFACE ATOMIC RATIOS AS DETERMINED BY ESCA, IN ATOMS C PER ATOM Y

	VELVA			WYODAK		RIVER KING	
Atomic Ratio	Raw	Dem	Dem*	Raw	Dem	Raw	Dem
C/O	4.1	4.8	16.6	6.1	30.7	8.5	22.7
C/N	107	134	60.7	132	136	68.5	ND
C/Na	747	403	456	159	ND	411	466
C/Si	16.6	403	152	56.6	951	30.4	ND
C/S	372	806	456	397	476	117	93.1
C/Ca	374	ND	ND	33.0	951	822	466
C/Al	83.0	806	182	41.7	476	31.6	103
C/Fe	ND	ND	ND	793	951	822	466

* 90 minute sputter
ND = Not Detected

reactive carbon functionalities on the surface of the particles. The change in inherent catalyst materials, sodium (Na), calcium (Ca), and iron (Fe), between raw coal char and demineralized coal char from the same coal differed for each of the coals. No pattern that would indicate a particular catalytic effect was observed for any of the three. Likewise silicon (Si), nitrogen (N), and sulfur (S) changes showed little correlation to the effect of demineralization that would facilitate a conclusion.

CONCLUSIONS.

All three coals responded to the addition of the K_2CO_3 catalyst in the char-steam reaction. Reactivity of the Velva char increased by factors of three to ten at a given temperature with the addition of the catalyst. However, the Wyodak char responded with greater increases in reactivity at the lower two temperatures upon catalyst addition, increasing reactivity six to ten times. The addition of catalyst to the River King char increased the reactivity by a factor of ~5 but the char reactivity was affected very little by temperature over the temperature range studied. Demineralization of the coals reduced the reactivity of the Velva char but increased the reactivity of the River King over that of their respective raw coal chars. Scanning electron microscopy showed that the char surface is affected by both demineralization and catalyst addition to the raw coal. Larger than expected aromatic carbonyl peaks were obtained in the ^{13}C NMR spectra of demineralized Velva and Wyodak chars:

REFERENCES

1. Timpe, R.C., R.E. Sears, and G.G. Montgomery, ACS Div. Fuel Preprints, 32, No. 4, 1, (1987).
2. Takarada, T., Y. Tamai, and A. Tomita, Fuel, 64, 1438, (1985).
3. Timpe, R.C., S.A. Farnum, S.J. Galegher, J.G. Hendrikson, M.M. Fegley, ACS Div. Fuel Preprints, 30, No. 4, 481, (1985).
4. Axelson, D.E., Solid State Nuclear Magnetic Resonance of Fossil Fuels, Chapters 2-3, Multiscience Pub. Ltd., Canada, (1985).
5. Botto, R.E., R. Wilson, and R.E. Winans, Energy and Fuels, 1, 173-181, (1987).

ACKNOWLEDGEMENTS

The authors would like to acknowledge Jan Lucht for assistance with the TGA experiments, George Montgomery for ESCA data, and Art Ruud for the ^{13}C NMR spectra. Gratitude is extended to Leland E. Paulson, Technical Project Officer, and Madhov Ghate, Chief, Combustion and Gasification Branch, Morgantown Energy Technology Center for their guidance and support. This work was carried out under DOE contract no. DE-FC21-86MC10637.

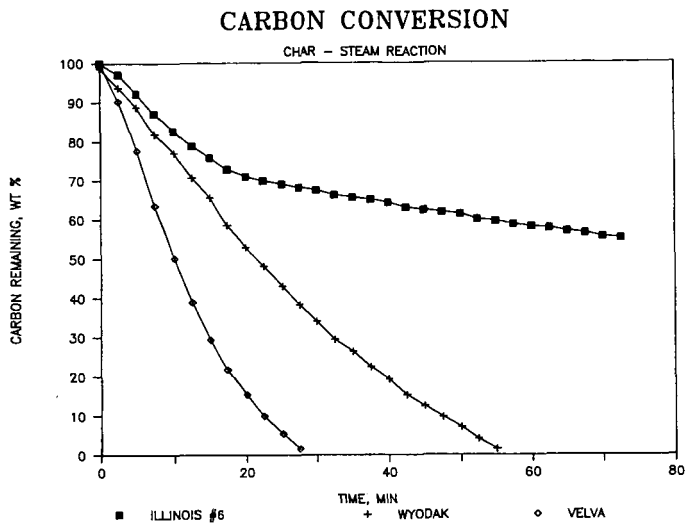

Figure 1. Conversion of Velva lignite, Wyodak subbituminous, and Illinois #6 char carbon on reacting with steam at 750°C.

(a) (b) (c)

Figure 2. SEM photos of chars of the raw (a, d, g) and demineralized (b, e, h) coals and chars of each coal with 10 wt % K_2CO_3 added (c, f, i). The photos shown are of chars of Velva lignite (a, b, c), Wyodak subbituminous (d, e, f), and Illinois #6 bituminous (g, h, i) coals.

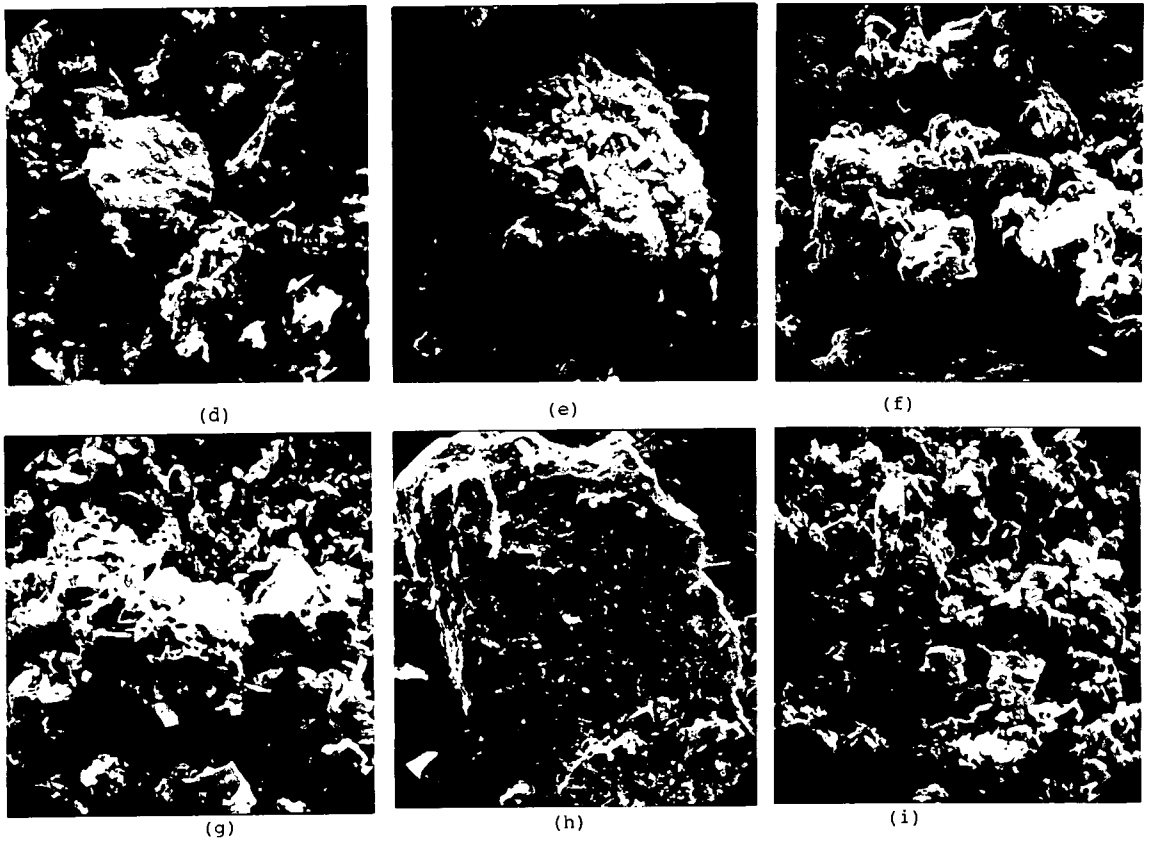

Figure 2 (continued).

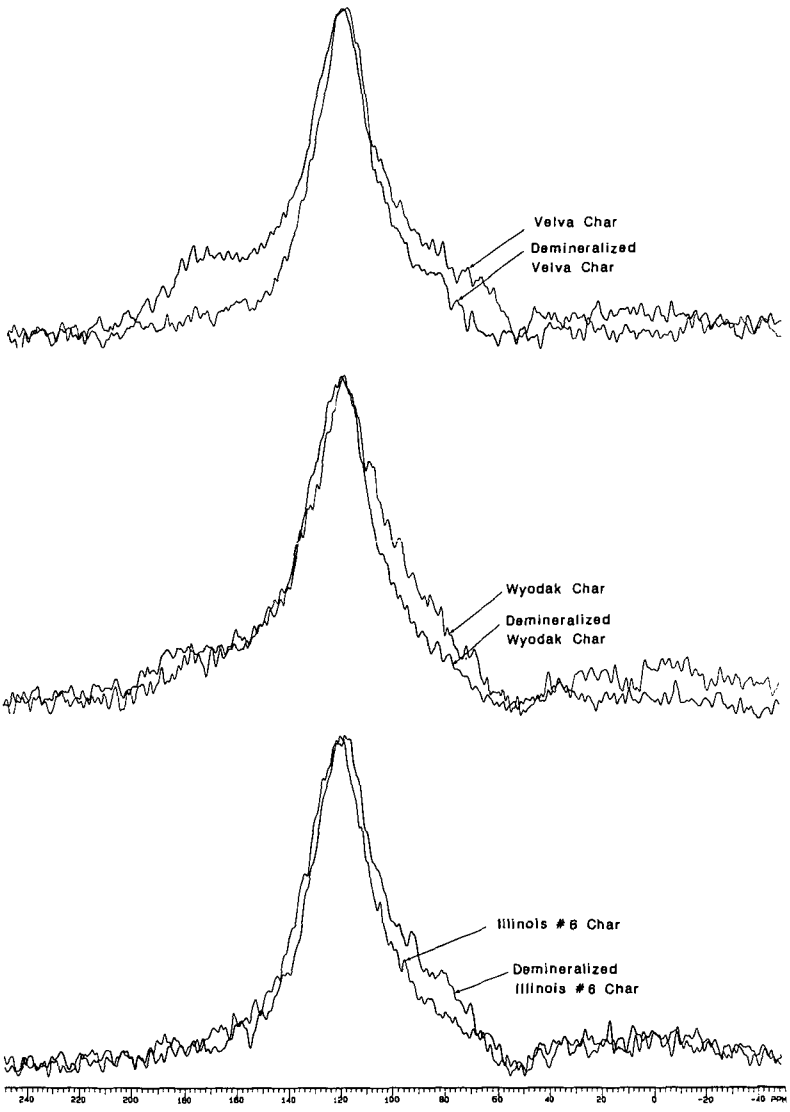

Figure 3. Solid ^{13}C NMR spectra of chars from raw and demineralized Velva lignite, Wyodak subbituminous, and Illinois #6 bituminous coals.

COAL LIQUEFACTION USING DEUTERIUM-LABELED ANTHRACENE OIL SOLVENT

T.R. Aulich, C.L. Knudson, and S.B. Hawthorne

University of North Dakota
Energy and Minerals Research Center
Grand Forks, North Dakota 58202

ABSTRACT

In order to better understand the reactions of heteroatom-containing organics which occur during liquefaction of subbituminous coal, it is necessary to distinguish between coal-derived and solvent-derived species. A coal-derived liquefaction solvent, AO4, was deuterium-labeled by a method developed at the University of North Dakota Energy and Minerals Research Center and found to be stable under liquefaction conditions. The deuterium-labeled AO4 was reacted in the presence of unconverted coal (tetrahydrofuran-insoluble material from a previous autoclave liquefaction test), water, carbon monoxide, and hydrogen sulfide at 350°C and 1000 psia for 30 minutes. No significant degradation in isotopic purity was observed in the mass spectra of the individual deuterated species comprising approximately 95 wt% of the deuterated solvent. Tests were also conducted with raw coal under similar liquefaction conditions to determine the amounts of coal-derived compounds evolved, and whether these compounds will undergo deuterium exchange with the deuterated solvent. Distillable products are being analyzed using GC/MS, and soluble and insoluble products are being analyzed using liquid proton and solid state C-13 NMR. The deuterium-labeling method has also been used to synthesize 16 model compounds including O-, S-, and N-containing aromatics to be used in future liquefaction tests. Analytical results including product component identification, coal conversion as determined by tetrahydrofuran solubility, and changes observed in NMR spectra will be presented.

INTRODUCTION

The purpose of the described research is to study the reactivity of heteroatom-containing organics in Wyodak subbituminous coal under liquefaction conditions. The liquefaction solvent specified for use in the research is a coal-derived anthracene oil (AO4). Several heteroatom-containing components of AO4 (dibenzofuran, dibenzothiophene, and carbazole) are thought to be produced from coal during liquefaction. Other coal-derived liquefaction products such as phenol, cresols, and quinolines are also present in AO4 as minor components. Clearly, a method is needed to distinguish between coal-derived and solvent-derived heteroatom-containing product species. By producing deuterium-labeled AO4 and examining its behavior under liquefaction conditions, it should be possible to differentiate between coal-derived and solvent-contained species with gas chromatography/mass spectrometry (GC/MS) and nuclear magnetic resonance (NMR) techniques.

SYNTHESIS OF DEUTERIUM-LABELED AO4 LIQUEFACTION SOLVENT

Approximately 30 grams of deuterium-labeled AO4 was synthesized

using a 1.0 liter autoclave constructed of "Hastelloy C", an alloy resistant to chloride ion corrosion. A six hour reaction at 300°C was carried out using 30 grams A04, and a 250 mL solution of 4% deuterium chloride in deuterium oxide with 10 mg/mL dissolved chromium metal. After cooling the autoclave overnight, the product was removed from the autoclave, dissolved in ether, washed, dried, and weighed to yield an approximate 97% recovery. Figure 1 shows a gas chromatogram of A04 before and after deuterium-labeling. The similarity in the two chromatograms demonstrates that essentially no degradation or loss due to volatilization of any major components occurred as a result of undergoing the deuteration reaction. Figure 2 shows representative mass spectra of several individual A04 components before deuteration (upper spectrum of each set) and after deuteration (lower spectrum). The spectra were obtained with a Hewlett Packard 5985 GC/MS using a 70 eV electron impact ionization potential. In general, isotopic purities of the individual aromatic components of the A04 were approximately 95%, as determined using GC/MS with low voltage (10 eV) electron impact ionization.

Proton NMR spectra obtained of the non-deuterated and deuterated solvents are presented in Figures 3a and 3b. Since deuterium is not detected with proton NMR, the area of the aromatic region (7-9 ppm) is greatly diminished relative to the aliphatic region (0.7-4.5 ppm) in the deuterated sample. This is because aromatic protons are more easily exchanged than aliphatic protons under the synthesis conditions utilized. Using data in Table 1, a calculation was made to estimate the extent of deuterium-for-hydrogen substitution required to produce the observed spectral difference between the deuterated and non-deuterated solvents. Assuming no exchange of deuterium for aliphatic protons, approximately 91% of the aromatic protons observed in the spectra of the original solvent would have to be replaced with deuterium to produce the observed spectra of the deuterated solvent. This value is in reasonable agreement with the 95% isotopic purity value calculated using GC/MS analysis.

STABILITY TESTING OF DEUTERIUM-LABELED A04

Following the synthesis of deuterium-labeled A04 it was necessary to determine the stability of the individual deuterated species in the solvent under liquefaction conditions. To do this, a reaction system was needed that simulated as closely as possible conditions that exist during liquefaction, without using coal. The absence of coal is required to ensure that possible degradation in the isotopic purity of a solvent-derived deuterated compound is not masked by the formation of the same compound from coal. In order to provide the system with the catalytic activity normally derived from the mineral content of coal, it was decided that the reaction mixture should contain tetrahydrofuran-insolubles (THFI) produced from an actual liquefaction reaction. To generate the THFI, an autoclave liquefaction reaction was run at 350°C and 1000 psia for 30 minutes using 383 grams Clovis Point Wyodak coal, 500 grams non-labeled A04, 36 psi H_2S, and 964 psi CO. (Based on moisture- and ash-content tests run prior to the autoclave reaction, 383 grams raw coal would provide 250 grams moisture- and ash-free (MAF) coal.) The product slurry contained 15.3% THFI, 19.4% of which was ash. The stability of deuterated A04 was tested by performing duplicate tubing bomb reactions using deuterated A04 (2.5 grams),

water, and THFI from the autoclave run. Water and THFI were added in quantities that would be supplied by a MAF coal charge of 1.25 grams. The amount of water added (Ø.36 grams) was calculated based on a moisture content of 2Ø.99 wt% raw coal, as determined immediately prior to the tubing bomb tests. The amount of THFI added (Ø.65 grams) was calculated based on the THF solubility of the product slurry resulting from the autoclave run. All other reaction conditions including H_2S and CO pressures, and reaction time and temperature were identical to the conditions of the autoclave run.

The most important result of the stability tests on deuterated AO4 is the finding that the deuterated species comprising approximately 95 wt% of the solvent underwent no significant degradation in isotopic purity. Figure 4 displays mass spectra (7Ø eV) of 4 major components of deuterated AO4 before and after exposure to liquefaction conditions. The fact that the before and after spectra are essentially identical will enable distinction to be made between coal-derived and solvent-derived species found in future liquefaction product slurries resulting from reactions with deuterated AO4 and coal. For example, the assumption can be made that any non-labeled dibenzofuran resulting from the liquefaction of coal using deuterated AO4, must be derived from the coal, since all solvent-derived dibenzofuran should remain deuterium-labeled throughout the reaction.

Several minor component species displaying various degrees of degradation in isotopic purity based on mass spectral data include phenol, two cresol isomers, quinoline, and carbazole. These compounds, while displaying molecular ions of smaller mass after stability testing than before, are still distinguishable from non-labeled isotopes. Figure 5 displays the mass spectra of deuterium-labeled phenol as it appears in deuterated AO4 prior to stability testing (top spectra), deuterium-labeled phenol as it appears in deuterated AO4 following stability testing (middle spectra), and non-labeled phenol as it appears in non-labeled AO4 (bottom spectra). Coal-derived phenol (molecular ion at 94) produced during future liquefaction tests in which deuterated AO4 is used, should be easily distinguishable from solvent-derived phenol (molecular ion at 96).

Another result of the stability testing of deuterated AO4 is the conversion of approximately 24 wt% of the THFI (which by definition is unconverted coal and ash) from one liquefaction reaction, to THF-soluble products through a second liquefaction reaction under nearly identical conditions. A partial explanation of this conversion may be the fact that the residence time for the THFI was double that of the raw coal. The 24 wt% conversion value was calculated based on the ash-free weight of THF-insolubles reacted.

LIQUEFACTION OF WYODAK COAL WITH DEUTERATED AO4

After demonstrating that deuterium-labeled AO4 is stable under the previously described liquefaction conditions, duplicate tubing bomb reactions were run using labeled AO4 with Wyodak (Clovis Point) coal. The feed slurry contained a 2/1 weight ratio of labeled AO4 to MAF coal. All reaction conditions were identical to those used in the previously described tubing bomb and autoclave reactions. Liquefaction conversion of the organic content of the coal was determined by THF solubility to be approximately 41 wt%.

The product slurries obtained were analyzed using GC/MS, and liquid proton NMR.

ANALYSIS OF PRODUCTS FROM COAL LIQUEFACTION WITH DEUTERATED AO4

All GC/MS analyses were performed using methylene chloride as the solvent. Comparison of the mass spectra of deuterated AO4 in product slurries from liquefaction runs made with and without coal, has indicated that the composition and isotopic purity of the deuterated solvent recovered from both reactions are essentially identical. In an effort to demonstrate the formation of coal-derived compounds, 8 compounds were selected for comparative quantitative analysis. The compounds chosen for study (phenol, 3 cresol isomers, tetralin, naphthalene, phenanthrene, and dibenzofuran) were selected primarily because they were present in detectable quantities in both the stability test and coal liquefaction product slurries. Since any coal-derived compounds would be non-labeled, to determine whether any of the 8 compounds were formed from coal, a method was needed to compare the quantity of each non-deuterated compound to the quantity of its deuterated counterpart in both product slurries. A mass spectral technique was employed which enables the relative quantitation of the amount of material having a specified molecular ion weight, using "area counts" as units of quantitation. For example, phenol has a molecular ion at 94 mass units, while deuterated (d_2-) phenol has a molecular ion at 96. The relative quantities (in area counts) of phenol and d_2-phenol can be obtained by integrating the area under each molecular ion peak. A ratio can then be calculated relating area counts of phenol to area counts of d_2-phenol. If this ratio is calculated for the phenol quantities in the product slurries from both the stability test reaction and the reaction with coal, it is possible to ascertain whether phenol was in fact produced from coal, simply by comparing the two ratios. Table 2 is a list of area counts for the 8 non-labeled and labeled compounds present in the product slurries from both reactions. Ratios of area counts non-labeled to labeled compounds are given in column E for both reactions. The fact that the ratio of area counts of non-labeled to labeled phenol produced from the reaction with coal is approximately 4 times greater than the same ratio for the reaction with THFI, is evidence for the presence of 4 times the quantity of non-labeled phenol in the coal reaction product slurry. Since conditions during the two reactions were identical, it is logical that the extra phenol came from the coal. There is also strong evidence pointing to low-temperature (350°C) production of cresol from the coal. Since the area counts are low for tetralin (see explanation at bottom of table) evidence suggests only the possibility of tetralin formation from the coal. Based on the ratios in column E, it appears that naphthalene, phenanthrene, and dibenzofuran are present in greater quantities in the THFI reaction products than in the coal reaction products. There are two explanations, both of which may be partially responsible for this result. The first centers on the longer residence time spent under liquefaction conditions by the THFI. Since the THFI were reacted twice as long as the coal, it is possible that species which take longer to form may be more concentrated in the product slurry of the longer reaction. The second explanation deals with adduction of AO4 solvent (non-labeled) to the solid THFI during the autoclave

reaction. When the A04-containing THFI were then subjected to liquefaction conditions a second time, A04 could have been released from the THFI and rendered soluble. The preparation of the THFI from the autoclave reaction involved their separation from THF-solubles through a vacuum filtration and extraction with THF. The insoluble fraction was then dried in an oven overnight at 120°C. The coarse powder remaining constituted the THFI which were then reacted a second time. In order to determine the contribution of solvent adduction to the presence of certain species in the THFI reaction, it may be necessary to use THFI which have been "cleaned", possibly through an extended Soxhlet extraction.

The product slurries from the reactions of THFI with deuterated A04, and coal with deuterated A04 were also compared using proton NMR. Figure 6 is the NMR spectrum of the deuterated methylene chloride solubles obtained from the reaction of deuterated A04 and THFI. (Since deuterium is not detected with proton NMR, reaction products were extracted with deuterated methylene chloride.) Figure 7 is the NMR spectrum of the deuterated methylene chloride solubles obtained from the reaction of deuterated A04 and coal. These spectra can be compared to the deuterated A04 spectrum in Figure 3b. The main peaks that stand out as unique are those associated with protons on bridge carbons found in fluorene at 3.9 ppm and acenaphthene at 3.4 ppm. The acenaphthene bridge protons make up 3.3% of the area in the spectrum of deuterated A04, 3.0% of the area in the spectrum of the THFI reaction products, and 7.1% of the area in the spectrum of the coal reaction products (see Table 1). Fluorene bridge protons make up 3.9, 12.8, and 9.8% of the three spectra areas, respectively. Protons (and deuterium atoms) in these bridge positions are labile. Higher percentages of hydrogen on bridge carbons in reaction products than in the deuterated solvent, could be due to hydrogen replacing bridge position deuterium during the reactions with THFI or coal. Sources of hydrogen could be non-substituted hydrogen from the solvent, hydrogen from the coal, or hydrogen from the hydrogen sulfide used in the reaction. According to GC/FID area percent data, acenaphthene comprises 3.6% and fluorene 3.5% of the total A04. According to GC/MS data, during the reaction with coal, approximately 75% of the acenaphthene and 90% of the fluorene bridge position deuterium was replaced with hydrogen. During the reaction with THFI, approximately 25% of the acenaphthene and 90% of the fluorene bridge position deuterium was replaced with hydrogen. This indicates that in the presence of coal, acenaphthene exchanges slightly less bridge deuterium than fluorene, and exchanges significantly less in the presence of THFI. Fluorene gives up its bridge deuterium with equal ease in the presence of THFI or coal. Based on this evidence it is likely that fluorene would be a more efficient hydrogen shuttler than acenaphthene.

THE FATE OF HETEROATOM-CONTAINING AROMATICS DURING LIQUEFACTION

Another aspect of this project involves monitoring the fate of heteroatom-containing species in coal under liquefaction conditions. A tubing bomb test was run with coal and non-labeled A04 which had been "spiked" with a set of 13 deuterated heteroatom-containing compounds and 3 deuterated aromatic hydrocarbons. All the heteroatom-containing organics used have been found in coal

liquefaction products, and many have also been identified as compounds emitted in substantial amounts during the pyrolysis of Wyodak coal (2). Analysis of the product slurry is currently in progress.

Deuterated compounds were synthesized using a reagent consisting of 4% deuterium chloride in deuterated water (deuterium oxide) with 10 mg/mL added chromium metal. The amount of reagent used in each reaction was calculated to give a reaction mixture containing a 20/1 molar ratio of deuterium to aromatic hydrogen. Syntheses were performed at 200 or 300°C for 2 or 15 hours as required to yield a product with both high isotopic and chemical purity (3,4). Table 3 is a list of the compounds along with their respective chemical and isotopic purities. Dihydrophenanthrene, dihydroanthracene, and hexahydropyrene are included in the table since these compounds served as hydrogen donors in another test involving the fate of hydrogen donors under liquefaction conditions. Most of the synthesized deuterated compounds had isotopic purities that approached 95% (as determined by 10 eV low-voltage EI mass spectrometry) which is the equilibrium value expected from using a reaction mixture containing a 20/1 molar ratio of deuterium to aromatic hydrogen. It is interesting to note that the hexahydropyrene showed 12 H/D exchanges even though only four aromatic hydrogens are present on the molecule. Proton NMR analysis of the deuterated product showed that the 8 aliphatic hydrogens bonded to the carbon atoms alpha to the aromatic rings were also replaced with deuterium during the synthesis. Aliphatic hydrogens were also replaced with deuterium during the synthesis of d_6-2-methylthiophene.

CONCLUSIONS

It has been demonstrated that deuterium-labeled A04 solvent undergoes no significant decrease in overall isotopic purity as a result of exposure to liquefaction conditions at 350°C and 1000 psia for 30 minutes. Although certain compounds such as phenol, cresols, acenaphthene, and fluorene undergo a reduction in isotopic purity under liquefaction conditions, the resulting mass spectra of the compounds are easily distinguishable from their non-deuterated counterparts. Despite a fairly low conversion, concrete evidence was found to substantiate the production of phenol and cresols during mild liquefaction of Wyodak coal. Production of tetralin was indicated but not substantiated by the data available. Analytical results from GC/MS and NMR were shown to correlate well.

REFERENCES

1. Hawthorne, S.B., D.J. Miller, T.R. Aulich, and S.A. Farnum. "A Simple Method for the Synthesis of Perdeuterated Aromatic Hydrocarbons and Heterocyclic Compounds," ACS Fuel Division Preprints, 32, 471, (1987)

2. Miller, D.J. and S.B. Hawthorne. "Pyrolysis GC/MS Analysis of Low-Rank Coal," ACS Fuel Division Preprints, 32, 10, (1987)

3. Werstiuk, N.H. and Kadai, T. Can. J. Chem., 52, 2169, (1974)

4. Werstiuk, N.H. and Timmins, G. Can. J. Chem., 51, 1485, (1981)

TABLE 1

PROTON NMR SUMMARY

Proton Type	ppm	Normalized Proton Distribution AO4	D-AO4	D-AO4 + IOM	D-AO4 + Wyodak
Aldehydic	10.0-9.0	0.3	0.1	0.0	0.1
Aromatic	9.0-5.9	73.4	18.6	29.2	24.1
Fluorenes	4.4-3.5	4.0	3.9	12.8	9.8
Acenaphthene Bridge H's	3.5-3.3	4.6	3.3	3.0	7.1
Alpha to Aromatic	3.3-1.9	11.7	29.4	23.1	25.0
Beta to Aromatic	1.9-1.5	0.4	11.4	8.1	5.0
Methylene	1.5-1.0	4.1	22.6	15.1	19.2
Methyl	1.0-0.0	1.5	10.7	8.6	9.7

TABLE 2

MASS SPECTRAL AREA COUNT DATA

A Compound	B Reaction	C Area Counts Non-labeled Compound	D Area Counts Labeled Compound	E Ratio C/D
Phenol	w/THFI	726	3959	0.24
Phenol	w/coal	3624	3863	0.94
m- & p-Cresol*	w/THFI	398	907	0.44
m- & p-Cresol*	w/coal	1146	1058	1.08
o-Cresol	w/THFI	124	399	0.31
o-Cresol	w/coal	265	387	0.68
Tetralin	w/THFI	19	80	0.24
Tetralin	w/coal	124	32	3.88
Naphthalene	w/THFI	460	47066	0.0098
Naphthalene	w/coal	59	38410	0.0015
Phenanthrene	w/THFI	2802	169659	0.017
Phenanthrene	w/coal	351	149507	0.0024
Dibenzofuran	w/THFI	722	60837	0.012
Dibenzofuran	w/coal	32	48272	0.0007

* m- and p-cresol elute as one species under the chromatographic conditions used.

Ratios in column E are area counts non-labeled aromatics to area counts labeled aromatics, in product slurries from liquefaction reactions with coal, and in product slurries from liquefaction reactions with THFI.

Area counts less than 100 are subject to substantial error and

should not be used as conclusive quantitative data. Low area counts are listed in this table solely to provide a potential indication of some of the detectable product quantities resulting from the two reactions.

TABLE 3

ISOTOPIC AND CHEMICAL PURITIES OF DEUTERATED COMPOUNDS

Compound	Isotopic Purity (%)	Chemical Purity (%)
d8-dihydrophenanthrene	96.6	81.5
d12-hexahydropyrene	97.0	86.3
d_7-dihydroanthracene	97.2	89.0
d10-phenanthrene	95.3	101.0
d10-pyrene	95.0	98.8
d10-biphenyl	94.9	98.5
d7-naphthol	89.7	97.7
d5-phenol	96.0	95.9
d4-o-cresol	91.0	97.5
d3-3-ethyl-5-methylphenol	94.1	96.1
d4-4n-propylphenol	96.5	53.1
d3-3-methylcatechol	97.0	91.4
d8-dibenzofuran	95.4	100.0
d9-phenanthridine	79.5	100.0
d7-quinoline	64.7	102.0
d_5-pyridine	99.0	100.0
d8-carbazole	94.7	105.0
d8-dibenzothiophene	95.3	100.0
d6-2-methylthiophene	94.8	82.3

Chemical purity values are + or - 5%.

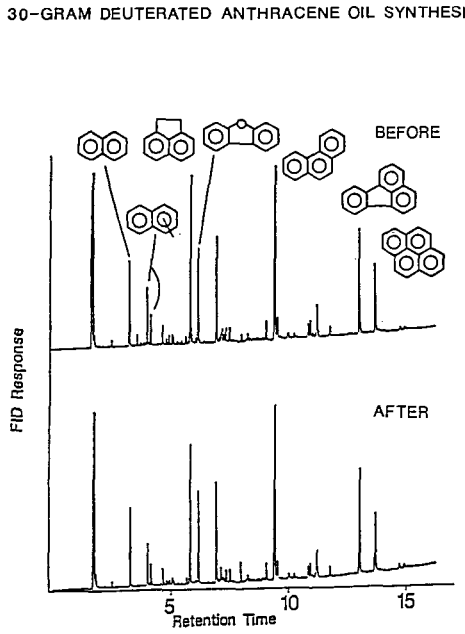

Figure 1. Gas chromatogram of AO4 before (top) and after (bottom) deuteration.

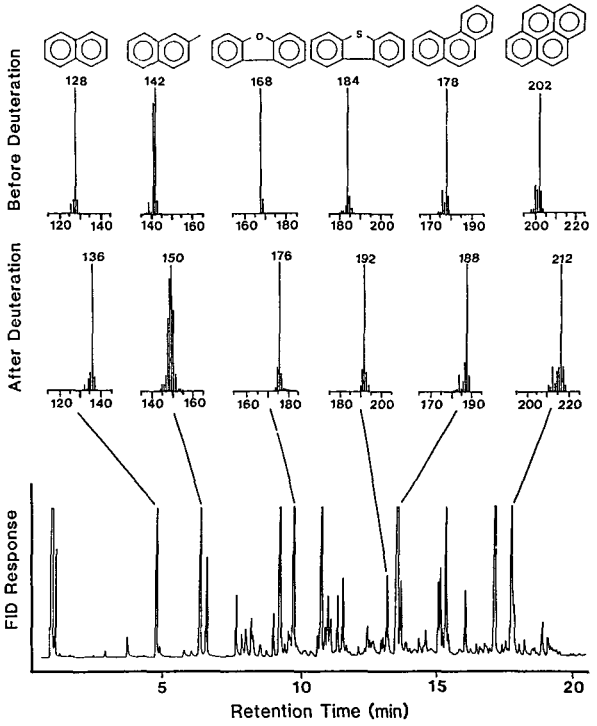

Figure 2. Mass spectra of components of AO4 before (top) and after (bottom) deuteration.

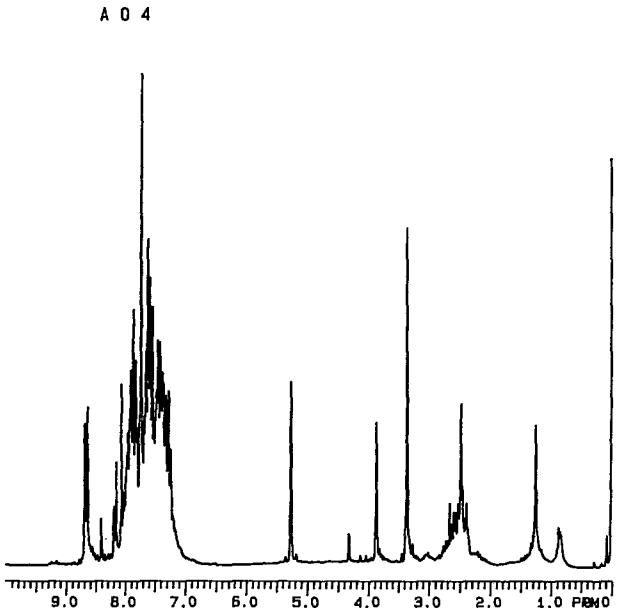

Figure 3a. Proton NMR spectrum of non-deuterated A04.

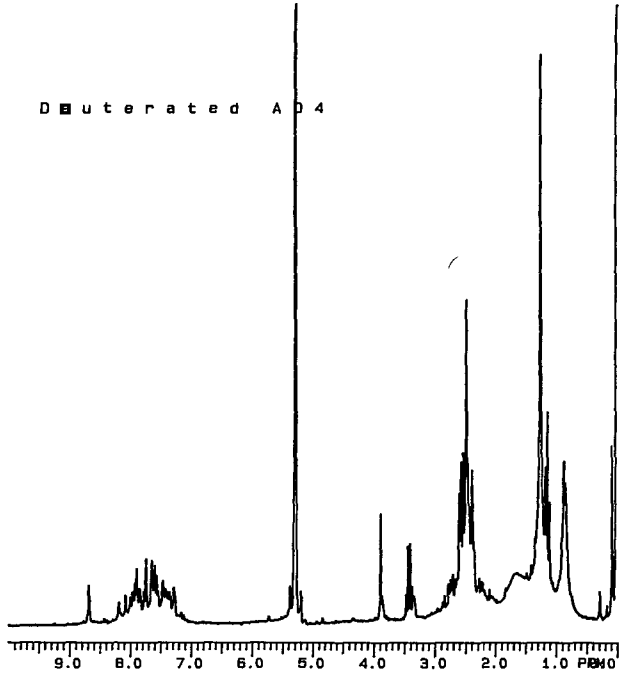

Figure 3b. Proton NMR spectrum of deuterated A04.

Before (left) and after (right) liquefaction.

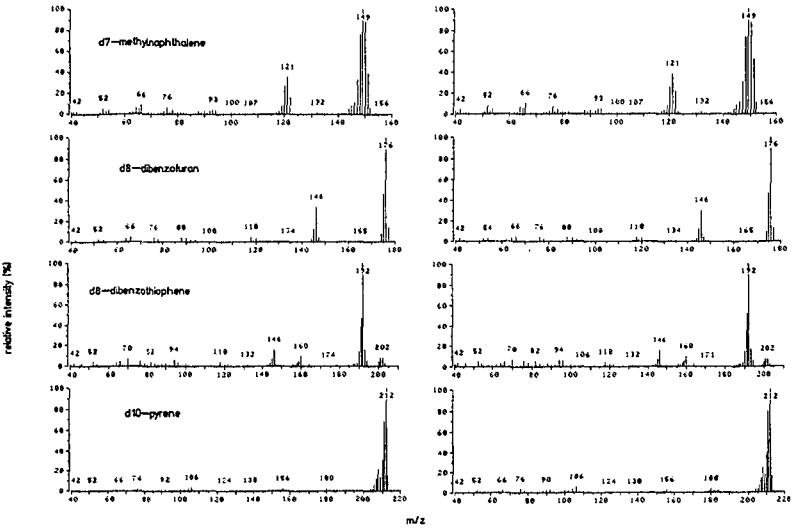

Figure 4. Mass spectra of 4 components of deuterated AO4 before (left) and after (right) exposure to liquefaction conditions with THFI, H_2S, CO, and water.

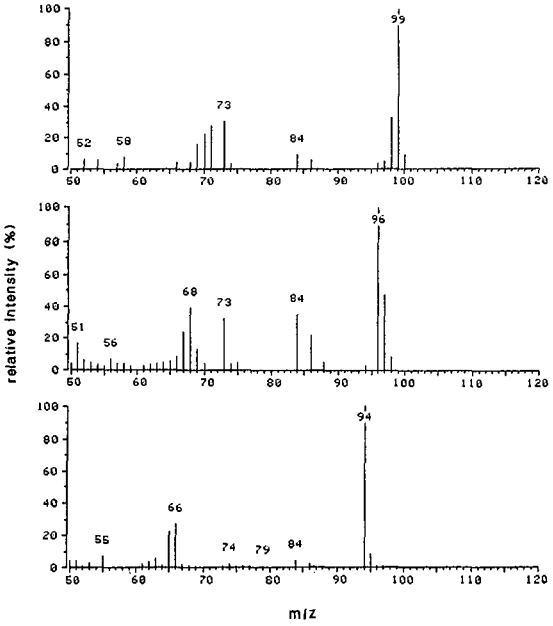

Figure 5. Mass spectra of d_5-phenol as it appears in deuterated AO4 prior to stability testing (top spectra), d_2-phenol as it appears following stability testing (middle spectra), and phenol as it appears in non-deuterated AO4 (bottom spectra).

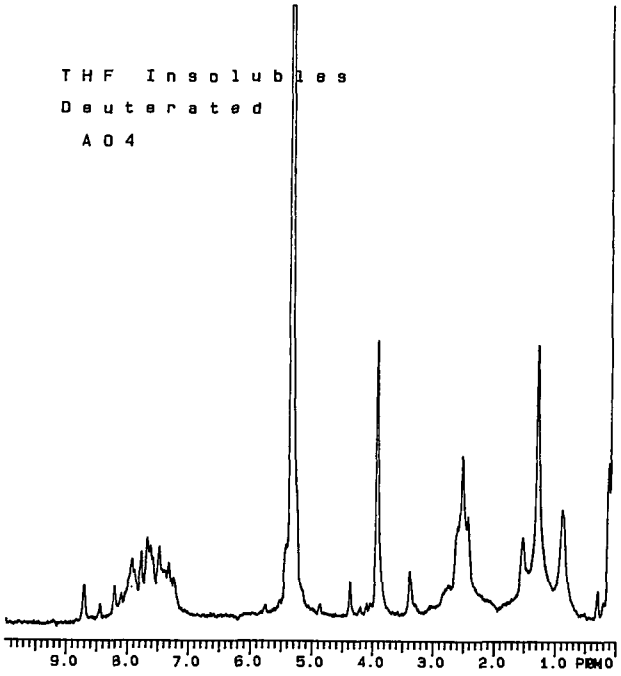

Figure 6. Proton NMR spectrum of methylene chloride solubles obtained from the reaction of deuterated AO4 and THF-insolubles.

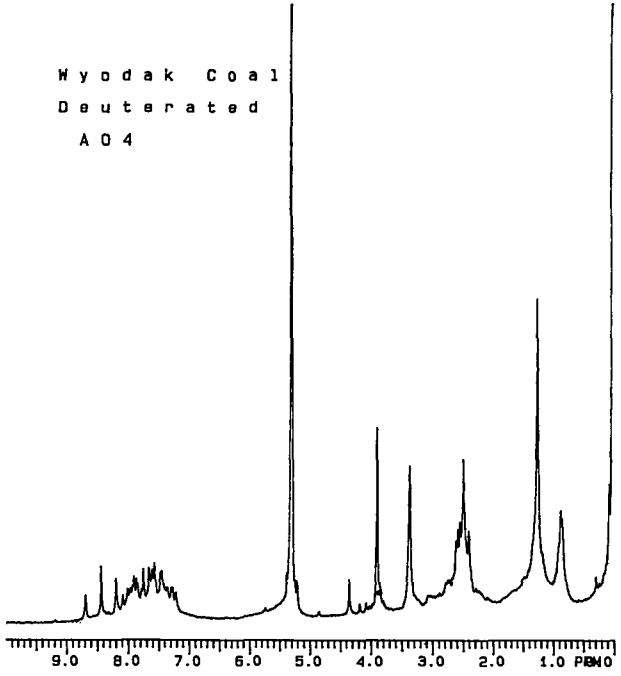

Figure 7. Proton NMR spectrum of methylene chloride solubles obtained from the reaction of deuterated AO4 and Wyodak coal.

Nitrogen Bases and Carbon Deposits on Coal Liquefaction Catalysts

Diane R. Milburn, Bruce D. Adkins, and Burtron H. Davis

Kentucky Energy Cabinet Laboratory
P.O.Box 13015, Lexington, KY 40512-3015

Introduction

The respective roles of coke and alkali as poisons of coal liquefaction catalyst activity have attracted the interest of numerous researchers in the past decade (1-17). It is believed that coke formation occurs on catalyst acid sites and that the basicity of coke precursors is an important factor in determining the propensity for coke formation. It is also well-known that alkali metals, especially sodium, can poison acid sites. The coal liquefaction catalyst environment often contains basic compounds (nitrogen bases) and alkali metals (in the coal ash).

Recently, we have correlated elemental analysis data obtained for catalyst samples from the Wilsonville, Alabama coal liquefaction pilot plant. We were surprised to find that a simple mechanistic model involving (a) nitrogen bases chemisorbed on acid sites, and (b) poisoning of acid sites by sodium, can explain virtually all of the interesting coke-formation trends seen in the Wilsonville process since the inception of the two-stage liquefaction (TSL) process mode. The purpose of this paper is to describe this model.

Experimental

Catalyst samples used in this work were from the Wilsonville runs summarized in Table 1. Two catalysts are represented: Shell 324M $NiMo/Al_2O_3$ and Amocat 1C $NiMo/Al_2O_3$. Two coals are represented: Wyodak sub-bituminous and Illinois #6 bituminous. Four basic processing configurations are shown: Integrated Two-Stage Liquefaction (ITSL), Doubly Integrated Two-Stage Liquefaction (DITSL), Reconfigured Integrated Two-Stage Liquefaction (RITSL) and Close-Coupled Integrated Two-Stage Liquefaction (CCITSL). A more detailed description of these runs and process configurations can be found in reference (18) and in the Wilsonville run reports (19).

The important hydrotreater feedstream components in the model are represented by the three product streams from the critical solvent deashing unit, (CSD). The first, called the ash concentrate stream, contains coal ash and "resid" (defined as a vacuum non-distillate at 650 F and 0.1 mm Hg). The second, called the "thermal resid" (TR) stream, typically consists of resid and less than 10% distillate solvent; the third, called the "light thermal resid" (LTR) stream, typically consists of resid and 20-30% distillate solvent. Because of chemical and/or physical fractionation in the CSD unit, the resids in these streams are different: in terms of average molecular weight, one could expect "ash concentrate resid" > "TR resid" > "LTR resid". The streams also differ in resid concentration. For a given resid input to the CSD, the "TR resid" and "LTR resid" typically constitute about 40-50% each of the total, while the "ash concentrate resid" is usually less than 10% of the total. Thus the model does not

include a separate provision for "ash concentrate resid", but does provide for effects associated with the presence or absence of "TR resid", "LTR resid", and the coal ash in the ash concentrate stream.

Catalyst samples in process solvent were shipped from the Wilsonville pilot plant to our laboratory. THF-soluble material was removed from the catalysts using a Soxhlet extraction apparatus. Residual THF was desorbed in a vacuum oven overnight at ca. 120 C. Details of the elemental analyses can be found in reference (20). The total weight of deposited contaminants (C, H, N, Fe, Ti, Na and traces of Ca, V, K) was between 10 and 15% in all cases. Data are uncorrected for differences in weight basis.

Results and Discussion

Proposed Model

The following model, utilizing reactions involving basic nitrogen compounds, sodium, and acid sites, fits virtually all of the Wilsonville catalyst coking trends for runs 246 through 250:

$$CH + LTR \underset{k_{d,LTR}}{\overset{k_{a,LTR}}{\rightleftharpoons}} C^{-}(LTRH)^{+} \qquad (1$$

$$CH + TR \underset{k_{d,TR}}{\overset{k_{a,TR}}{\rightleftharpoons}} C^{-}(TRH)^{+} \qquad (2$$

$$CH + ANa \underset{k_{d,Na}}{\overset{k_{a,Na}}{\rightleftharpoons}} CNa + AH \qquad (3$$

$$BH + ANa \underset{k'_{d,Na}}{\overset{k'_{a,Na}}{\rightleftharpoons}} BNA + AH \qquad (4$$

where LTR represents nitrogen bases correlated with light thermal resid (or with distillate solvent), and TR represents nitrogen bases which correlate with thermal resid. CH represents an acid site that may react with either basic nitrogen or sodium, while BH represents a site that reacts with sodium alone. ANa represents sodium that is present in some ionic form in coal ash. $C^{-}(LTRH)^{+}$ and $C^{-}(TRH)^{+}$ represent the acid-base adducts, which are designated chemisorbed bases, and CNa and BNA represent the Na-exchanged acid sites, which are designated chemisorbed Na. Simplifying assumptions are that, on the average, base molecules contain only one nitrogen atom, and that saturation corresponds to one nitrogen atom per acid site. It is also assumed that CNa and BNA are not reactive towards nitrogen bases. In this model, the chemisorbed bases contain as much as 100% of the carbon on the catalyst at any time. The remainder of the carbon, if present, is assumed to be present as an essentially constant amount of non-nitrogen-containing process-derived coke.

The model, as written, is for Brönsted acid sites. However it can be written for combined Bronsted and Lewis acidity, or only Lewis acidity, with no loss of applicability. Of course, the

protonated nitrogen base must be held to the surface for Brönsted acidity to lead to carbon deposition by this model. Also, at this stage of development the model neglects condensation and/or hydrodenitrogenation (HDN) reactions of the chemisorbed nitrogen bases, since desorption of these bases is a key feature. The true coke formation mechanism is almost certainly more complicated than the model presented here.

Catalyst Characterization

Wyodak Coal, Shell 324M Catalyst. Figure 1 shows the %C, %N and %Na determinations for Shell 324M catalyst in Wilsonville runs using a Wyodak sub-bituminous coal. The series shown (246-DITSL, 246-ITSL and 249-RITSL) is especially interesting because a single catalyst charge was used for all three runs. The entire catalyst lifetime is thus depicted from left to right in Figure 1.

DITSL operation (LTR, no TR or ash) is characterized by essentially constant C and N levels during the operating period, and no Na accumulation. This represents a rapid saturation of acid sites by LTR-bases; the N level at saturation for this catalyst is about 0.7%.

On switching to the ITSL mode (LTR and TR, no ash) C increases, N remains constant, and Na does not accumulate. In our model, this corresponds to a gradual exchange of LTR-bases with TR-bases. Assuming that a pseudo-saturated surface exists during the exchange period, this requires that TR bases have a higher average molecular weight than the LTR bases. This is certainly consistent with the resids contained in the LTR and TR streams. Stohl and Stephens (8) published C analyses for the last month of 246-ITSL which clearly show the establishment of a new saturation level at ca. 10% C. This level, sketched in Figure 1, is consistent with the carbon level at the start of the 249-RITSL run period.

Finally, in the RITSL period, C and N decrease while Na increases. In fact, N decreases to essentially zero while at the same time Na shows evidence of reaching a saturation level. In our model this is due to a gradual exchange of nitrogen poisoned acid sites with Na-poisoned sites. It is clear that coal ash is the source of Na deposited on the catalyst.

Illinois #6 Coal, Shell 324M Catalyst. Figure 2 shows the characterization data for Shell 324M catalysts when Illinois #6 bituminous coal was used. Runs 248-DITSL and 248-ITSL represent a single batch of catalyst subjected to first DITSL, then ITSL, processing, but Run 247-RITSL was conducted with a separate catalyst batch. In this respect the data obtained with Illinois #6 coal feed are different than the Wyodak data in Figure 1.

DITSL data for Illinois #6 coal are virtually identical to that for Wyodak coal with a saturation level of ca. 0.7% N and 8% C. On switching to the ITSL mode, the C level increases with no change in N or Na, again consistent with an exchange of LTR-base with TR-base at pseudosaturated conditions. It is, as before, not clear if the exchange with TR-base has gone to completion at the end of Run 248-ITSL. However, it is obvious that the TR-bases derived fron the Illinois #6 coal have a higher C/N ratio than TR-bases from the Wyodak coal because the C levels in 248-ITSL are higher than in 246-ITSL. Assuming an average of one N atom per base molecule, the average molecular weight of the Illinois #6 TR-

bases is 50% to 100% greater than that of the Wyodak TR-bases.

Run 247-RITSL data again show C and N decreasing as Na increases. In comparison to the Wyodak coal (Run 249-RITSL) data, more C is desorbed per desorbed N, again indicating Illinois #6 TR-bases have a higher average molecular weight than Wyodak TR-bases. Also, in comparison to Run 249, the N and Na levels at the end of Run 247 indicate that poisoning of acid sites had not reached completion when run 247 was terminated.

Since this RITSL catalyst was not previously subjected to the DITSL-ITSL exchange, the initial levels of C and N must correspond to a rapid saturation at startup; however, this saturation was not with LTR-bases, as occurs in DITSL mode. Instead, saturation occurs with the higher average molecular weight TR-bases. In contrast to organic base exchange, which is probably desorption-limited, adsorption on unsaturated sites should be rapid at process temperatures, and the rapid saturation with N indicates this to be the case. Stohl and Stephens (5) have shown that the presulfided Shell 324M catalyst will chemisorb N from a nitrogen-containing polycyclic aromatic coal liquid fraction rapidly enough to achieve saturation, reported by them to be 0.6% N, in two hours at 300 C. The initial C level in Run 247 shows reasonable agreement with the levels reached in 248-ITSL; this suggests the exchange of LTR and TR bases was near completion at the end of 248-ITSL.

Illinois #6 Coal, Amocat 1C Catalyst. The two periods of Run 250-CCITSL shown in Figure 3 used Illinois #6 coal and Amocat 1C $NiMo/Al_2O_3$ catalyst. These two periods are 250-CCITSL-NAR (no ash recycle) and 250-CCITSL-AR (ash recycle). They represent two separate batches of the Amocat 1C catalyst. Both batches indicate rapid initial saturation at ca. 12% C and 0.5% N, followed by a decrease in C and N levels and corresponding Na increase. The data taken in the ash-recycle period shows a more rapid increase in Na, and concurrent decrease in C, than the data for the no-ash-recycle period. This is most easily explained as a Na concentration effect, with the Na deposition rate increasing with sodium concentration in the reactor. The larger relative error in N determination makes the N trends less definite.

Elemental Correlations. Figure 4 shows plots of N versus C, normalized to moles per g catalyst, for all samples used in this study. Two distinct data clusters are immediately obvious: DITSL-ITSL data and RITSL-CCITSL data. All of the DITSL-ITSL data show essentially constant N content while for RITSL-CCITSL samples a direct relationship between C and N exists. The slope of the C-N data suggests stoichiometries for the desorbing bases. Trends show that the desorbing material is mainly coal-dependent: it has an average stoichiometry of about $C_{14}N$ for Wyodak sub-bituminous coal, and about $C_{24}N$ for Illinois #6 bituminous. These calculations are subject to the assumption that all of the net carbon loss is due to desorption of nitrogen bases. Also, the trends in the Amocat data are less well defined simply because the N-Na exchange is slower on this catalyst. Assuming that the initial coverage in all RITSL and CCITSL runs is essentially all TR base, then these average stoichiometries can be assigned to the TR bases.

Average stoichiometries for the bases chemisorbed on the catalyst when LTR and distillate derived from from the Wyodak or Illinois #6 coals can be calculated from 246-ITSL and 248-ITSL

data; in the model this represents exchanges from essentially 100% LTR coverage to 100% TR coverage. Assuming the LTR- and TR-saturation points indicated by the surrounding DITSL and RITSL data in Figures 1 and 2, and using the $C_{14}N$ and $C_{22}N$ stoichiometries calculated for the appropriate TR-bases, we next calculate an average stoichiometry for LTR bases derived from both coals of about C_8N, with no strong dependence on coal type. This number is less certain than the TR-base calculations as both TR-base numbers and the absolute %C numbers were required. Nevertheless, the numbers summarized in Table 3 represent our best estimate of the average stoichiometries of the nitrogen bases required to fit the characterization data to our model.

Figure 5 shows N plotted against Na, both in moles per g catalyst, for the RITSL and CCITSL data (DITSL and ITSL data show no Na uptake). The correlation here is good: all of the Shell 324M data fall on one line, and all of the Amocat 1C data falls on another. This relationship should reflect characteristics of the acid site populations of the two catalysts. For Shell 324M catalyst, three Na atoms are chemisorbed for each N atom desorbed; for Amocat 1C, two Na atoms are chemisorbed for each N atom desorbed. Assuming one N atom (or one Na atom) per CH site, and one Na atom per BH site, and assuming that all CH sites can react with Na (strongly suggested by the desorption of essentially all N in Run 249, for Shell 324 catalyst, but not strongly indicated for Amocat 1C, for which complete desorption of N was not seen) then two BH sites exist for every CH site on the Shell 324M catalyst, and one BH site for every CH site on the Amocat catalyst.

Laboratory Desorption of LTR-Bases

A key point in this model is the desorption of basic nitrogen compounds under coal liquefaction conditions. A laboratory experiment was performed recently in a 300 mL CSTR to duplicate the desorption of these bases indicated by the pilot plant data. A 100 g blend of various Wilsonville DITSL catalysts, still in the oil in which they were shipped, was placed in the reactor. THF was flowed over the catalyst bed at ca. 120 C until the oil was removed. This took approximately one week. Analysis of the catalyst at this point indicated about 0.45% N, which is somewhat lower than the saturation coverage of 0.7% N seen in the Wilsonville catalysts after THF Soxhlet extraction. As a separate check, a Wilsonville DITSL catalyst was Soxhlet extracted for almost 1000 hours and the %N level was found to remain constant. Temperature measurements indicated Soxhlet extraction occurs at about 65 C. It is possible that the CSTR extraction at 120 C causes bases to desorb that do not desorb in the Soxhlet apparatus.

After THF extraction in the CSTR, the feed was switched to tetralin at about 6 ml/hr and the temperature was increased to 350 C. H_2 was supplied only in makeup amounts, i.e. to enough to keep reactor pressure at about 2000 psi. The catalyst bed was gently stirred during the experiment. The reactor was cooled, and samples taken, twice weekly for the next month.

Results are shown in Figure 6. A significant loss of N, from 0.45% to a relatively stable 0.15% did occur during the run (figure 6b). The average stoichiometry calculated for the desorbing compounds (figure 6c), was $C_{30}N$, which is closer to TR-

base stoichiometry (estimated from process exchange) than the LTR-base stoichiometry. One possible explanation for the discrepancy could be the formation of non-nitrogen-containing coke on acid sites concurrent with nitrogen base exchange. Evidence for this was seen near the end of the CSTR experiment (figure 6a). Since only %C was used to estimate the LTR-base stoichiometry from the DITSL-ITSL exchanges, the C_8N figure could be low for this reason. Also, accumulation and loss of bases may be complicated than a simple adsorption/desorption process. A kinetic analysis of the nitrogen content based on a first-order desorption mechanism is shown in Figure 6d. The rate constant for desorption of N in this experiment, $k_{d,TR}$, is 0.04 day^{-1}, which is within a factor of four of rate constants calculated from the data for the spent catalysts from the Wilsonville runs. Thus the CSTR experiment is in qualitative agreement with the kinetic analysis of the spent Wilsonville catalyst data. Most importantly, the lab experiment confirms the reversibility of the N contained in the organic residue on the catalyst.

Conclusion

In this model, acid sites on the sulfided catalyst rapidly saturate with basic nitrogen compounds on start-up. These bases (called LTR-bases) are either in the LTR material, or in the distillate solvent. In turn these bases gradually exchange with nitrogen bases having a higher average molecular weight when the TR stream is introduced to the feed. This correlation does not necessarily imply any chemical difference in the two resids (LTR and TR), but may simply reflect an increase in the relative concentrations of distillate solvent and resid. On introduction of coal ash, the nitrogen-containing compounds desorb, and sodium is adsorbed on the catalyst. Coal dependence is seen in the TR-bases, with the Illinois #6 coal producing a higher average molecular weight deposit than the Wyodak coal; this is not seen for LTR-bases. Sodium adsorption demonstrates a catalyst dependence, indicating differences in acid site populations for the two Shell and Amocat catalysts.

Reversibility of the chemisorption of nitrogen bases has been demonstrated in our laboratory. Future experiments will concentrate on other key features of the model, such as base exchange and sodium poisoning.

Acknowledgement

This work was performed at the Kentucky Energy Cabinet Laboratory (KECL). The KECL is operated by the University of Louisville for the Kentucky Energy Cabinet.

Table 1.

Summary of Wilsonville Runs Correlated in This Work

Run	Coal	Configuration	Catalyst	Comments
246A	Wyodak	DITSL	Shell 324M NiMo	
246B	Wyodak	ITSL	Shell 324M NiMo	Started with catalyst from end of 246A
247	Illinois #6	RITSL	Shell 324M NiMo	
248A	Illinois #6	DITSL	Shell 324M NiMo	
248B	Illinois #6	ITSL	Shell 324M NiMo	
249	Wyodak	RITSL	Shell 324M NiMo	Started with catalyst from end of 246B
250-II	Illinois #6	CCITSL	Amocat^{R} 1C NiMo	No ash recycle
250-III	Illinois #6	CCITSL	Amocat^{R} 1C NiMo	With ash recycle

Table 2.

Hydrotreater Feed

	TR Present?	LTR Present?	Coal Ash Present?
DITSL	No	Yes	No
ITSL	Yes	Yes	No
RITSL	Yes	Yes	Yes
CCITSL	Yes	Yes	Yes

Table 3.

Best Estimate of Average Nitrogen Base Stoichiometry Required to Fit Our Model to Wilsonville Catalyst Data

Coal	LTR-Bases	TR-Bases
Wyodak Sub-bituminous	C_8N	$C_{14}N$
Illinois #6 Bituminous	C_8N	$C_{22}N$
CSTR Laboratory Study	$C_{30}N$	

Figure Captions

Figure 1. Elemental analyses for Shell 324M catalyst and Wyodak sub-bituminous coal.

Figure 2. Elemental analyses for Shell 324M catalyst and Illinois bituminous coal.

Figure 3. Elemental analyses for Amocat 1C catalyst and Illinois bituminous coal.

Figure 4. C-N trends for all data.

Figure 5. N-Na correlations for all data.

Figure 6. Desorption of LTR-bases from Run 248 DITSL catalysts in CSTR at 350"c.

References

1. P. Holloway, Sandia National Labs Report SAND78-0056 (1978).

2. A. Ocampo, J.T. Schrodt and S.M. Kovach, Ind. Eng. Chem. Prod. Res. Dev. 17 (1), 56 (1978).

3. T.L. Cable, F.E. Massoth and M.G. Thomas, Fuel Proc. Tech. 4, 265 (1981).

4. D.S. Thakur and M.G. Thomas, Ind. Eng. Prod. Res. Dev. 23, 349 (1984).

5. F.V. Stohl and H.P. Stephens, ACS Div. Fuel Chem. Prepr. 31, 251 (1986).

6. F.V. Stohl, ACS Div. Fuel Chem. Prepr. 33, 325 (1987).

7. F.V. Stohl, Q.A. Qader, F.E. Massoth and D.S. Thakur, Ind. Eng. Chem. Res. 26, 840 (1987).

8. F.V. Stohl and H.P. Stephens, Ind. Eng. Chem. Res. 26, 2466 (1987).

9. I. Mochida, K. Sakanishi, Y. Korai and H. Fujitsu, Fuel 65, 1090 (1986).

10. Y. Yoshimura, T. Sato, H. Shimada and A. Nishijima, Fuel Sci. Tech. Int'l. 4, 621 (1985).

11. Y. Yoshimura, H. Shimada, T. Sato, M. Kubota and A. Nishijima, Appl. Catal. 29, 125 (1987).

12. Y. Yoshimura, K. Hayamizu, T. Sato, H. Shimada and A. Nishijima, Fuel Proc. Techm 16, 55 (1987).

13. A. Nishijima, H. Shimada, Y. Yoshimura, T. Sato and N. Matsubayashi, Catalyst Deactivation 1987, B. Delmon and G. Froment, Eds., Amsterdam, p. 39 (1987).

14. E. Furimsky, Erdol und Kohle 35, 455 (1982).

15. S.M. Kovach, L.J. Castle, J.V. Bennett and J.T. Schrodt, Ind. Eng. Chem. Prod. Res. Dev. 17 (1), 62 (1978).

16. D. Garg and E.N. Givens, Fuel Proc. Tech. 9, 29 (1984).

17. J. R. Baker, R.L. McCormick and H.W. Haynes, Jr., Ind. Eng. Chem. Res. 26, 1895 (1987).

18. B.D. Adkins, S.R. Adkins, B.H. Davis and D.R. Milburn, in Catalyst Deactivation 1987, p. 469, B. Delmon and G. Froment, Eds., Elsevier, Amsterdam 1987.

19. Catalytic, Inc. "Run 250 with Illinois #6 Coal", Technical Progress Report DOE/PC/50041-81; "Run 249 with Wyodak Coal", Technical Progress Report DOE/PC/50041-75; "Run 248 with Illinois #6 Coal", Technical Report DOE/PC/50041-71; "Run 247 with Illinois #6 Coal", Technical Report DOE/PC/50041-67; "Run 246 with Wyodak Coal", Technical Report DOE/PC/50041-61.

20. B.D. Adkins, K. Cisler and B.H. Davis, Appl. Catal. 23, 111 (1986).

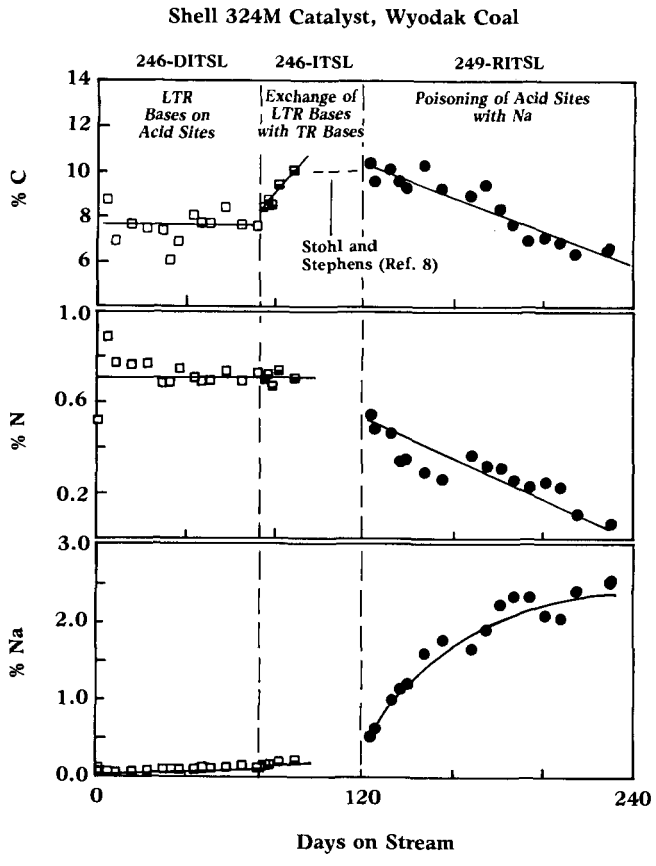
Shell 324M Catalyst, Wyodak Coal
246-DITSL
246-ITSL
249-RITSL
LTR Bases on Acid Sites
Exchange of LTR Bases with TR Bases
Poisoning of Acid Sites with Na
Stohl and Stephens (Ref. 8)
% C
% N
% Na
14
12
10
8
6
1.0
0.6
0.2
3.0
2.0
1.0
0.0
0
120
240
Days on Stream

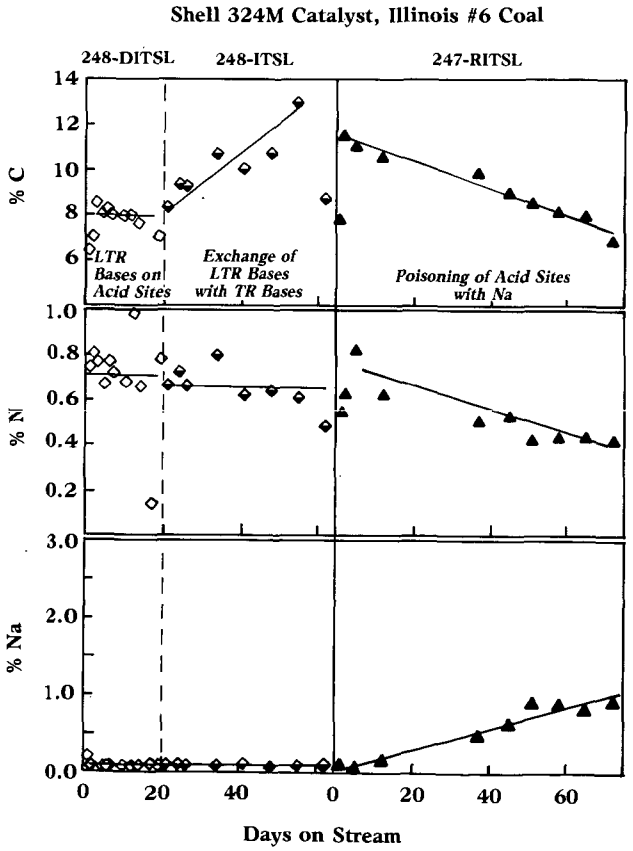
Shell 324M Catalyst, Illinois #6 Coal
248-DITSL
248-ITSL
247-RITSL
% C
% N
% Na
LTR Bases on Acid Sites
Exchange of LTR Bases with TR Bases
Poisoning of Acid Sites with Na
Days on Stream

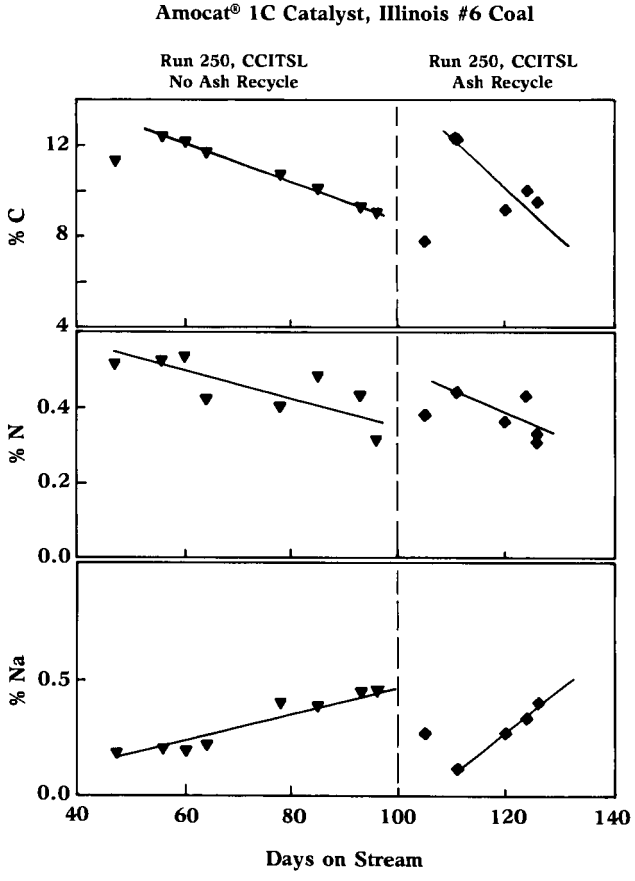
Amocat® 1C Catalyst, Illinois #6 Coal
Run 250, CCITSL
No Ash Recycle
Run 250, CCITSL
Ash Recycle
% C
12
8
4
% N
0.4
0.2
0.0
% Na
0.5
0.0
40
60
80
100
120
140
Days on Stream

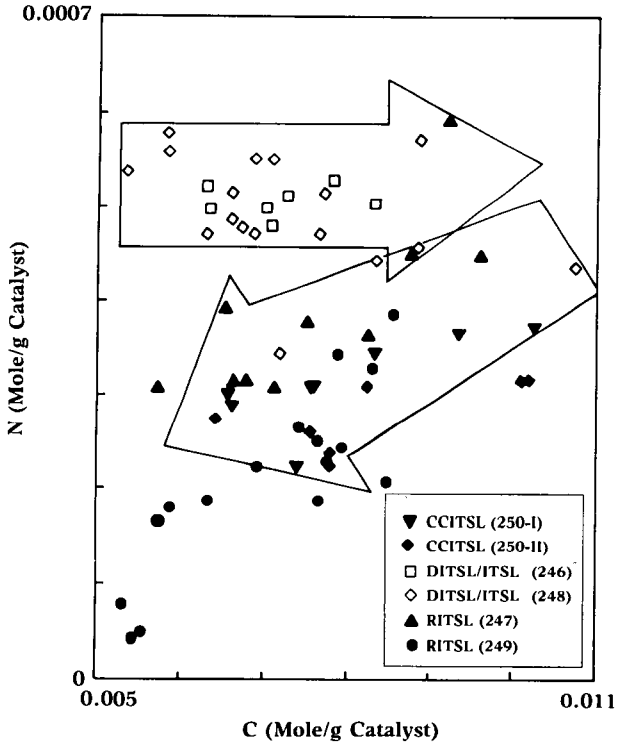
0.0007
N (Mole/g Catalyst)
0
0.005
0.011
C (Mole/g Catalyst)
CCITSL (250-I)
CCITSL (250-II)
DITSL/ITSL (246)
DITSL/ITSL (248)
RITSL (247)
RITSL (249)

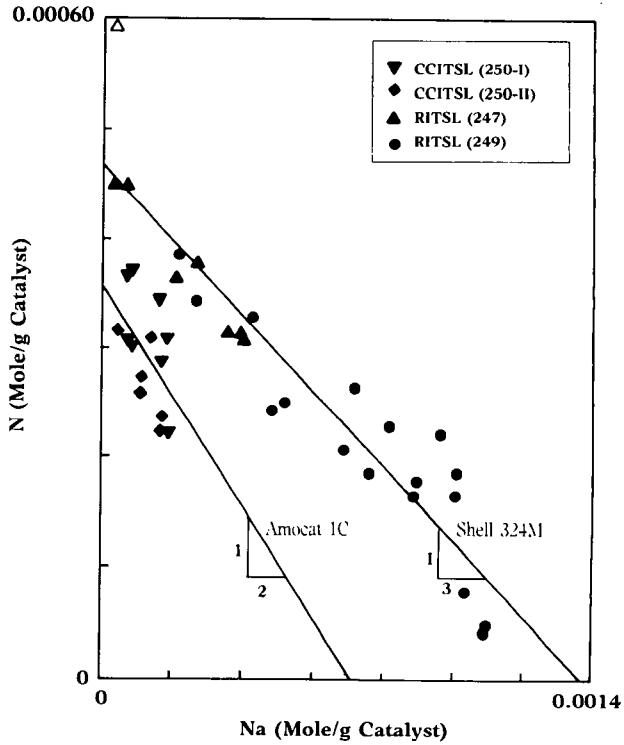
0.00060
N (Mole/g Catalyst)
0
0
0.0014
Na (Mole/g Catalyst)
CCITSL (250-I)
CCITSL (250-II)
RITSL (247)
RITSL (249)
Amocat 1C
1
2
Shell 324M
1
3

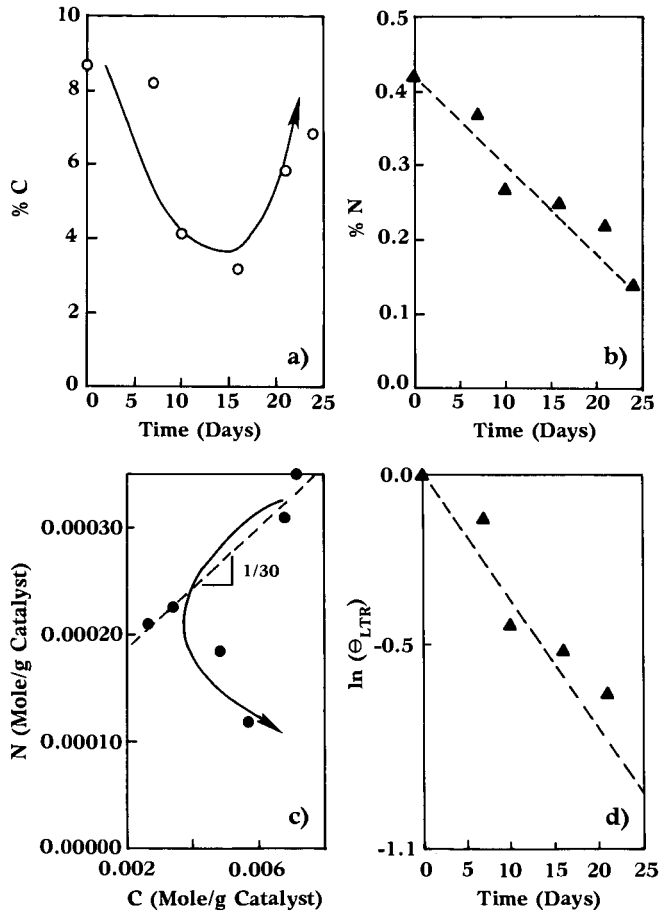
% C
Time (Days)
a)
% N
Time (Days)
b)
N (Mole/g Catalyst)
C (Mole/g Catalyst)
1/30
c)
ln (Θ_{LTR})
Time (Days)
d)

ANOMALOUSLY HIGH FLAMMABILITY OF LOW VOLATILITY FUELS DUE TO ANOMALOUSLY LOW IGNITION TEMPERATURES.

Joseph L. Walker, William W. Bannister,
CAPT Edward T. Morehouse, USAF, and Robert E. Tapscott

Fire Technology Branch, AFESC, Tyndall AFB, FL 32403

Fuel flammability is usually predicated on flash points, resulting from exposure of fuel to flame. Low molecular weight (high volatility) fuels have lower flash points and thus are judged more flammable than low volatility fuels. A startling reversed relationship has been shown to exist, however, for lower members of the alkane series, between molecular weight and ignition temperature (IT), occasioned by contact with hot surfaces: up to a point, less volatile higher molecular weight fuels have lower IT's and are more easily ignited when exposed to hot surfaces. For higher members of the alkane family this trend reverses, resulting in minimum IT's for the C_5 - C_9 alkanes. Branched chain alkanes, arenes and olefins also have anomalously high IT's. Free radical effects are unimportant among factors influencing ignition temperature; ionic effects may be important, as is the case for fires involving active metal, phosphorus, thermite and similar inorganic incendiary agents. This may be useful in fuel selection, if fires are anticipated to result from contact with hot metal surfaces, as in aircraft crashes, fuel spills on hot engine surfaces, or similar effects, instead of by contact with flame. Molecular modelling considerations will be discussed to explain the anomalous trends.

I. Ignition Temperatures (IT).

Ignition temperature is a poorly understood fuel characteristic which has received little previous attention. This is despite the fact that ignition temperature may arguably be the single most important fuel characteristic in terms of catastrophic ignition by gunfire, aircraft crashes, fuel spills on hot engine surfaces, and other instances of obvious military (and commercial) aviation interest. From the standpoint of fire prevention, and in particular design of practical jet fuels capable of resisting ignition from such effects while fulfilling normal operational combustion performance requirements, it is suggested that IT's should be given an in depth examination.

Fuel ignition can be initiated by either of two effects: contact of the fuel with a flame, or with a hot surface. For ignition by flame contact, the important fuel characteristic is the flash point (FP); for ignition from a hot surface, ignition temperature is important.

Flash points are routinely measured by heating a sample of the liquid in either a closed or open cup assembly, with a small flame continually passed over the surface of the liquid. The flash point is the lowest temperature at which the fuel vapors ignite with propagation of the flame beyond the source of ignition. Since it is principally a measure of fuel volatility, flash point is most associated with the molecular weight of the fuel component within a given chemical family.

IT measurements are not as precise. Typically, fuel is directed onto a hot surface at a given temperature, and allowed to heat for up to ten minutes. (1) The IT is the lowest temperature at which a flame occurs (in some cases, exothermic decompositions not necessarily accompanied by a flame). Often the flammable liquid will decompose to other

materials during the heating period. Thus, ignition temperature may not really be a characteristic of the original material, but rather of its decomposition products. In addition to rate and duration of heating, other variables also affect IT measurements: shape and size of the test chamber, air concentration, nature of the heated surface (including catalytic effects), and temperature of the surface. Therefore, IT measurements are frequently only poorly reproducible: ignition temperature data for a compound, taken by different individuals, can have very greatly differing values. (2)

II. Free Radical Fire Effects, and the Fire Tetrahedron. (3)

Until twenty years ago, there were three important requirements known for a fire -- fuel, oxygen, and heat. These were commonly considered as components of the "fire triangle", the removal of any one being sufficient to extinguish a fire, and the presence of all three required for fire initiation and propagation. As free radicals became more understood, the "fire triangle" was expanded to the "fire tetrahedron".

Free radicals are non-ionic high energy intermediates which form easily in high temperature reactions. Fire growth involves an avalanching oxidative propagation of free radicals in vaporized fuel-air mixtures: one free radical creates several others, and with descendent free radicals forming in profusion in a continuing and proliferating propagation throughout the fuel-air mixture.

Today, therefore, fires are characterized by the "fire tetrahedron" (fuel, heat, air, and the presence of propagating free radicals).

For ignition of fuels by contact with flame, in which flash points have most meaning, free radical events are entirely operational. In such fires, the flame ignition source actually is a free radical plasma, from which high energy free radicals are transferred to fuel vaporized by heat of the flame. Situations which promote free radical formation are conducive to ignition of the fuel under these conditions; and agents such as the Halons which quench free radical formation are thus optimum fire extinguishing agents for such fires.

III. Ionic Fire Effects: A Return to the Fire Triangle?

This discussion will attempt to point out that not all fires should be characterized by the "fire tetrahedron". In fact, many fires of military and commercial importance may best be characterized by the "fire triangle", with free radicals being totally unimportant.

Thus, fires arising from ignition of magnesium, titanium, and other active metals would best be described as involving ionic (not free radical) effects in both initiation and growth of the fire.

e.g., $Mg^{O} + 1/2\ O_2 \text{ -----> } Mg^{++}\ O^{=}$ 1)

"Ionic fires" can perhaps best be differentiated from free radical fires in terms of the ionic pathways and products of the ionic reactions, with no role of free radical propagating intermediates. The "flame" of an ionic fire is a plasma of incandescent ions, lacking in free radical components.

Phosphorus, thermite and other inorganic or pyrotechnic fires also would appear to be ionic and not free radical in nature. For ignition

of other combustibles by active metal or other inorganic incendiaries, it is now suggested that the mode of such ignitions may be that of contact with a hot surface rather than by contact with a flame.

Along these lines, Halons which quench free radicals and thus prevent propagation of "free radical" types of fires are completely ineffective against active metal "ionic" types of fires.

IV. Possible Ionic Effects in Ignition Temperature Correlations.

For fires resulting from ignition by contact of the fuel with hot surfaces, this discussion will attempt to demonstrate that while free radicals are certainly formed due to energy transfer and resulting bond breakages, the initiating events are not free radical in nature. In actuality, those fuels which would appear to be most susceptible to free radical formation often are among the most resistant to ignition by contact with hot surfaces! Thus, olefins and alkyl-substituted benzenes are far more susceptible to free radical substitution than are alkanes, due to resonance stabilization of the resulting free radical intermediates. (4) On the other hand, when comparing olefins and arenes with alkanes of similar volatility, the olefins and arenes frequently have higher ignition temperatures. Branched chain alkanes also undergo free radical reactions more readily than straight chain alkanes, but have higher IT's; and cyclopentanes are more reactive to free radicals than are cyclohexanes, but again the cyclopentanes have higher IT's (4,5) Representative data is shown in Table I.

Table I. Ignition Temperatures (IT) and Boiling Points (BP), in ^{O}F, for Alkanes, Olefins and Arenes. (2,6,7)

Alkane	BP	IT	Olefin	BP	IT	Arene	BP	IT
butane	31	826	1-butene	21	829			
methyl-cyclohexane	214	545				Toluene	232	1026
methyl-cyclopentane	161	624						
octane	257	428						
2,2,4-trimethyl-pentane	211	784						

In Figure 1, moreover, there is an anomalous decrease in ignition temperature of alkanes with increasing molecular weight, for the range of alkanes from methane (C_1) through octane (C_8). Precise data is not prevalent for the higher alkanes. As shown in the lower projected track of the IT values for the various alkanes, one possibility certainly lies in an asymptotic sweep along a 400^{O} IT isotherm, for alkanes beyond C_8. An inescapable suspicion lurks here, however,that a possible thermal cracking may occur at this temperature if the hydrocarbon is permitted to linger at the heated surface for up to ten minutes, in accordance with the ASTM operating procedures for this determination. (1) Thus, alkanes larger than nonane could conceivably have higher ignition temperatures; but by undergoing slow pyrolysis at 400^{O} F, some alkanes in the minimum IT region characeristic of C_5 - C_9

would form, with these igniting at this spuriously low temperature.

There is indeed some evidence for a possible increase in IT's for the higher alkanes; i.e., a minimum zone of IT's may exist for alkanes in the region of pentane through nonane (C_5 - C_9). This is shown in Figure 1 as the upper projected track for the alkanes beyond C_9. It is obvious that either track could actually pertain, and that currently available data is insufficient and good values are probably poorly available with existing equipment and technique.

If this mimimum zone for ignition temperatures indeed exists, the hexane through decane range of alkane would appear to represent the most dangerous species in jet fuel formulations: these alkanes have unsuitably low flash points and ignition temperatures. In terms of ignition from hot surfaces, these would be highly prone to enflame due to the low ingition temperatures, and then would promote uncontrollable proliferation of the fire because of the low flash points.

Experimental evidence is too sparce to fully support an ionic event for typical hot surface ignitions. However, it has previously been demonstrated that the nature of the hot surface can have significant effects on ignition temperatures. Thus, benzene exhibits quite higher ignition temperatures in iron containers than in quartz, and even higher in zinc. (2) As will be discussed below, this may be most consistent with the relative emissivities of these materials. However, silica (quartz) can be acidic; and ferric oxide is significantly more acidic than zinc oxide. Thus, there may be cationic catalysis provided by an acidic surface, which can serve to greatly favor bond ruptures in alkanes. (4) Cationic and emissivity effects may be of importance with regard to incorporation of metals or coatings for aircraft parts which may be anticipated to be most likely to come into contact with fuel leaks in combat gunfire or in controlled crash situations.

V. Surface Emissivity Effects.

Emissivity is the energy radiated from a unit area of a surface, in a unit of time. This is greatly dependent on the nature of the surface: for example, rough surfaces are more emissive than smooth surfaces. With regard to the decreasing ignition temperatures noted above, with zinc surfaces influencing a higher IT for benzene than iron, and quartz surfaces providing the coolest IT of all three, this is consistent with the relative trend of increasing emissivities: quartz is a more efficient heating surface than smooth unoxidized iron or zinc.

VI. Molecular Effects Which May Influence Ignition Temperatures.

Fuel component characteristics have been identified as having possible impact on the ignition temperatures are described below. None of these appear in any way to be associated with free radical effects.

1. Molecular weight, and speed and inertia effects.

Since the anomalous decrease of ignition temperatures with increasing molecular weight is observed only from methane through nonane, other effects in the alkanes must offset any role of molecular weight in reducing ignition temperatures. Molecular weights are inversely proportional to molecular velocities, however, as shown in Figure 2. Since the heavier molecules have lower velocities, there is an increased residence time for these in the vicinity of a hot surface,

with increased time for energy transfer to the molecule. Heavier molecules also have greater inertia and thus less ability to move away from a hot surface than would a lighter molecule.

2. Molecular rigidity.

This appears to be a very important effect, not only in the straight chain alkane family, but even more so for branched chain alkanes, cycloalkanes, olefins and aromatics. As stated previously, these species are particularly susceptible to free radical reaction systems; but surprisingly, these are frequently very considerably more stable than are the alkane analogs, with regard to ignition by fuel contact with hot surfaces. Examinations of molecular models reveal that, compared to the straight chain alkanes, all these other species are very considerably more rigid, with very considerably reduced rotational degrees of freedom within the molecular structures. This would then impart a pronounced decrease in "floppiness" of the molecule in its impact with a hot surface, allowing the more rigid structure to rebound readily and rapidly, with correspondingly considerably reduced residence times in the vicinity of the hot surface, and considerably reduced energy transfer from the surface to the fuel molecule.

This effect may be of importance in design of new fuel compositions: olefinic, branched chain, cyclic (napthenic) and aromatic moeities would impart higher ignition temperature characteristics.

3. Specific molecular heat.

For the smaller molecules, apparently, factors of relative speed and relative rigidity are overpoweringly important. Within the lower range of the alkanes, each addition of a methylene unit imparts a significant increase in molecular weight and in internal degrees of rotational freedom. In going from ethane to propane, for example, there is a 17% decrease in speed at 1000° F; whereas decane is only 5% slower than nonane at this temperature. Internal rotational degrees of freedom are even more considerably enhanced for propane, which is very flexible compared with ethane, which is remarkably rigid; but decane and nonane have very little difference in "mushiness" due to this effect. Thus, decreased speed and rigidity effects arising from increased molecular weight are very much less important for the higher alkanes.

Moreover, higher alkanes begin to enjoy the benefit of increased "molecular specific heat". When lower alkanes such as ethane or propane are energized by radiational heat, all atoms of the small molecule are fairly equally irradiated. For significantly larger molecules, some atoms will be in the shadow of others. The hotter surface atoms can then transfer some of their increased energies to the cooler internal atoms. Thus, a higher ignition temperature will be required to attain decomposition energies for a molecule large enough to provide shadowing by some of its atoms to other neighboring atoms.

Thus, the anomalous high ignition temperatures for higher alkanes seen in Figure 1 may actually represent valid IT's; and the lower points constituting the asymptotic sweep at the 400° isotherm for these higher alkanes may prove to be unrealistically low.

VII. Recommendations for an IT Differential Scanning Calorimeter.

If more realistic IT determinations had lower time requirements

(perhaps a second instead of ten minutes), IT values for fuel components would probably be considerably increased. Modification of a conventional differential scanning calorimeter (DSC) could provide a convenient and accurate determination. Minute samples of the fuel components could be periodically injected, at higher and higher temperatures, until a sudden exotherm signal is attained. The first derivative appearance of the IT point with this scheme may make for a more reproducible determination. Automatic injection devices, coupled with automatic temperature controlling, should provide rapid and easy injections with minimum attention requirements for the determination.)

VIII. Fuel Design for Fire Prevention.

It may be possible to design fuels meeting operational combustion requirements, (i.e., burning satisfactorily when ignited with a flame), at the same time providing maximum resistance to ignition on contact with a hot surface (as in aircraft crashes, leakage of fuel onto hot engine surfaces, and similar situations). From the foregoing preliminary considerations, attention could be given to elimination of alkane content in the region C_5 - C_{10}), since these components may be in the minimum zone of IT's and also suffer from unduly low flash points. This cut could be catalytically dehydrogenated to olefinic or aromatic stocks, or catalytically rearranged to branched chain isomers or cyclolalkane analogs. It could also be alkylated with isobutylene to provide higher molecular weight and branched chain character. All of these should result in higher ignition temperatures, lower vapor pressure, increased density, and decreased viscosity effects, which should prove desirable from the standpoint of fuel characteristics.

REFERENCES

1. "Autoignition Temperature of Liquid Chemicals", ASTM Designation E 659 - 78 (Reapproved 1984).

2. "Fire Hazard Properties of Flammable Liquids, Gases and Volatile Solids", National Fire Protection Association, Boston, MA (1960).

3. Hucknall, D. J. "Chemistry of Hydrocarbon Combustion", Chapman and Hall, New York (1985).

4. March, J. "Advanced Organic Chemistry: Reactions, Mechanisms and Structure", McGraw-Hill Book Co., New York (1968), pp. 153 - 155.

5. Brown, H.C.; Borkowski. J. Am. Chem. Soc. **1952**, 74, 1894; Brown, H.C.; Brewster, J. H.; Schechter, H. J. Am. Chem. Soc. **1954**, 76, 467.

6. Lange, N. A. "Handbook of Chemistry", 9th ed., Handbook Publishers, Inc., Sanduskey, OH (1956), 324.

7. Perry, J. "Chemical Engineering Handbook", 3rd ed., McGraw-Hill Book Co., New York (1950), pp. 1584-5.

8. Lange, N. A. "Handbook of Chemistry", 9th ed., Handbook Publishers, Inc., Sanduskey, OH (1956), 824.

9. "Handbook of Chemistry and Physics", 58th ed., CRC Press, Inc., Boca Raton, FL (1978, E-229-230.

Figure 1. Correlations of Ignition Temperatures and Flash Points for n-Alkane Components.

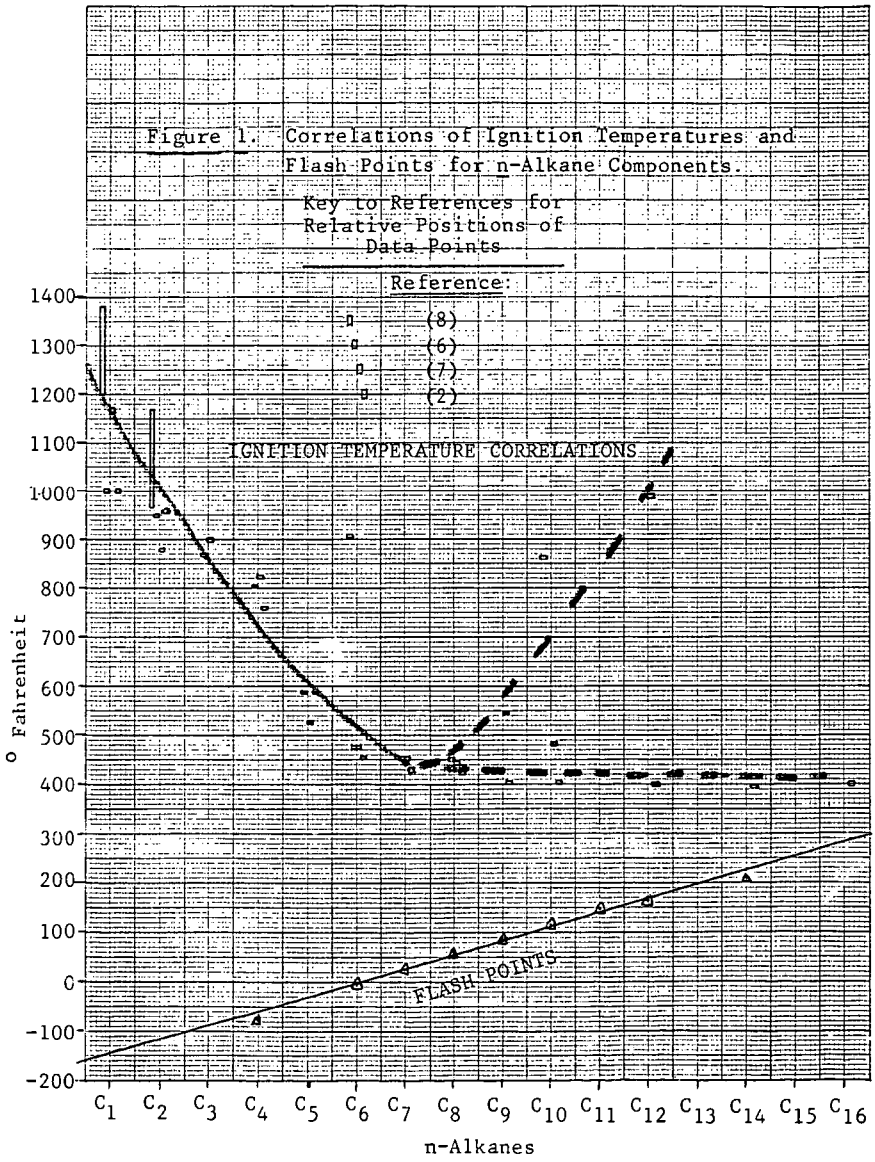

Figure 2. Molecular Characteristics Affecting Ignition Temperatures.

Typical JP-8 component (A): dodecane

$CH_3-CH_2-CH_2-CH_2-CH_2-CH_2-CH_2-CH_2-CH_2-CH_2-CH_2-CH_3$

(slow movement of massive molecule)

Typical JP-4 component (B): heptane

$CH_3-CH_2-CH_2-CH_2-CH_2-CH_2-CH_3$

(smaller, rapid movement)

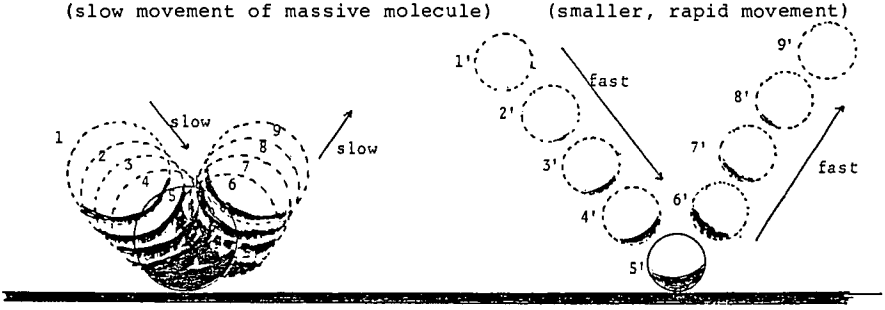

[(1), (2), (3) ... (8), (9) above indicate positions of molecules **A** and **B** at same time intervals, relative to hot surface area.]

Molecular velocity at temperature (T, ^{o}K) is inversely proportional to the molecular weight (M); smaller molecules have greater speed.

$$\text{Average velocity} = 14{,}600(T/M)^{\frac{1}{2}} \text{ cm/sec}$$

The slow moving heavy molecule **A** (above) is therefore near the hot surface longer than the lighter and faster **B**, and **A** has more time available to absorb energy from the hot radiating surface.

The larger molecule **A** has more mobile C-C bonds and therefore more rotational degrees of freedom than the smaller **B**. Thus, A will tend to be "mushier" with less elastic recoil on impact with the hot surface than the smaller, more rigid **B** which can bounce away more readily. Again, molecule **A** will have more time to energize than B.

To offset this, and although the larger molecule has greater surface area enabling it to absorb more heat than the smaller molecule, the large molecule's volume is increased even more than is the surface area (by comparison with the smaller molecule). Absorbed heat is then dissipated more through the large molecule, which accordingly is cooler than the small molecule. This effect is more pronounced with increased molecular weights (and volumes). In this case **A** (dodecane) needs more heat (with a higher ignition temperature) to energize it to its decomposition point than does **B** (octane). For smaller molecules (e.g., comparing hexane [C_6] and propane [C_3]), this offsetting factor of increased molecular specific heats is not as important as the molecular speed and rigidity effects: in such cases the heavier molecule has the lower ignition temperature.

X-RAY DIFFRACTION, MÖSSBAUER SPECTROSCOPIC AND ELECTRON MICROSCOPIC STUDY OF TIN "TITANATES" CATALYSTS USED FOR COPROCESSING MIXTURES OF COALS AND HEAVY OILS

Georges Dénès[a]1 and Jacques Monnier[b]

(a) Department of Chemistry and Laboratories for Inorganic Materials, Laboratory of Solid State Chemistry and Mössbauer Spectroscopy, CONCORDIA UNIVERSITY, 1455 West, de Maisonneuve Boulevard, Montréal, Québec, CANADA, H3G 1M8.
(b) Energy Research Laboratories, CANMET, Energy, Mines, and Resources Canada, 555, Booth Street, Ottawa, Ontario, CANADA, K1A 0G1.

ABSTRACT

Tin "titanate" catalysts were prepared by ion exchange of sodium hydrous "titanate" $NaTi_2O_5H$ support in aqueous solutions of $SnCl_2 \cdot 2H_2O$, and tested as catalysts for coprocessing of subbituminous coals and heavy oils. The catalysts were characterized at each stage of preparation and use, i.e. before and after ionic exchange, after calcination and after use, using X-ray powder diffraction, ^{119}Sn Mössbauer spectroscopy and scanning electron microscopy. The samples are microcrystalline (30 - 300 Å particle diameter). Most of the tin is in the stannic form. The SnO_2 and TiO_2 polymorphs (rutile, anatase) present in the catalysts are stable during coprocessing. A $Ti_{1-x}Sn_xO_2$ rutile-type solid solution, found in some calcined catalysts, decomposes during coprocessing, with reduction of tin(IV) to tin(II) followed by sulfidation to SnS. This decomposition also leads to formation of TiO_2 anatase.

INTRODUCTION

The large deposits of coal and heavy oil in Western Canada have prompted extensive research on coprocessing at CANMET (1-6). Hydrogenation of coal in the presence of bitumen or heavy oil of petroleum origin yields better conversions and higher quality liquids if catalysts are added to the liquid slurry (7). Recently, the Sandia National Laboratories of the US Department of Energy developed new catalyst supports for coal hydrogenation utilizing metal-exchanged hydrous titanates (8,9).

As interesting results have been obtained using tin catalysts for hydroliquefaction of coal (10-13), new tin catalysts on hydrous "titanate"[2] supports were prepared and tested at CANMET for coprocessing of heavy oil and coal (5). The present study reports the characterization of the catalysts by electron microscopy, X-ray powder diffraction and ^{119}Sn Mössbauer spectroscopy (15). The structure and texture of the catalysts are discussed as a function of the method of preparation, and their effect on the catalysts behavior is examined.

1 Author to whom all correspondence should be addressed.
2 Although no structural data suggest that discrete titanate ions are present in the catalysts, we use the name "titanates", as do Dosch, Stephens, and Stohl (8,9) The name "titanates" for these type of compounds is also used in well known inorganic chemistry textbooks (14).

EXPERIMENTAL SECTION

Preparation of the Catalysts

Metal-exchanged hydrous "titanates" (MEHT) were prepared according to Dosch, Stephens, and Stohl (8,9). Reaction of titanium(IV) 2-propoxide, $Ti[OCH(CH_3)_2]_4$ with a solution of sodium hydroxide in methanol produces a soluble intermediate, which yields sodium hydrous "titanate" precipitate, $NaTi_2O_5H$, upon addition of a mixture of 10 wt % water in acetone. The precipitate is washed with water and acetone, and then dried under vacuum, yielding hydrous titanate support, in the form of a white fluffy powder. Then, the support is loaded with tin in an aqueous solution of stannous chloride dihydrate, $SnCl_2 \cdot 2H_2O$, washed with water and acetone and dried under vacuum overnight. Before hydroprocessing tests, the titanate catalysts are calcined in air at 400 °C for 2 hours. Analytical results for the metals, obtained by neutron activation, are shown in TABLE I. The samples contain much more titanium than tin or sodium. The ratio of ionic exchange of Na by Sn is 70 % for MB-586 and 46 % for MB-599.

TABLE I
Metal Content of the Catalysts

Catalyst[a]		Weight %			Atomic Ratios		
		Ti	Sn	Na	Ti/Sn	Na/Sn	Na/Ti
MB-586	nc	41.88	11.44	-	9.10	-	-
	c	43.20	12.70	1.08	8.43	0.44	0.05
	u	-	1.56	-	-	-	-
MB-599	nc	-	-	-	-	-	-
	c	36.50	16.80	3.86	5.38	1.19	0.22
	u	-	2.64	-	-	-	-

a: nc = non-calcined, c = calcined, u = used.

Characterization Techniques

The texture of the catalysts and the particles shape and size were studied by scanning electron microscopy (SEM), which was performed using a Hitachi S-520 instrument with the filament energized at 15 kV. The samples were dried at 120 °C overnight to remove adsorbed water, stored in a dessicator and then gold coated.

X-ray powder diffraction (XRD), performed on a Picker X-ray diffractometer/X-ray fluorescence spectrometer dual instrument, using the Ni-filtered K_α radiation of Cu ($\lambda K_\alpha Cu = 1.54178$ Å), provided information on the crystalline phases present in the catalyst, namely their identification and crystalline form, and the crystallite size.

Identification of the tin species and the degree of oxidation of tin in the catalysts were obtained by Mössbauer spectroscopy, using the 8.58 % natural abundance of the ^{119}Sn probe. The 23.875 keV Mössbauer γ-ray was obtained using a 15 mCi $Ca^{119m}SnO_3$ source purchased from Amersham. A 0.1 mm thick Pd foil was used to filter the 25.04 and 25.27 keV X-ray lines. The detector was a Harshaw Na(Tl)I scintillation counter operating at 900 V. Based on the analytical data of TABLE I, the appropriate amount of sample containing 10 mg $Sn.cm^{-2}$ were enclosed in a teflon holder with a thin window and tight fitting cap. Both source and absorber (sample) were maintained at ambient temperature for the measurements. The Doppler velocity was provided by an Elscint driving system, including a MVT-4 velocity

transducer, a MFG-N-5 function generator and a MDF-N-5 driver generator, located on a vibration-free table, and operating in the triangular mode in the velocity range -8.5 $mm.s^{-1}$ to +8.5 $mm.s^{-1}$. The signal was fed to a Tracor Northern 7200 multichannel analyzer operating in the multiscaling mode. After accumulation of 500,000 to 1,000,000 counts per channel, data acquisition was stopped and the data were stored on a diskette. The Doppler velocity was calibrated using $CaSnO_3$ and α-SnF_2 standard absorbers. Computer fitting was performed on a CDC Cyber 835 main-frame computer using GMFP5 (16), a revised version of the General Mössbauer-Fitting Program (GMFP) of Ruebenbauer and Birchall (17). All chemical isomer shifts are referenced relative to $CaSnO_3$ at room temperature as zero shift.

RESULTS AND DISCUSSION

Scanning Electron Microscopy

FIGURE 1 shows SEM micrographs of the hydrous titanate support (FIGURE 1a), the MB-586 catalyst before (FIGURE 1b) and after calcination (FIGURE 1c), and of MB-599 before calcination (FIGURE 1d). The support is a fine powder, non-agglomerated with particle diameters up to 2 μm. Further magnification shows that the particles have no internal structure, and therefore are probably amorphous.

After ion-exchange (FIGURE 1b), a significant change has taken place as large blocks (10 - 50 μm edge) with no particular geometrical shape are observed, together with the powder. However, magnification of such a block to 8000X reveals that it is made of loosely bound powdered particles, which again have no internal structure. After calcination (FIGURE 1c), similar types of large blocks are observed, but these are still mixed with powder and show no smaller scale structure. The loosely bound powder inside these blocks are identical to those observed before calcination, and indicate that no sintering took place. FIGURE 1d reveals that the situation is the same for the MB-599 catalyst. Scanning electron microscopy shows that all catalysts have a low degree of ordering, at all steps of preparation, with little texture. This indicates that most likely they are amorphous or microcrystalline.

X-Ray Powder Diffraction

The X-ray diffraction results for the two catalysts at various stages of preparation and use are given in FIGURES 2 and 3. FIGURE 2a shows the hydrous titanate support before ion exchange is totally amorphous. After ion-exchange (FIGURE 2b), a low degree of ordering is observed, in the MB-586 catalyst, in the form of weak, very broad bumps on the background, indicating the presence of microcrystallinity. Calcination results in significant crystallite growth, giving identifiable Bragg peaks for TiO_2 in the anatase and rutile forms and SnO_2 rutile. Little change is observed after the catalyst has been used in the coprocessing reaction, except that a few extra weak peaks indicate the formation of a small quantity of SnS and maybe some β-Sn.

For the MB-599 catalyst (FIGURE 3), the non-calcined catalyst after ionic exchange (FIGURE 3b) is also microcrystalline. Contrary to MB-586, the powder pattern of calcined MB-599 (FIGURE 3c) contains only a few very broad peaks; however, no TiO_2 anatase, TiO_2 rutile or SnO_2 rutile seem to be present. Instead, a broad peak is observed between the positions that would be occupied by any (hkl) peak of TiO_2 rutile and the same (hkl) peak of SnO_2 rutile. This is indicative of the formation of a rutile-type $Ti_{1-x}Sn_xO_2$ solid solution with unit-cell parameters intermediate between those of TiO_2 and SnO_2 (TABLE II).

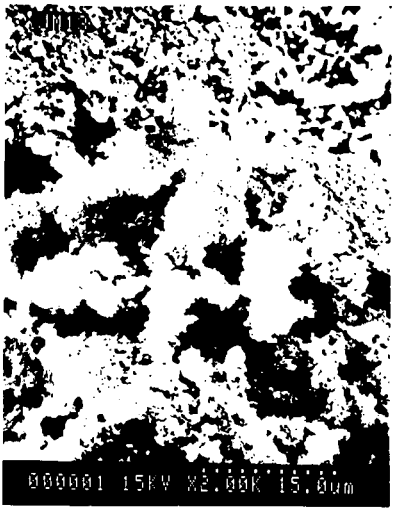

a: $NaTi_2O_5H$ support: SEM micrograph before cationic exchange, magnification= 5,000.

b: MB-586 catalyst before calcination: SEM micrograph at magnifications of 800 (top) and 8,000 (bottom).

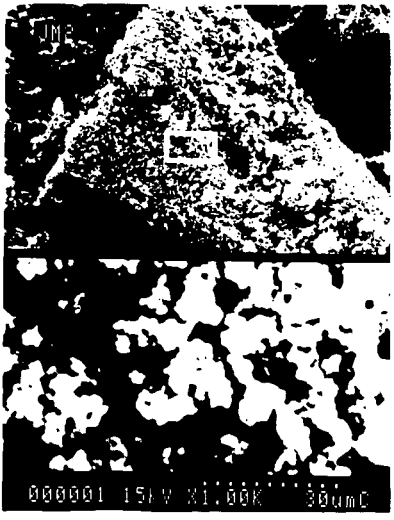

c: MB-586 catalyst after calcination: SEM micrograph at magnifications of 1,000 (top) and 10,000 (bottom).

d: MB-599 catalyst before calcination: SEM micrograph at magnifications of 800 (top) and 8,000 (bottom).

Figure 1

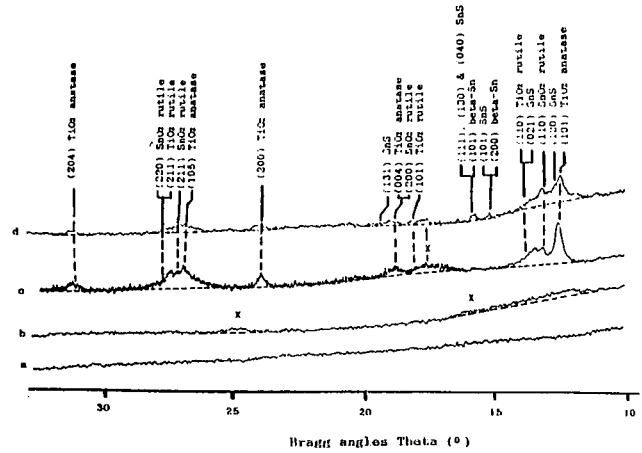

Figure 2: X-ray powder pattern (K Cu) of MB-586;
a: support
b: non-calcined ion-exchanged catalyst
c: calcined catalyst
d: used catalyst
X= unidentified peaks

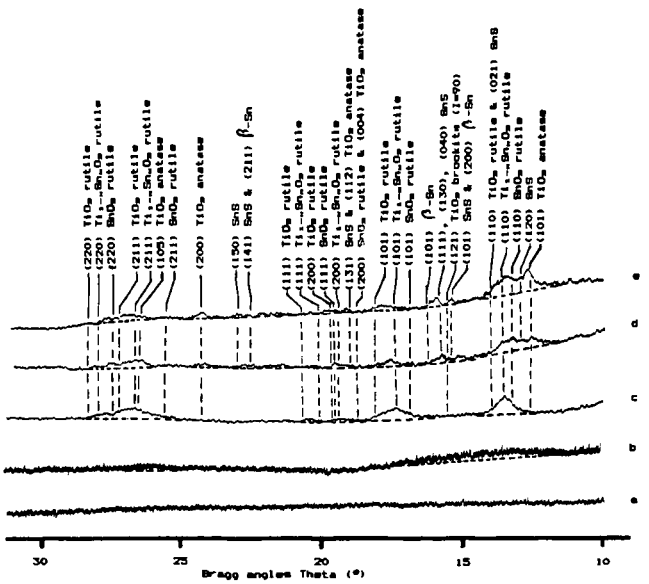

Figure 3: X-ray powder pattern (K Cu) of MB-599;
a: support
b: non-calcined ion-exchanged catalyst
c: calcined catalyst
d: used calcined catalyst
e: used non-calcined catalyst

TABLE II

Unit-Cell Parameters of TiO_2, $Ti_{1-x}Sn_xO_2$, and SnO_2 Rutile-Type

Unit-cell parameters	TiO_2	$Ti_{1-x}Sn_xO_2$	SnO_2
a (A)	4.594	4.643	4.738
c (A)	2.958	3.100	3.188
V (A^3)	62.43	66.83	71.51

Contrary to MB-586, a drastic change takes place in MB-599 upon use (FIGURE 3d and 3e), as a mixture of TiO_2 anatase, TiO_2 rutile, SnO_2 rutile, SnS, and possibly β-Sn, is observed in addition to some unreacted $Ti_{1-x}Sn_xO_2$ solid solution. The details of the changes for the first group of peaks are given on FIGURE 4.

The MB-586 and MB-599 catalysts were prepared following the same procedure, except that, for MB-599, the sodium hydroxide solution was kept below 0 °C to minimize temperature rise during addition of titanium(IV) 2-propoxide, whereas for MB-586, this NaOH solution was not cooled before preparation of the soluble titanium intermediate. This difference in experimental procedure, not brought up in the literature, must be at the origin of the difference in the nature of the solid catalysts. It is most likely that additional intermediate species, precursors of TiO_2 anatase, are formed upon hydrolysis of titanium(IV)· 2-propoxide at room temperature.

The catalyst are microcrystalline at all stages, even after calcination and use, as shown by the large linewidth of the Bragg peaks. Below 1000 A particle diameter, line broadening occurs, and below ca. 50 A, the peaks are so broad they cannot be distinguished from the background. The average particle size of each phase was estimated by using the Scherrer's formula (18), corrected for instrumental broadening with Warren's method (18). The results are given in TABLE III.

TABLE III

Average Particle Size of Catalysts as Determined by Scherrer's Method from the Broadening of the Bragg Peaks

Catalysts[a]	$\theta(K_\alpha Cu)(°)$	$B_M(°)$[b]	$B_S(°)$[b]	$B(°)$[b]	t(A)[b]	Phase
Support	*	*	*	*	< 50	microcrystalline
MB-586 nc	#	#	#	#	50-100	TiO_2 microcryst. SnO_2 microcryst.
MB-586 c	12.70	0.32	0.17	0.27	300	TiO_2 anatase
MB-586 u	12.70	0.52	0.18	0.49	170	TiO_2 anatase
MB-599 nc	#	#	#	#	50-100	TiO_2 microcryst. SnO_2 microcryst.
MB-599 c	13.58	0.70	0.17	0.68	120	$Ti_{1-x}Sn_xO_2$ rutile
	17.40	1.05	0.17	1.04	80	$Ti_{1-x}Sn_xO_2$ rutile
MB-599 u-c	17.60	0.80	0.17	0.78	107	$Ti_{1-x}Sn_xO_2$ rutile
MB-599 u-nc	12.64	0.30	0.17	0.25	330	TiO_2 anatase
	17.60	0.50	0.17	0.47	177	$Ti_{1-x}Sn_xO_2$ rutile

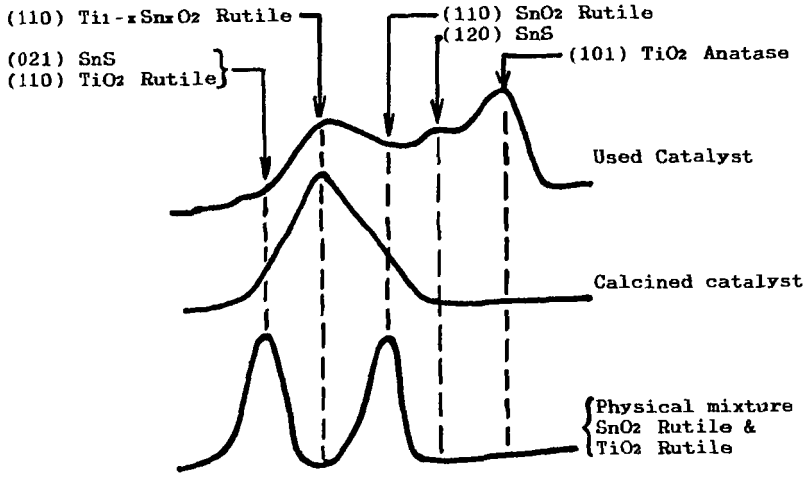

Figure 4: Comparison of the first Bragg peak of $Ti_{1-x}Sn_xO_2$ Rutile type solid solution in MB-599 calcined catalyst with a physical mixture of rutile type SnO_2 and TiO_2 and with the used catalyst.

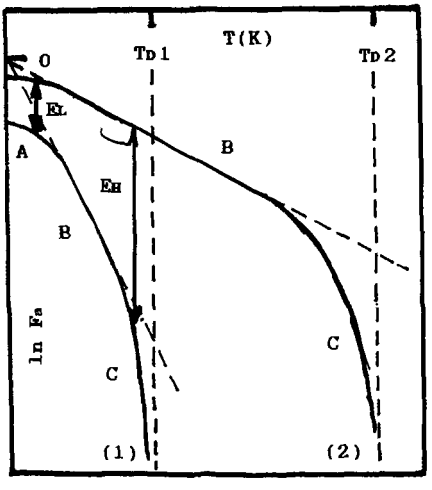

Figure 5: Evolution of the recoil-free fraction with temperature as a function of lattice strength

A= Zero point motion
B= Harmonic thermal vibrations
C= Anharmonic thermal vibrations
E_L = Low temperature difference
E_H = High temperature difference
f_a = Absorber recoil-free fraction
T_{D1}, T_{D2}= Debye temperatures
(1)= Soft lattice
(2)= Hard lattice

a: nc = non-calcined, c = calcined, u = used, u-c = used calcined catalyst, u-nc = used non-calcined catalyst.
b: Scherrer's formula: $t = (0.9\lambda)/(B.\cos\theta)$ with t (A) = average particle size, B (°) = broadening at half-height due to small particles, λ (A) = wavelength, θ (°) = Bragg angle.
* No Bragg peak observed.
\# Very broad peak, cannot be measured.

X-ray diffraction results corroborate the information obtained from the SEM photographs, i.e. all samples are microcrystalline. It is not surprising that the particles of 1-2 μm diameter observed by SEM appear to have no internal structure. Indeed, each of them is made of about 10^{10} much smaller particles (diameter ca. 1000 times smaller) randomly distributed relative to one another. The support gives no Bragg peak at all, and therefore is amorphous or microcrystalline with particle diameter below 50 A. The non-calcined ion-exchanged catalysts shows very broad features barely distinguishable from the background, indicative of a particle size close to 50 A. The rutile-type $Ti_{1-x}Sn_xO_2$ solid solution has particle dimensions of about 100 A, while TiO_2 anatase has the largest crystallites (~ 300 A). Some crystallite growth occur upon calcination; however, all samples are still microcrystalline. No further crystal growth was observed during the tests.

Mössbauer Spectroscopy

^{119}Sn Mössbauer spectroscopy provides a direct probing of all tin sites, regardless of the degree of crystallinity or presence of other phases. This is very important for obtaining information on the oxidation state and the coordination of the active sites of these catalysts. Furthermore, of all metal-exchanged catalysts tested in (5), i.e. Mo, Co, Pd, Sn, and Ni, only tin has a Mössbauer isotope[3]. The Mössbauer results for MB-586 and MB-599 are summarized in TABLE IV.

The non-calcined ion-exchanged catalysts contain minor divalent tin and a major tetravalent tin species, both coordinated with oxygen. Sn(IV) is in pseudooctahedral coordination like in SnO_2, with various degrees of distortion relative to regular octahedral symmetry. The oxygenated ligands can be bridging oxygen, OH^- or H_2O molecules. The sample prepared at low temperature (MB-599) contains a larger proportion of Sn(II). Upon calcination in air, all tin(II) is oxidized to tin(IV) as expected. After coprocessing test, some stannous sulfide SnS is produced, in very small quantity (1 %) for MB-586, in much larger quantity (10 - 15 %) for MB-599. No ß-Sn was observed by Mössbauer spectroscopy; therefore, if it is indeed formed, it is in very small quantities.

Mechanism of formation of TiO_2 anatase and SnS during the coprocessing reaction

The X-ray diffraction results of FIGURES 2 to 4 and the Mössbauer data presented in TABLE IV show that, during coprocessing, a profound change takes place in the solid catalyst provided it was

---

3 Co catalysts can be studies by ^{57}Fe Mössbauer spectroscopy; however, this requires preparing the catalyst using radioactive ^{57}Co radioisotope, thus giving rise to additional experimental complications. In addition, electron-capture decay, and the following Auger cascade, often give extra Mössbauer lines and unexpected oxidation states of Fe, making the interpretation of the spectra more difficult (19).

TABLE IV

Room Temperature ^{119}Sn Mössbauer Parameters for MB-586 and MB-599 Tin Titanate Catalysts

Catalysts[a]	δ(mm.s^{-1})[b]	Δ(mm.s^{-1})[c]	Oxi[d]	Contr(%)[e]	Assignment[f]
MB-586 nc	- 0.09	0.15	+4	95	Sn/O octa sd
	3.04	1.59	+2	5	Sn(II)/O
MB-586 c	- 0.03	0.30	+4	100	Sn/O octa di
MB-586 u	- 0.03	0.40	+4	99	Sn/O octa vd
	3.16	0.98	+2	1	SnS
MB-599 nc	- 0.09	0.40	+4	75	Sn/O octa vd
	3.13	1.78	+2	25	Sn(II)/O
MB-599 c	- 0.03	0.00	+4	100	Sn/O octa ud
MB-599 u-c	- 0.03	0.00	+4	85	Sn/O octa ud
	3.22	0.86	+2	15	SnS
MB-599 u-nc	- 0.03	0.00	+4	90	Sn/O octa ud
	3.28	0.86	+2	10	SnS

a: nc = non-calcined, c = calcined, u = used, u-c = used calcined catalyst, u-nc = used non-calcined catalyst.
b: chemical isomer shift relative to $CaSnO_3$ at room temperature, error bar = 0.01 mm.s^{-1}.
c: quadrupole splitting, error bar = 0.01 mm.s^{-1}.
d: oxi = tin oxidation state.
e: contr = % contribution of each tin site to the total spectrum, error bar = 1 %.
f: Sn/O octa = tetravalent tin in octahedral or pseudo-octahedral coordination of oxygen, ud = undistorted, sd = slightly distorted, di = distorted, vd = very distorted, Sn(II)/O = divalent tin coordinated by oxygen.

formed of $Ti_{1-x}Sn_xO_2$ solid solution (MB-599). The amount of solid solution is reduced while a large amount of TiO_2 anatase is formed and ca. 15 % SnS. On the other hand, if the calcined catalyst contains TiO_2 anatase and rutile and SnO_2 rutile, and no $Ti_{1-x}Sn_xO_2$ (MB-586), no significant change is observed and little SnS is formed (1 %). Obviously, there is a correlation between the simultaneous disappearance of $Ti_{1-x}Sn_xO_2$ and the appearance of TiO_2 anatase and SnS. As the reaction with calcined MB-599 gives the highest yield in SnS, reduction of tin(IV) to tin(II) by hydrogen and/or coal first takes place, followed by sulfidation of the tin(II) formed (EQUATION 1), sulfur being provided by the oils (5 wt % S) and coals (0.5 wt % S).

$$\text{Sn(IV)} \xrightarrow{C + H_2,\ 410\ ^\circ C} \text{Sn(II)} \xrightarrow{\text{oil, coal}} \text{SnS} \qquad 1)$$

As formation of SnS is observed only if $Ti_{1-x}Sn_xO_2$ is present, the reactions given in EQUATIONS 2 and 3 take place at 410 °C under 3.4 MPa pressure of hydrogen.

$$xS^{2-} + Ti_{1-x}Sn_xO_2 + 2xH_2 \longrightarrow (1-x)TiO_2 + 2xH_2O + xSnS + 2xe^- \quad 2)$$
rutile → anatase

$$xS^{2-} + Ti_{1-x}Sn_xO_2 + 2xC \longrightarrow (1-x)TiO_2 + 2xCO + xSnS + 2xe^- \quad 3)$$
anatase → anatase

Reactions 2 and 3 produce TiO_2 anatase and SnS and consume $Ti_{1-x}Sn_xO_2$, and therefore, account for the experimental observations. The reason the reaction works well with $Ti_{1-x}Sn_xO_2$ and not for SnO_2 rutile is probably that the SnO_2 lattice is much more stable. Indeed, the strain induced by the presence of two cations of significantly different size (Sn(IV) = 0.83 Å, Ti(IV) = 0.735 Å, in coordination number six) (20) in $Ti_{1-x}Sn_xO_2$ reduces the lattice energy and makes it more susceptible to the destabilizing power of chemical attacks.

The amount of SnS formed depends on the presence of the $Ti_{1-x}Sn_xO_2$ rutile-type solid solution, and is not favored by prior presence of tin(II) in the catalyst. The data of TABLE V show that the calcined MB-599 (0 % Sn(II)) yields 15 % SnS, while non-calcined MB-599 catalyst (25 % Sn(II)) gives 10 % SnS, i.e. less. Even in the case of the test with non-calcined MB-599, the used catalyst contains less divalent tin (10 %) than the catalyst before use (25 %), showing that direct sulfidation of tin(II) already present does not take place. To the contrary, presence of $Ti_{1-x}Sn_xO_2$ is required showing that its decomposition leads to SnS and TiO_2 anatase, according to equations 2 and/or 3.

TABLE V
Amount of SnS versus Test Conditions

Catalyst	c/nc[a]	T_S[b]	pH_2 (psi)[c]	T_R (°C)[d]	Time[e]	% SnS
MB-586	c	RT	500	410	3h45	1
MB-599	c	< 0 °C	500	410	3h45	15
MB-599	nc	< 0 °C	500	410	3h45	10

a: c = calcined, nc = non-calcined.
b: T_S = temperature of preparation of support.
c: pH_2 = pressure of hydrogen (continuous flow) in the reactor during the test.
d: T_R = temperature of reaction for the tests.
e: Time = time of the test reaction.

A surprising feature is the high amount of Sn(IV) in the catalysts before calcination, i.e. the large amount of divalent tin oxidized to tin(IV) during ion-exchange. TABLE V compares the relative amount of tin(II) as a function of the conditions of ion exchange.

TABLE VI
Relative amount of divalent tin in ion-exchanged non-calcined catalysts as a function of preparative conditions

Catalyst	Water Degassing	pH	Stirring Time (min)	Sn(II)/total Sn (%)
MB-586	No	2.8	60	5
MB-599	Yes	1.83	105	25
MB-585	Yes	2.4	60	10

Although one could expect that prolonged exposure to dissolved atmospheric oxygen would increase the amount of tin(IV), the above data clearly indicate that the pH of the solution is the most important factor, followed by degassing. Most likely, at low pH less hydrolysis of tin(II) occurs, which is known to favor oxidation. However, a pH lower than 1.8 cannot be used because it dissolves the sodium titanate support. Oxidation to tin(IV) during calcination could be expected.

CONCLUSION

Tin exchanged hydrous "titanates" have been prepared and characterized by some of the solid state techniques. The method of preparation, texture and structure of the catalysts, as well as the nature of the tin site, are important parameters for the understanding of their behavior during coprocessing reactions. The catalysts are microcrystalline in all stages of preparation, although significant crystallite growth of TiO_2 anatase occurs during calcination, from ca. 50 A to 300 A. The method of preparation of the support is critical as a room temperature reaction yields mostly TiO_2 anatase, while low temperature syntheses result in a rutile-type $Ti_{1-x}Sn_xO_2$ solid solution being formed, which easily decomposes upon reduction of tin(IV to tin(II), producing SnS and TiO_2 anatase at coprocessing conditions. X-ray diffraction and Mössbauer spectroscopy show that no Sn(IV) or Sn(II)/Sn(IV) mixed oxidation state sulfide is formed. In addition, no titanium sulfide or sodium-containing species was detected, despite the non-negligible sodium content (TABLE I). The coal/hydrogen reducing medium reduces Sn(IV) from $Ti_{1-x}Sn_xO_2$ and not from SnO_2, followed by sulfidation to SnS, using the natural sulfur content of coals and oils. TiO_2 anatase and rutile and SnO_2 rutile seem very stable.

The relative contribution of each tin species to the total Mössbauer spectrum, is not equal to the real amounts of these species in the samples if their recoil-free fractions are not the same, and the difference, which is a function of their Debye temperature, is temperature dependent, as shown on FIGURE 5. A variable temperature study is presently being undertaken in order to minimize the error due to recoil-free fraction difference. Calculations of equilibrium constants (21) for the reduction of oxides of Sn, Mo, Co, and Ni, at the temperature of the coprocessing reactions show that SnO_2 is more difficult to reduce in H_2 than NiO, CoO and MoO_3. If reduction of SnO_2 occured, NiO, CoO and MoO_3 would also be reduced in the reactions of (5). As no data are available on the equilibrium constant for $Ti_{1-x}Sn_xO_2$, reduction of NiO, CoO, and MoO_3 cannot be confirmed. The detailed study of the tin catalysts, which was possible because of the ^{119}Sn Mössbauer probe, provides a model for catalysts containing other metals, which have no Mössbauer nuclide.

ACKNOWLEDGMENT

We wish to thank Prof. N. Kapoor, Ms. J. Fitzgerald, and Mrs. M. Dénès at Concordia University for technical assistance in electron microscopy and X-ray diffraction. Financial assistance from Concordia University for the purchase of the Mössbauer spectrometer and technical assistance from the Concordia University Science Technical Center are acknowledged. G.D. thanks the Natural Sciences and Engineering Research Council of Canada for a University Research Fellowship. This work was conducted under Supply and Services Canada Contract Serial Number OST85-00243.

REFERENCES

1. J.F. Kelly, S.A. Fouda, P.M. Rahimi, and M. Ikura, Proceedings of the Coal Conversion Contractors' Review Meeting, J.F. Kelly Edit.; CANMET, Energy, Mines and Resources Canada, Ottawa, Ontario, Canada, 397 (1985).
2. J. Monnier and J.F. Kriz, Ind. Eng. Chem. Prod. Res. Dev. 25, 537 (1986).
3. S.A. Fouda and J.F. Kelly, Proceedings of the 1987 International Conference on Coal Science; J.A. Moulijn et al. Eds., Elsevier Science Publishers, 387 (1987).
4. P.M. Rahimi, S.A. Fouda, and J.F. Kelly, Proceedings of the 12th EPRI Annual Fuel Science and Conversion Conference, Palo Alto, California, USA (1987).
5. J. Monnier, G. Dénès, J. Potter, and J.F. Kriz, J. Energy & Fuels 1, 332 (1987).
6. J. Monnier, C.W. Fairbridge, J.R. Brown, and J.F. Kriz, Proceedings of the 9th International Congress on Catalysis 1, 182 (1988).
7. J. Monnier and J.F. Kriz, 10th Canadian Symposium on Catalysis, Preprints, 1 (1986).
8. R.G. Dosch, H.P. Stephens, and F.V. Stohl, US Patent 4 511 455 (1985).
9. H.P. Stephens, R.G. Dosch, and F.V. Stohl, Ind. Eng. Chem. Prod. Res. Dev. 24, 15 (1985).
10. S.W. Weller, in "Catalysis IV", P. Emmett Edit., Reinhold, New York, CHAPTER 7 (1956).
11. S.J. Cochran, M. Hatswell, W. Roy Jackson, and F.P. Larskins, Fuel 61, 831 (1982).
12. M. Mizumoto, H. Yamashita, and S. Matsuda, Ind. Eng. Chem. Prod. Res. Dev. 24, 394 (1985).
13. P.S Cook and J.D. Cashion, Fuel 65, 146 (1986).
14. F.A. Cotton and G. Wilkinson, "Advanced Inorganic Chemistry", 4th Ed., Wiley-Interscience, New York, USA, p. 695 (1980).
15. G. Dénès, "Characterization of Tin Catalysts by Mössbauer Spectroscopy", Final Report to CANMET under Supply and Services Canada Contract Serial Number OST85-00243; Department of Chemistry, Concordia University, Montréal, Québec, Canada (1987).
16. J. Monnier, G. Dénès, and R.B. Anderson, Can. J. Chem. Eng. 62, 419 (1984).
17. K. Ruebenbauer and T. Birchall, Hyperfine Interact. 7, 125 (1979).
18. B.D. Cullity, "Element of X-ray Diffraction", 2nd Ed., Addison-Wesley, Don Mills, Ontario, Canada, pp. 192, 284 (1978).
19. N.N. Greenwood and T.C. Gibb, "Mössbauer Spectroscopy", Chapman and Hall Limited, London, UK, p. 330 (1971).
20. R.D. Shannon, Acta Crystallogr. A32, 751 (1976).
21. I. Barin and O. Knacke, "Thermochemical Properties of Inorganic Substances", Springer-Verlag, West-Berlin, Germany, and New York, USA (1973).

A NEW DETERMINATION OF EXCHANGEABLE OXYGEN IN COALS

Edwin S. Olson and John W. Diehl

University of North Dakota Energy and Mineral Research Center
Box 8213, University Station
Grand Forks, ND 58202

Introduction

All facets of research on a coal sample require accurate knowledge of the moisture content, which obviously changes during any chemical or physical processing. The elemental analysis of coal significantly depends on the determination of the moisture content of the coal; and thus during the combustion (ultimate) analysis of a sample, the amount of water initially present in the coal sample must be accounted for in the water of combustion measured in the experiment, in order to determine the amount of hydrogen present in the coal sample. The amount of water present also must be known to determine the oxygen content. Although the weight loss drying method is standard practice for determining moisture, there are errors possible, especially in the low-rank coals, which may contain over 30 percent moisture. These errors could be due to incomplete drying or possibly oxidation during the determination.

Finseth has recently reported a new method for the determination of water in coals which utilizes isotope dilution (1). In this technique, a known amount of water which was enriched in ^{18}O was added to the weighed coal sample in a tube. Carbon dioxide was also added and the tube sealed and then heated to equilibrate the added labeled water with the natural abundance water present in the sample. The tube was then opened and the carbon dioxide analyzed by mass spectrometry to determine the isotopic ratio, from which the coal moisture could be calculated. The carbon dioxide acted as a probe molecule to facilitate the mass spectrometric analysis, since its oxygens exchange completely with those of the water. The results of Finseth's moisture determinations were compared with ASTM values for a number of Argonne premium coal samples and were in all cases somewhat larger than the ASTM values.

The mass spectrometers available in our laboratories are not adaptable to analysis of the CO_2, hence we sought an alternative for the analysis of the isotope ratio in the isotopically equilibrated water samples. The reaction of the water with several orthoesters to give the ester containing the water-derived oxygen (labeled oxygen) in the carbonyl group was investigated (see Equation 1). The orthoester selected for the analysis was trimethyl orthobenzoate, since it gave methyl benzoate which could be conveniently analyzed in our GC/FTIR/MS system.

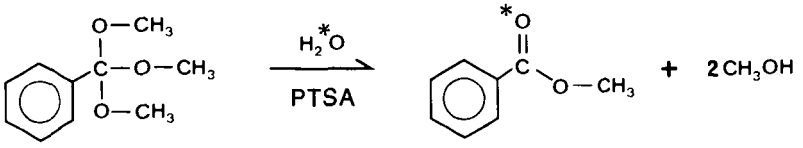

Equation 1. Reaction of trimethyl orthobenzoate with water.

Results and Discussion

The reaction of water with the trimethyl orthobenzoate proceeded somewhat slowly; hence several catalysts for the reaction were investigated. Boron trifluoride etherate was unsuccessful since it appeared to catalyze the exchange of labeled oxygen of the water with the glass or possibly with the solvent. Methanesulfonic acid similarly gave poor results. A very dilute solution of p-toluenesulfonic acid in glyme was selected as the catalyst which gave the best reproducibility and calibration.

The isotope ratio of the natural and labeled methyl benzoate which results from the reaction of water with the trimethyl orthobenzoate was determined both from mass spectra and infrared spectra of the methyl benzoate peak eluting from the GC column. Adequate peak shape was obtained using a 60 m x 0.32 mm column with a 1.0 μ DB-5 film, so that reproducible integration of the peak for the quantitation could be obtained.

In the mass spectral measurement, the ratio of the integrated intensity of the $(M-31)^+$ ion corresponding to the labeled methyl benzoate (at m/e = 107) to that of the natural methyl benzoate (at m/e = 105) over the corresponding peaks was determined. A representative mass spectrum from the GC/MS determination of one of the known mixtures is shown in Figure 1 along with the reconstructed total ion chromatogram which shows the ^{18}O-labeled and natural methyl benzoate peak and the unreacted trimethyl orthobenzoate peak.

A linear calibration plot (Fig. 2) was used for the mass spectral isotope ratios, since there were no overlapping peaks from the labeled compound (m/e = 107) and natural abundance analyte (m/e = 105). The small amount of m/e 105 peak in the spectrum of the labeled ester was due to the small amount of ^{16}O water (2 percent) in the ^{18}O water plus a small amount in the glyme solvent used in the reaction of the water with the orthoester. The glyme was purified and dried over lithium aluminum hydride and distilled onto molecular sieves. The m/e 105 peak in the standard will not affect the linearity but will change the intercept.

The absorbance reconstructed GC peaks of the natural methyl benzoate (over the range 1750 to 1742 cm^{-1}) and labeled methyl benzoate (over the range 1720 to 1712 cm^{-1}) were integrated to obtain the area ratios (A/S) of natural to labeled ester. A representative infrared spectrum from the GC/FTIR determination of one of the known mixtures is shown in Figure 3.

The calibration plot (Fig. 4) of the infrared data (amount ratio versus area ratio) was not linear since the absorption bands for the labeled and natural ester overlap slightly. The calibration data were fitted to a polynomial expression, which was then used for the determination of the unknown isotope ratios.

Three methods were investigated for the equilibration of the coal moisture with the added isotopically enriched standard. The equilibration was first carried out by adding a solution of the ^{18}O water in dried and purified glyme to the coal and heating in the sealed vial at 100°C overnight. Decent calibration curves were obtained by using volumetric aliquots of known concentrations of natural abundance and isotopically enriched water in glyme. The area ratios were reproducible, with deviations less than one percent for most points. Tests of the calibration with known concentrations of water in glyme showed that the method was accurate. However, tests with coal samples gave obviously poor results using this method. Exchange with the ether oxygen of the solvent appears to have occurred in the coal determinations, rendering the method useless. The same reaction in the absence of the coal but with an amount of natural abundance water corresponding to that expected in the coal gave no exchange with the solvent, even in the presence of acid catalyst. Acetonitrile was investigated as the solvent, but the methyl benzoate did not form.

The equilibration was then investigated using no solvent as Finseth has reported. To generate the calibration curves, the ^{18}O water and natural abundance

water were pipetted into a vial using micropipettes. Trimethyl orthobenzoate and catalyst were added and the vial was crimped. The methyl benzoate product was analyzed with GC/FTIR/MS as described above. The resulting calibration curves were somewhat erratic, and although points from the same solution were reproducible, tests of the calibration with new known mixtures gave large errors. The large errors and erratic calibration curves were attributed to errors in the volumetric measurements using the micropipettes, probably due to incomplete drainage.

Finally, the solutions for the calibration were made up by weighing milligram amounts of ^{18}O water and natural water. A linear calibration curve was obtained from the mass spectral data, and a smooth curve was obtained from the infrared data, from which a polynomial expression was derived. The infrared integrated absorbance ratios were reproducible within one percent, and the mass spectral intensity ratios were within one percent in the middle of the calibration curve and within four percent at each end. A test of the calibration using a new known solution gave errors of 1.8 percent using the infrared data and 4.5 percent using the mass spectral data.

The method was tested using a Beulah lignite sample by adding an analytically weighed amount of the ^{18}O water. The sample was sealed with a torch in such as manner as to leave a capillary at the sealed end. After equilibration in an oven overnight, the sample was then removed from the oven and placed in an oil bath so that the coal in the bottom of the tube was warmed and the moisture collected in the capillary tube. The tube was opened and the equilibrated water was obtained from the capillary and reacted with trimethyl orthobenzoate and p-toluenesulfonic acid catalyst. The analysis of the methyl benzoate with the GC/FTIR/MS system gave values for the exchangeable oxygen reservoir of 39.8 percent from the infrared data and 38.6 percent from the mass spectral data. The close agreement of these determinations was encouraging and demonstrated that the instrumental methodology was working extremely well. On the other hand, the large value obtained was not expected, since the ASTM drying weight loss method gave 33.6 percent moisture in this sample. The equilibration with the isotopically enriched water, of course, determines the size of the exchangeable oxygen reservoir. The problem is that we do not know if this includes portions of the organically bound oxygen, such as carboxylic acid groups. Finseth demonstrated that benzoic acid does not exchange under these conditions, however, we cannot be certain that the coal carboxylate and carboxylic acid groups do not exchange, considering that there may be catalysts for the exchange present in the coal.

The exchangeable oxygen determination was then performed on two of the Argonne premium coal samples and a sample of Big Brown lignite. Table 1 compares the values obtained using the isotope dilution GC/FTIR and GC/MS data with the fast drying ASTM method and the Finseth isotope dilution (CO_2) MS method. The values obtained for the Argonne premium sample of Illinois #6 bituminous coal and the Argonne premium Beulah-Zap lignite were very similar to those obtained by Finseth (1) and were somewhat higher than those found using the ASTM method. Further work with the Argonne premium samples will be undertaken to evaluate the infrared and mass spectral methods for water determination.

Experimental

Coal samples were equilibrated with the weighed amount of ^{18}O water in sealed tubes at 100°C for 15 hours as reported by Finseth (1). The seal on the tubes was fashioned so that it formed a narrow capillary portion. After equilibration, the bottom of the tube was warmed so that moisture was trapped in the capillary portion of the tube. The capillary tube was then broken off, and the upper part containing the collected water was quickly transferred to a reaction vial, where it was crushed and the reagents added. For preparation of the derivative, 1 μ of a solution containing 1 mg/ml of p-toluene-sulfonic acid in dried glyme and 100 mg of trimethyl orthobenzoate were added to the vial, which was sealed with a crimped cap. The vial was heated for 1 hour at 100°C. Instrumentation for the GC/FTIR/MS determination was described earlier (2). All glassware was dried several hours at 110°.

References

1. Finseth, D. ACS Div. of Fuel Chem. Preprints, (1987) 32(4), 260-5.
2. Olson, E.S. and Diehl, J.W., Anal. Chem. (1987) 59, 443.

Acknowledgements

Financial support of this work was provided by the U.S. Department of Energy under Contract No. DOE-FE21MC10637.

TABLE 1. MOISTURE (EXCHANGEABLE OXYGEN) DETERMINATIONS

COAL	ID/GC/FTIR	GC/MS	ID/MS(CO_2)*	ASTM
AR. B-Z LIGNITE	34.3%	32.8%	34.4%	32.8%
AR. ILL #6	9.4%	9.9%	9.6%	8.8%
UND B-Z LIGNITE	39.8%	38.6%		33.6%
UND BB LIGNITE	28.9%	29.4%		27.8%

* Values from Finseth (Reference 1)

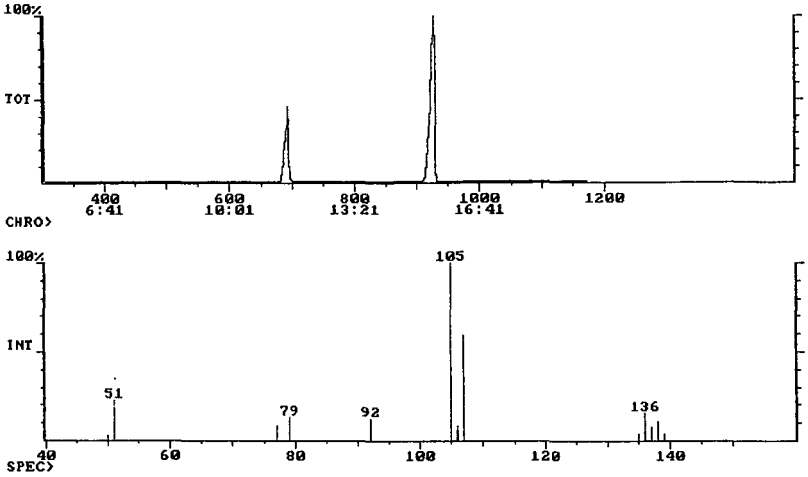

Figure 1. (a) Reconstructed total ion chromatogram of mixture of ^{18}O- and ^{16}O-labeled methyl benzoate, (b) Mass spectrum of above mixture.

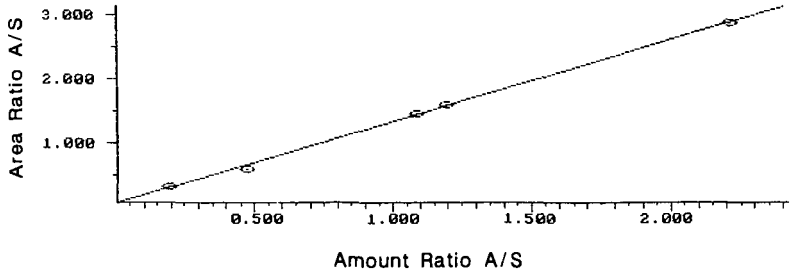

Figure 2. Mass spectra calibration curve for isotopic methyl benzoate ratios.

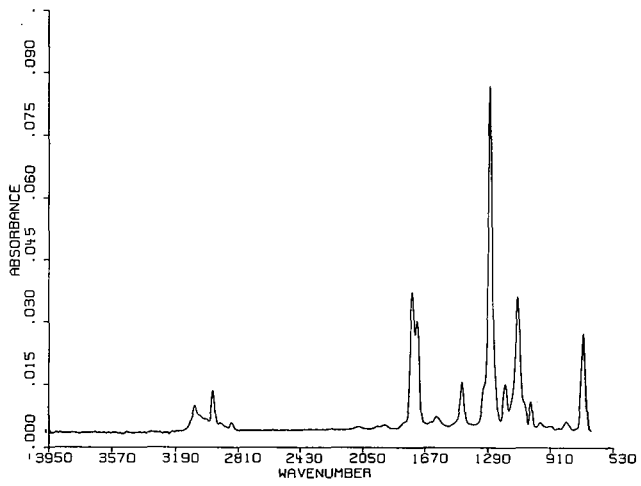

Figure 3. Infrared spectrum of mixture of ^{18}O and ^{16}O-labeled methyl benzoate.

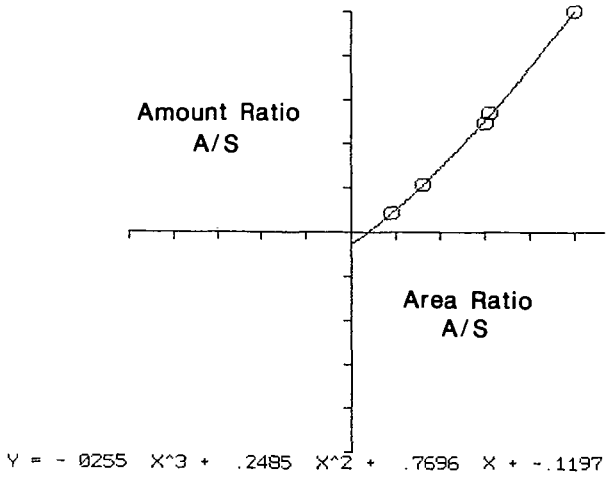

Figure 4. Infrared calibration curve for isotopic methyl benzoate ratios.

ANALYSIS OF NONDISTILLABLES FROM COAL LIQUIDS BY SIZE EXCLUSION CHROMATOGRAPHY/FOURIER TRANSFORM INFRARED SPECTROMETRY (SEC/FT-IR)

C. V. Philip and R. G. Anthony

Kinetics, Catalysis and Reaction Engineering Laboratory
Department of Chemical Engineering, Texas A&M University
College Station, Texas 77843

INTRODUCTION

Coal liquids may contain as much as 50% or more nondistillables. Most of the nondistillable materials are soluble in solvents such as tetrahydrofuran (THF) or pyridine. Currently, the nondistillables are characterized by elemental analysis, nuclear magnetic resonance (NMR), Fourier Transform infrared (FT-IR) spectrometry and heating values. The nondistillable and distillable fractions of a coal liquid can be separated and analyzed by size exclusion chromatography (SEC) (1-8). SEC separates molecules based on "linear molecular" size (3,4). The application of SEC is limited only by the solubility of the sample in a solvent. Although SEC has been used primarily for the separation and characterization of polymers based on molecular size or molecular weight, its use has been extended to the separation of smaller size molecules (10-13).

The separation of coal liquids by SEC is easily achieved with appropriate columns. Because coal-derived mixtures have several components of a similar size, the use of SEC alone is not adequate for the purpose of identification. Gas chromatography (GC) coupled with mass spectrometry (MS) has been used in conjunction with the SEC (14,15,16). The use of these three analytical techniques [SEC, GC, and MS] is a powerful analytical method for the analysis of the distillables of coal liquids, recycle solvents and anthracene oils (14, 15, 16).

Analysis of SEC fractions of nondistillables by FT-IR spectrometry is very useful in characterizing the coal liquids produced under different reaction conditions. Conventional FT-IR techniques are rather unreliable as well as time consuming, because the mass of coal liquid in a SEC fraction is very small. A new technique, which is more reliable and requires less time than the conventional techniques, is developed for the analysis of small samples. The residues from SEC fractions are spotted onto a potassium bromide (KBr) pellet. The spotted samples are then analyzed using a narrow focused beam in the Microbeam accessory of a Nicolet 60 SXR FT-IR spectrometer. The paper discusses the analytical technique as well as the FT-IR spectra of SEC fractions.

EXPERIMENTAL

The low rank coal used in the liquefaction experiments (15) was Zap-2 Indian Head lignite from North Dakota. Minireactors (6.3 and 20 *ml*), which were made from Autoclave high pressure fittings (7) were used. The liquefaction solvents included anthracene oil and water under supercritical conditions. Hydrogen, carbon monoxide and hydrogen sulfide were the reactive gases. The experimental conditions are listed in Table 1, and the yields are listed in Table 2 (15).

Coal liquids from these experiments were separated by distillation at 230^{o}C and 1 Torr. The nondistillables were dissolved in THF and separated using a 60 cm long, 5 um, 10 nm PL gel column and THF as the mobile phase. The effluents were monitored by a Waters refractive index detector (Model 401). The SEC fractions were collected as one *ml* fractions. Most samples were separated into

10 fractions. The THF in these fractions was evaporated using a slow dry stream of nitrogen and occasionally warming the vials with warm air from a hot air blower. The residues were used for FT-IR analysis.

A Nicolet 60SXR FT-IR Spectrometer with Microbeam accessory and a MCT-A detector was used for the FT-IR analysis. The samples were dissolved in 2-5 *ml* and spotted on a 13 mm potassium bromide (KBr) pellet (100 mg) using a 5 *ml* syringe with a fused silica needle. The pellets were dried on a hot plate. Six 1-2 mm diameter sample spots were deposited on each KBr pellet. Each pellet was scanned using a motorized sample stage which is both manual and computer software controllable. The Microbeam accessory is used to focus the IR beam either manually or by the 60 SXR software. A narrow beam (0.1 mm dia.) was used for the analysis. The Microbeam accessory enables analysis of a sample as small as 0.1 mg with good absorption spectrum with about 2 absorbance unit for the largest peak. Absorptions due to water vapor and CO_2 were subtracted from all spectra. The spectra were subjected to baseline correction as well as the normalization of the largest peak to 2.00 absorbance units.

RESULTS AND DISCUSSIONS

The coal liquids contained substantial amounts of nondistillables, which varied depending on the reaction conditions. Figure 1 shows the distribution of various chemical species in a coal liquid. A coal liquid from Wyodak subbituminous coal is used for the illustration.

One of the major results of SEC-GC-MS analysis of the distillables is the discovery of an orderly pattern (14,15,16), by which various isomers and homologues of similar chemical species exist in coal liquids. Direct coal liquefaction produces chemical species, which differ from each other by size and extent of isomerization but with an orderly continuous pattern. Alkanes ranging from $C_{12}H_{26}$ and $C_{44}H_{80}$ are detected in almost any coal liquid. Most of these are straight chain alkanes showing an orderly continuous pattern. Neither is a particular n-alkane almost absent nor is it present in a disproportionate amount. Exceptions exist for some branched alkanes such as pristine, phytane, and hopanes. These species are also called biomarkers and their concentration varies depending on the sample. The nondistillable fraction of coal liquids are expected to contain larger alkanes as a continuation of the alkane pattern. Since alkanes larger than $nC_{44}H_{80}$ are almost insoluble in THF, their presence in THF soluble nondistillables is limited and they may exist as nondistillables in the THF insoluble fractions.

Phenols are a major group of species present in coal liquids and have basically one or more aromatic ring structures with alkyl substituents. Methyl, ethyl and propyl are the most common alkyl substituents (14,15,16). The number of possible isomers increases as the possible number and size of alkyl substituents increases. It is expected that higher degrees of alkylation can produce larger molecules with a greater number of isomeric forms. Separation of these isomers is rather difficult even by high resolution GC methods. The larger phenols should be present in the nondistillables. If pattern observed for the distillables is continuous, the phenols are heavily alkylated and may contain other functional groups including additional hydroxy groups. SEC can separate these phenols based on "linear size" (length obtained from valence bond structures), and FT-IR gives an insight into the structural details. Interpretation of the FT-IR is difficult (17-20) and requires extensive use of the literature as well as conformation from other analytical methods.

The number of isomers of alkylated aromatics is enormous. Increased alkylation causes an increase in the number of isomers. In the case of both alkylated phenols and aromatics various isomers exist in a continuous pattern

(14,15,16). A low amount of alkylation gives a few well-resolved isomers. For aromatic species which have been extensively alkylated a large number of isomers are produced but in small concentrations. The two types of aromatics are expected in the nondistillables. Polycyclic aromatics such as pyrenes and corones are the first type which appear in SEC fraction 10. The second type is the alkylated aromatics which are heavy due to size and number of alkyl side chains. The trend in distillables indicates that the number of possible isomers is enormous. The use of FT-IR with SEC allows one to identify the functional groups for molecules with a known linear molecular size.

The THF soluble nonvolatiles shown in Figure 1 represent the nondistillables in a coal liquid. If we assume that the heavy alkanes are insignificant due to their limited THF solubilities, the nonvolatiles contain two major chemical species, i.e.alkylated phenolics and aromatics. Phenolic species will be found in the first few SEC fractions and the aromatics in the last few fractions.

Figures 2-4 illustrate the separation of three coal liquids by SEC. By using the Microbeam accessory on the FT-IR and the new technique, the small samples in the SEC fractions are readily analyzed. The Microbeam accessory is used to focus the IR beam to less than 0.5 mm diameter, and analyze small samples deposited as spots on a KBr pellet. This technique allows the analysis of up to six sample spots on a single 13 mm diameter pellet. Another advantage of this technique is that the area between the spots on the pellet is used for background subtraction to eliminate the absorptions from contaminants in the pellet such as absorbed water.

FT-IR has been used to characterize spectroscopic analysis of complex substances such as coal, oil shale, petroleum crude and various products derived from them (18-20). These fossil fuels as well as coal liquids are composed of various species with functional groups whose characteristic absorption bands may overlap and interfere with the interpretation of the spectra. We have shown (3,4) that SEC separates molecules on the basis of linear molecular size, and that the phenolics hydrogen bond with the THF. Thus SEC with THF solvent is capable of separating phenolics and aromatics. Therefore, SEC separation prior to FT-IR analysis is used to resolve some of the uncertainties associated with spectral interpretation.

Figure 5 shows the FT-IR spectra of 10 one ml SEC fractions of nondistillables from a liquefaction reaction in where water under supercritical conditions was used as the solvent along with reactive gases such as H_2, CO and H_2S (See Table 1 & 2 for experimental conditions and product yields). Most reports on FT-IR analysis of coal points out the difficulties associate with the interpretation of the spectrum. A good discussion about the band assignments of functional groups found in coal and coal liquids is presented in a recent paper (19). Figure 6 shows the SEC/FT-IR analysis of anthracene oil distillate which was also used as solvent for liquefaction experiments. The effect of reaction time on the SEC/FT-IR data for the nondistillables produced when using anthracene oil distillate and water under supercritical conditions is illustrated in Figure 7.

Comparison of Figures 1,2,3 & 4 shows that any coal liquid sample can be separated over a 10 ml THF flow time. The first five fractions contain most of the nondistillables and the latter five fractions have most of the distillables.

The broad absorbing peak at 3400 cm^{-1} in all spectra shown in Figures 5-7 indicate the species with phenolic or alcoholic hydroxy groups. The nondistillables from all four liquefactions experiments have species with hydroxyl group in the first six SEC fractions. SEC fractions 7 through 10

showed smaller amounts of phenols in two experiments(TEH 11 & 22) and very little in the other two experiments (THE 13 & 23). The product from the two short reaction time experiments (TEH - 13 and 22) have a larger broad peak at 3400 cm^{-1} indicating more large molecular size phenols than the product produced in the two longer reaction time experiments (TEH 11 and 23). The absorption due to the phenolics reaches a maximum for SEC fraction 6 for two runs (TEH 22 & 23) where supercritical water was the solvent, and at SEC fraction 4 for one run (TEH-11) where anthracene oil and long reaction time were used. Short reaction time experiment (TEH-13) with anthracene oil followed an intermediate trend. The absorption at 2900 cm^{-1} due to alkyl groups maximized in SEC fraction 5 for all coal liquid samples.

The broad absorption peak at 1700 cm^{-1} is due mostly to various carbonyl groups. Short reaction time experiments (TEH-13 & 22) showed an increase in the amount of carbonyl groups in SEC fractions 2-5 as indicated by the single broad peak at 1700 cm^{-1}. Longer reaction time experiments (TEH 11 & 23) show smaller absorptions in SEC fractions 2-5 with a split broad peak. Longer reaction time experiment (TEH-11) showed an increase in the amount of carbonyl absorption in SEC fraction 6-10, compared to the shorter reaction time experiment (TEH -13). The absorption at 1600 cm^{-1} appears to be due to aromatic species with substituents such as alkyl, carbonyl and hydroxy groups. These species did not show any trend in any of the SEC fractions, or with reaction conditions.

CONCLUSION

The use of Microbeam accessory and the spotting of the sample on the KBr pellet enables the study of small samples of coal liquids by FT-IR combined with SEC. The analysis time is short and reproducible. The complex and unknown chemical composition of nondistillables in coal liquids makes the determination of the chemical significance of each IR absorption peak rather difficult. This is particularly the case with the limited number of experiments used in this report. But it appears that the nondistillables and distillables contain species with similar functional groups. The determination of the structure of nondistillables may be possible by use of the FT-IR data, and by extrapolation, using the known chemical nature of major species in distillables.

ACKNOWLEDGEMENTS

The financial support of this project by the Center for Energy and Mineral Resources, a Texas A&M University agency is very much appreciated. Mr. Terry Helton conducted all the liquefaction experiments, and Ms. Joan Perry separated nondistillable samples into fractions by size exclusion chromatography. The authors acknowledge their professional help. The Energy Research Center at University of North Dakota furnished lignite samples and the anthracene oil for the study.

REFERENCES

1. Philip, C. V., Anthony, R. G., *Fuel Processing Technology*, 1980, 3, p. 285.
2. Zingaro, R. A., Philip, C. V., Anthony, R. G., Vindiola, A., *Fuel Processing Technology*, 1981, 4, 169.
3. Philip, C. V., Zingaro, R. A., Anthony, R. G., Ed. Sullivan, R. F., *ACS Symposium Series No. 156*, 1981; p.239.
4. Philip, C. V., Anthony, R. G., *Fuel*, 1982, 61, 351.
5. Philip, C. V., Anthony, R. G., *Fuel*, 1982, 61, 357.
6. Philip, C. V. and Anthony R. G., "Size Exclusion Chromatography", Ed. Prouder, T., *ACS Symp. Series*, 1984, 245, 257.
7. Philip, C. V., Anthony, R. G. and Cui, Z. D., Chemistry of Low-Rank

Coals, Ed. Schobert, H. H., *ACS Symp. Series*, 1984, 264, 287.
8. Philip, C. V., Bullin, J. A. and Anthony, R. G., *Fuel Processing Technology*, 1984, *9*, 189.
9. Philip, C. V. and Anthony, R. G. *Chromatographic Science*, 1986, *24*, 438.
10. Hendrickson, J.G., *Anal. Chem.*, 1968, 40:49.
11. Majors, R.E.J., *Chromatog. Sci.*, 1980, 18, 488.
12. Caze, J. and D. R. Gaskill, *Sep. Sci.*, 1969 4, 15.
13. Krishen, A. and R. G. Tucker, *Anal. Chem.*, 1977 49, 898.
14. Philip, C. V., Moore, P. K., and Anthony, R. G. Advances in Size Exclusion Chromatography, *ACS Symposium Series*, 1987, 352, 183.
15. Anthony, R. G., Philip, C. V. and Moore, P.K., Final Technical Report for Low Rank Coal Liquefaction, March 15, 1983 - October 31, 1986, DOE/FC/1060-13.
16. Philip, C. V., and Anthony, R. G. *Am. Chem. Soc. Div. Fuel Chem. Preprints*, 1987, 32, 368.
17. Soloman, P. R., Carangelo, R. M. and Horn, E., *Fuel*, 1986, 65, 650.
18. Soloman, P. R., and King, H. H., *Fuel*, 1984, 63, 1302.
19. Cooke, N. E., Fuller, O. M. and Gaikwad, R. P., *Fuel*, 1986, 66, 1255.
20. Painter, P. C., Snyder, R. W., Starsinie, M., Colman, N. M., Kuehn, N. W., and Davis, A., *Applied Spectroscopy*, 1981, 35, 475.

Table 1. Liquefaction conditions

Run No.	Temp. (K)	H_2 (%)	CO (%)	H2S (%)	Time (min.)	Max P (MPa)	Solvent
TEH-11	681	38.4	44.1	17.5	22.8	29.2	A04
TEH-13	690	38.4	44.1	17.5	4.4	23.2	A04
TEH-22	695	33.2	41.8	25.0	4.5	34.6	H_2O
TEH-23	695	33.2	41.8	25.0	19.8	34.6	H_2O

Table 2. The Percentage yields based on dmmf lignite.

Run No.	NDTHFS	Distillables
TEH-11	30.40	49.93
TEH-13	50.76	6.79
TEH-22	33.04	16.38
TEH-23	47.22	18.58

THF = Tetrahydrofuran, NDTHFS = THF soluble nondistillables.

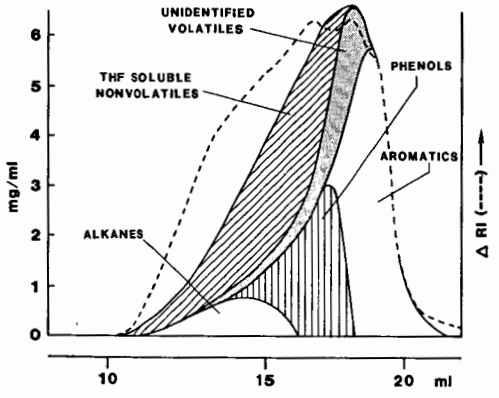

Fig. 1 SEC separation of Wyodak recycle solvent. The reconstructed chromatogram is shown to illustrate the size distribution various chemical species.

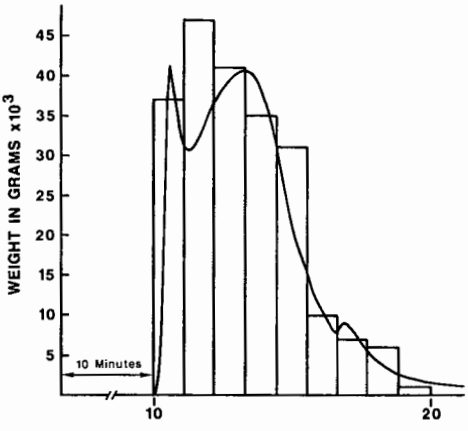

Fig. 3 SEC separation of THF soluble nondistillable from liquefaction experiment TEH-11. The solid curve shows the ΔRI responded.

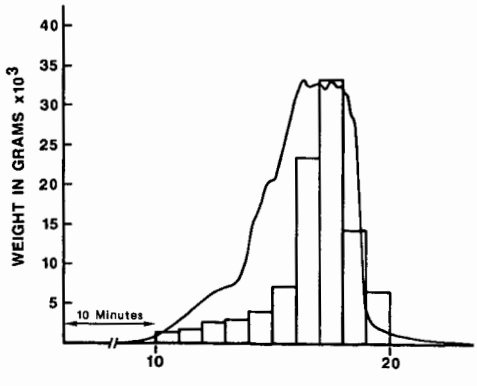

Fig. 2 SEC separation of Anthrazene oil which was used in liquefaction experiment TEH-11. The solid curve shows the ΔRI responded.

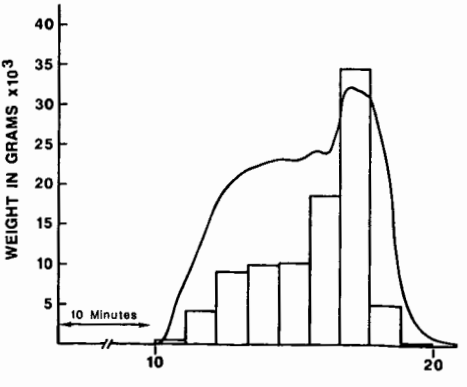

Fig. 4 SEC separation of THF soluble products from liquefaction experiment TEH-11. The solid curve shows the ΔRI responded.

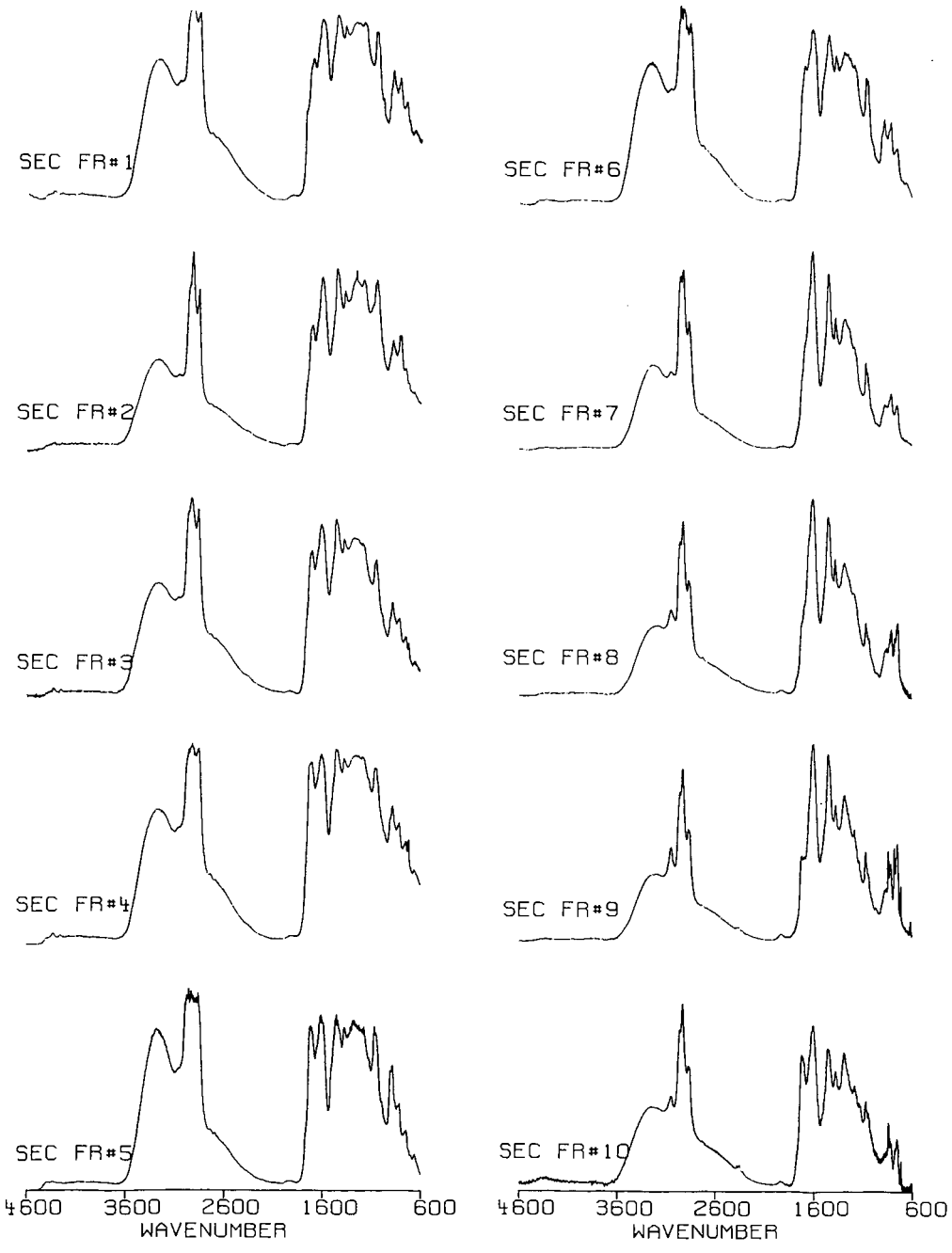

Fig 5. FT-IR spectra of SEC frs. of nonvolatiles from Zap-2 lignite liquefield using water under supercritical condition. See Table 1 & 2 for the reaction conditions & yield of TEH 22.

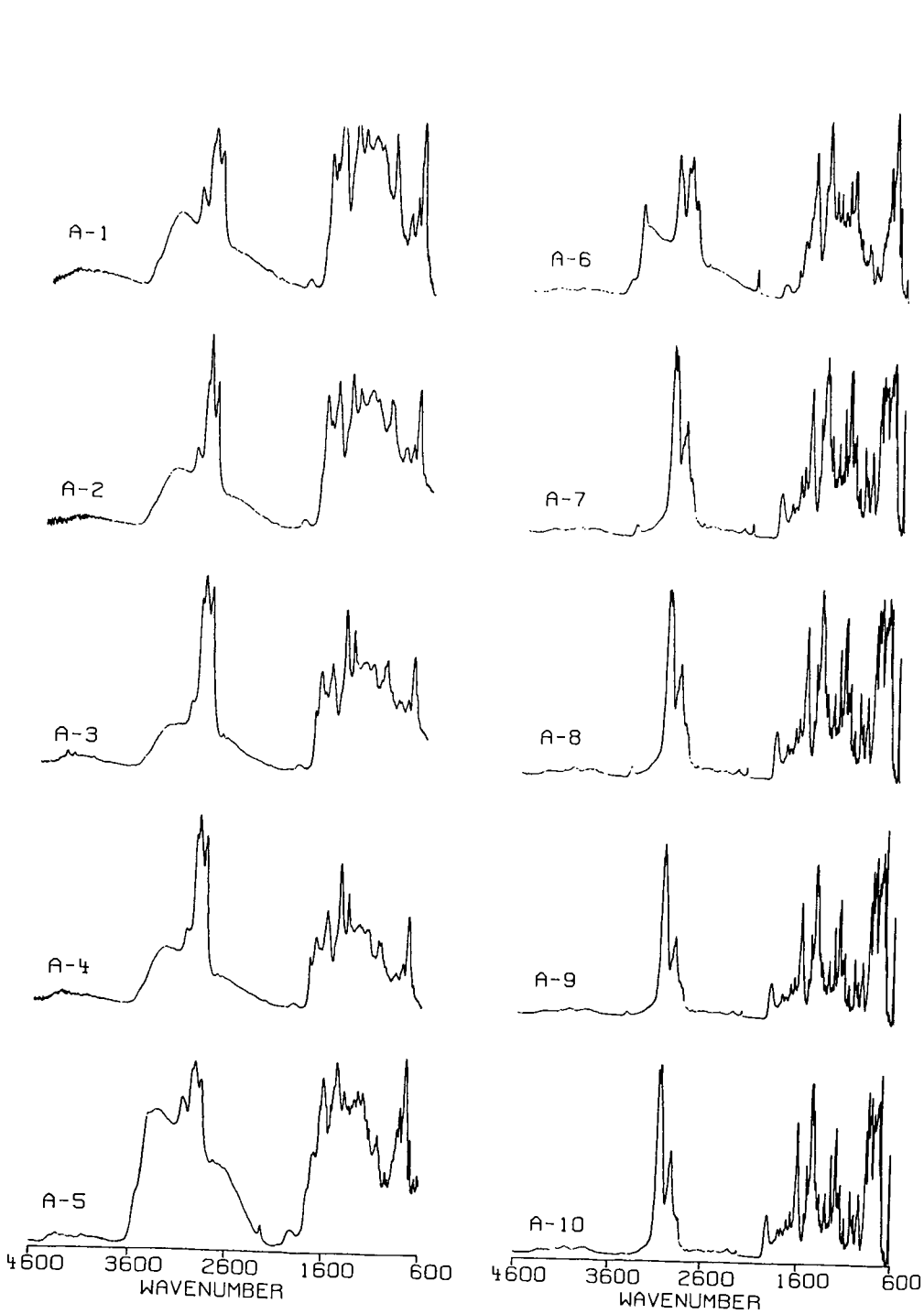

Fig 6. FT-IR spectra of SEC fractions of Figure 2 Anthracene oil distillate (A04). Figure 2 shows the SEC of A04.

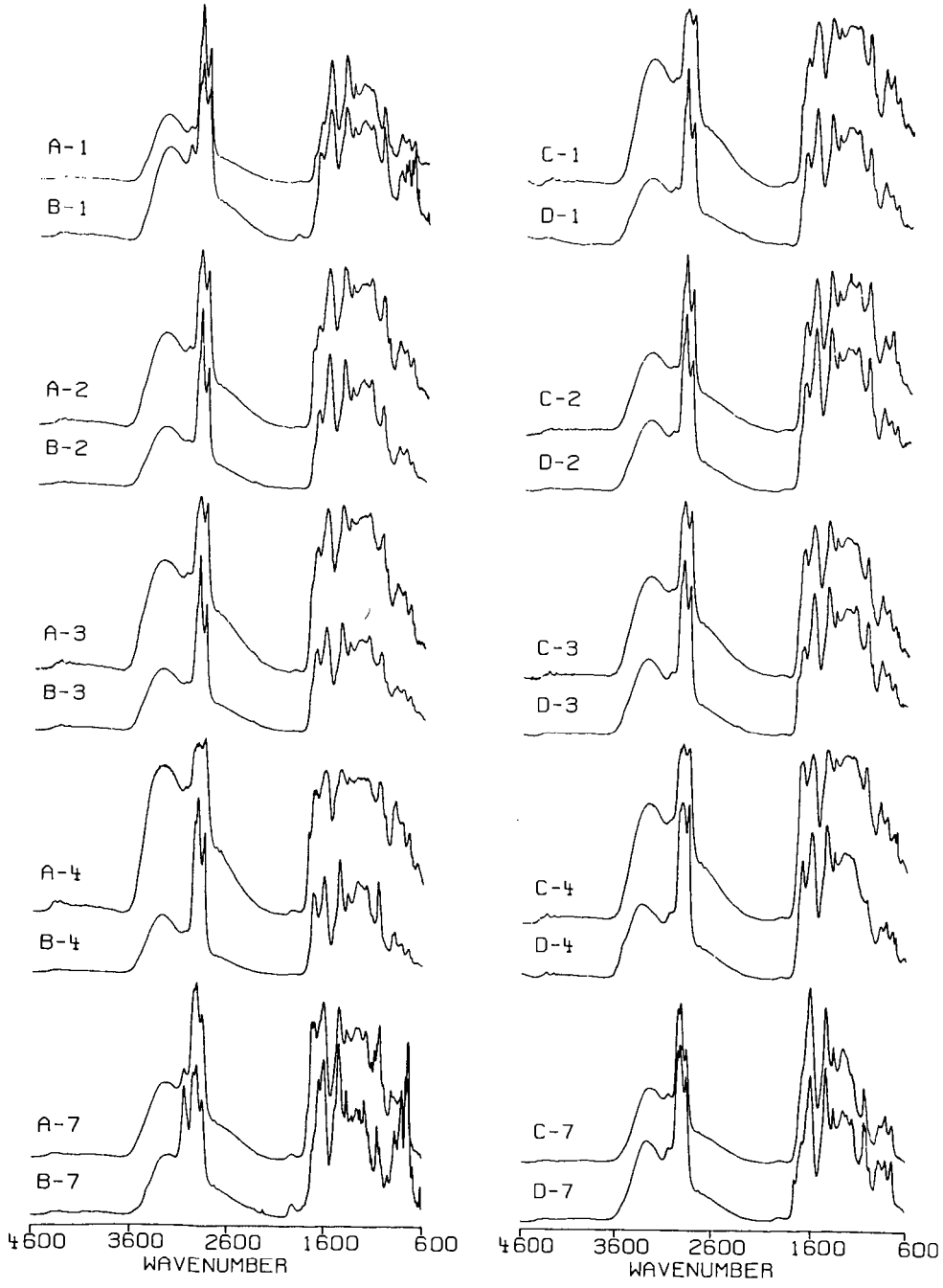

Fig 7. Comparison of FT-IR spectra of SEC fractions of non distillate obtained from four liquefaction experiments - A = TEH 13 and B= TEH 11 c= TEH 22 and D=TEH 23.

Luminescence in Coal. The Effect of Mineral Matter, Air, and Swelling

Rita K. Hessley

Department of Chemistry, Western Kentucky University, Bowling Green, KY 42101

Introduction

Based on the work of Coyne et al (1), who showed that simple dehydration of clay minerals results in measurable spontaneous emmission of light, we have undertaken the investigation of spontaneous light emmission in coals (2). Coal is frequently found in regions where clay minerals are abundant. Following Coyne, our initial study (2) monitored light emission from coal when an aqueous slurry of micronized coal was subjected to dehydration over $CaSO_4$. That work showed that luminescence did occur in a coal containing relatively little inorganic material (3% ash) as well as in a coal with a substantially higher (18%) content of mineral matter.

Several questions arose from that study. In particular, because the addition of as little as 1-2% (w/w) kaolinite to a coal sample exhibited a marked increase in luminescence, it was critical to determine, if possible, whether the photon release was caused only by the mineral matter content and not by the effect of dehydration on the coal structure itself. Thus, one goal of this phase of the investigation was to look for spontaneous luminescence in ash-free coal.

A second question was whether the phenomenon was related to, or dependent upon, excitation of the oxygen or nitrogen in air. Thus, the second goal of this work was to examine samples prepared with the exclusion of air.

Finally, Coyne et al (3) have also shown that kaolinites exhibit pronounced spontaneous luminescence as they swell in a slurry prepared with various amines. Because coal, also, generally swells readily in amine solvents, several measurements were carried out to determine whether coal luminescence could be detected as a function of solvent swelling.

EXPERIMENTAL

Preparation of Samples

The coal used for this study is a Western Kentucky hvA bituminous coal obtained from the Western Kentucky University Center for Coal Science. A summary of the analysis of the coal is given in Table I.

Table I

Analysis of Coal Bank Sample #86025

Moisture(as det.)	4.07	Carbon	66.74
Ash	15.50	Hydrogen	4.59
VM	35.3	Nitrogen	1.42
fixed Carbon	49.2	Sulfur	4.55
BTU	11,012	Oxygen(diff)	6.71

A portion of the 60-mesh coal was beneficiated in $ZnCl_2$ media of specific gravity 1.30. After cleaning, the recovered coal was micronized for 2 minutes in a Union Process Model 1-S stirred ball attritor mill. This effectively reduced the average particle size of the sample to 10 microns. Unbeneficiated 60-mesh coal was subjected to exhaustive solvent extraction with refluxing Dimethylformamide (DMF) under N_2. The

residue was then washed repeatedly with refluxing methanol under N_2 before being dried in a vacuum oven. The extracted material was recovered from the DMF and was also washed, and dried in vacuo.

The ash from the same coal was obtained according to ASTM D3173. The ash analysis is shown in Table II.

Table II

Major and Minor Metal Oxides in Ash from Coal Bank Sample #86025

	Raw	Clean
% SiO_2	42.9	41.4
% Al_2O_3	16.3	19.7
% Fe_2O_3	33.3	21.2
% CaO	1.10	.61
% MgO	.51	.33
% K_2O	1.46	1.10
% MnO_2	.04	.01

Measurement of Luminescence

Spontaneous luminescence was measured as a function of time. Single photon monitoring was carried out using the Packard Model 1500 "TriCarb" liquid scintillation counter. Data were recorded as counts per minute and were printed at one minute intervals for 99 minute maximum monitoring period.

A sample slurry was prepared by direct weighing and mixing of the solid and water. Typically, a coating of about 2.5 cm was applied to the inside of a standard scintillation vial above about 1 cm of indicating $CaSO_4$. For all trials, the slurry was applied manually and it was difficult to apply precisely the same amount of sample each time. Generally, 80-120 mg samples were used which consisted of at least a water:coal ratio of 2:1. For swelling experiments, the method described by Coyne (3) was used to prepare the samples. Pyridine and DMF were used as the swelling solvents. To prepare samples in an air-free environment, a stream of argon was used to purge the vial prior to and during application of the slurry.

RESULTS AND DISCUSSION

Figure 1 shows a portion of the photon output for the dehydration of the whole coal #86025 (15.5% ash). As in our previous study, the photon count was observed to decay monotonically until spontaneous luminescence occurred at some time after initiation of drying. Figure 2 shows data for the beneficiated sample (1.25% ash). These data confirm our earlier observations that even low ash coals exhibit luminescent behavior. Figure 3 shows that extraction residue, which retains most if not all of the inorganic matter in coal, also displays spontaneous luminescence during dehydration. The traces in these figures cannot be compared directly with regards to the time required for the on-set of photon emmission nor with regards to the intensity. Our earlier work showed that time and intensity differences between samples are dependent on the sample size (thickness) and total moisture content.

Figure 4 shows the trace of counts per minute with time for the material extracted from coal with refluxing DMF. This material is essentially ash-free, and shows no spontaneous luminescence during the period monitored. This is striking evidence that ash-free coal does not exhibit luminescent behavior. Of course, the extract from additional samples needs to be studied in order to confirm this observation conclusively. Measurement of photon emmission in recovered ash (Figure 5) was difficult to measure and was not nearly as impressive in its intensity as is

observed with kaolinite (1). The ash was very granular and difficult to grind sufficiently fine to prepare a smooth paste. It may also be important that the ash obtained from the coal used in this study was brick-red and contained 33.3 % (w/w) Iron oxide and, correspondingly, a smaller quantity of aluminum and silicon oxides. For comparison, the luminescence during dehydration for a coal ash containing much less iron oxide (based on its white coloration) was recorded and is shown in Figure 6. These data suggest that photon emmission from ash may be affected by its overall composition.

All attempts to induce measurable photon emmission in either whole coal or coal extract by solvent swelling have been unsuccessful. One explanation is that the small (mg) quantities of coal being used swell rapidly enough in the two amine solvents tested that luminescence accompanying swelling may be dissipated in the time required to grind and prepare the sample (3). These experiments are being continued using other, less vigorous, swelling solvents.

Using kaolinite, there is no change observed for spontaneous luminescence in samples prepared under argon. However, there remains some question whether the sample vials are air-tight throughout the counting period. Thus, our initial trials to determine the effect of air on the presence and intensity of spontaneous luminescence in coal are incomplete.

CONCLUSIONS

It has been shown that spontaneous luminescence in coal during dehydration is dependent directly on the ash, or mineral matter content of the coal. In the absence of any ash, no photon emmission is observed. Coal extraction residue retains the property of luminescenc during dehydration; coal ash also exhibits luminescence, but appears to be affected strongly by the presence of iron oxide (or by the actual clay mineral content). Quantities of ash as small as a few percent by weight dispersed throughout the coal matrix are sufficient to cause the phenomenom to be observable. Work is continuing to explore the effects of air and solvent swelling.

REFERENCES

1. Coyne, L. M., N. Lahav and J. G. Lawless, Nature, 292, 27 August, 819 (1981); Lahav, N., L. M. Coyne and J. G. Lawless, Clays Clay Miner., 30(1), 73 (1982).

2. Hessley, R. K. and L. M. Coyne, Preprints, Amer. Chem. Soc. Div. Fuel Chem., Denver, 32(1), 547 (1987).

3. Coyne, Lelia M., Glenn Pollack and Roger Kloepping, Clays Clay Miner., 32(1), 58 (1984).

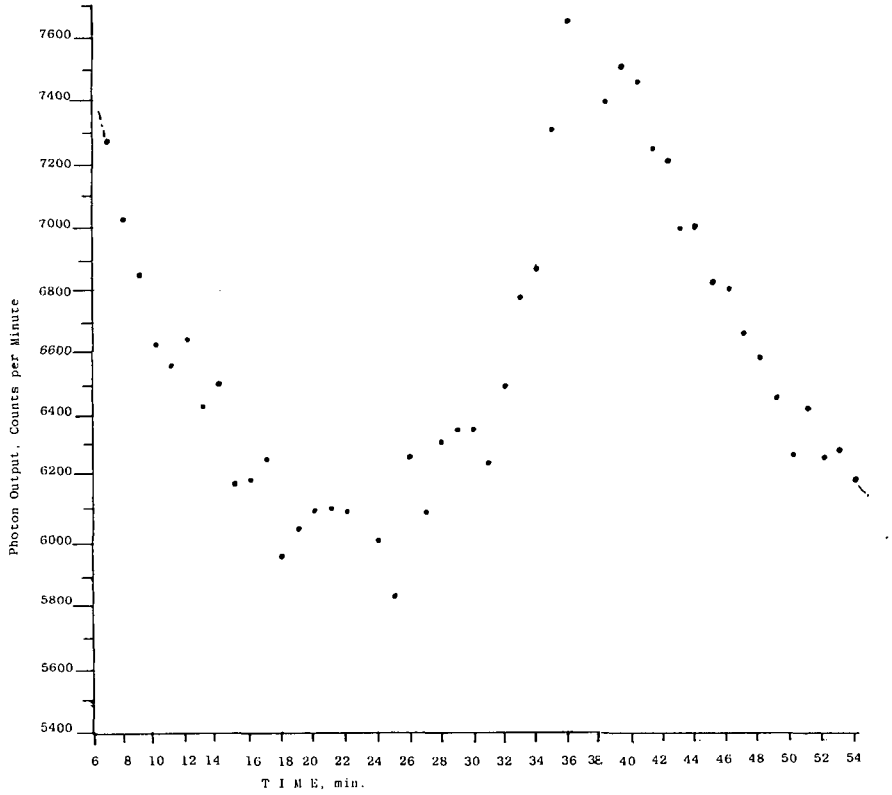

Figure 1. Photon output for Dehydration of whole coal (15.5% ash)

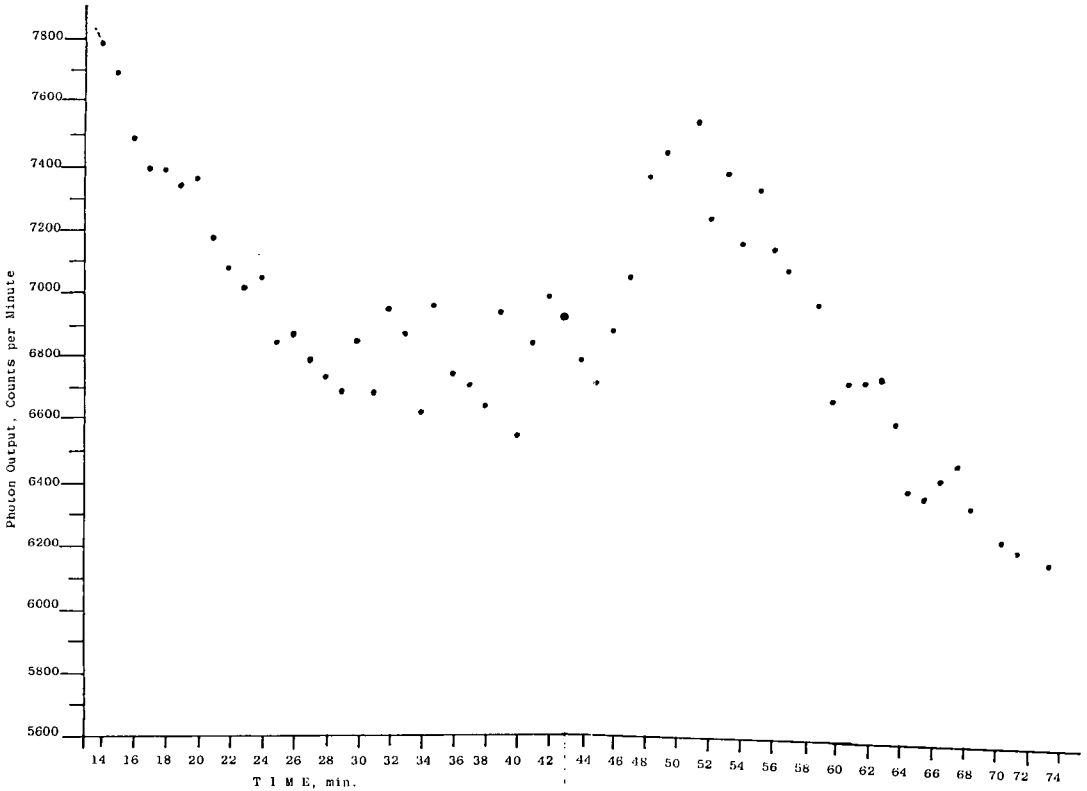

Figure 2. Photon Output for Beneficiated coal (1.25% ash).

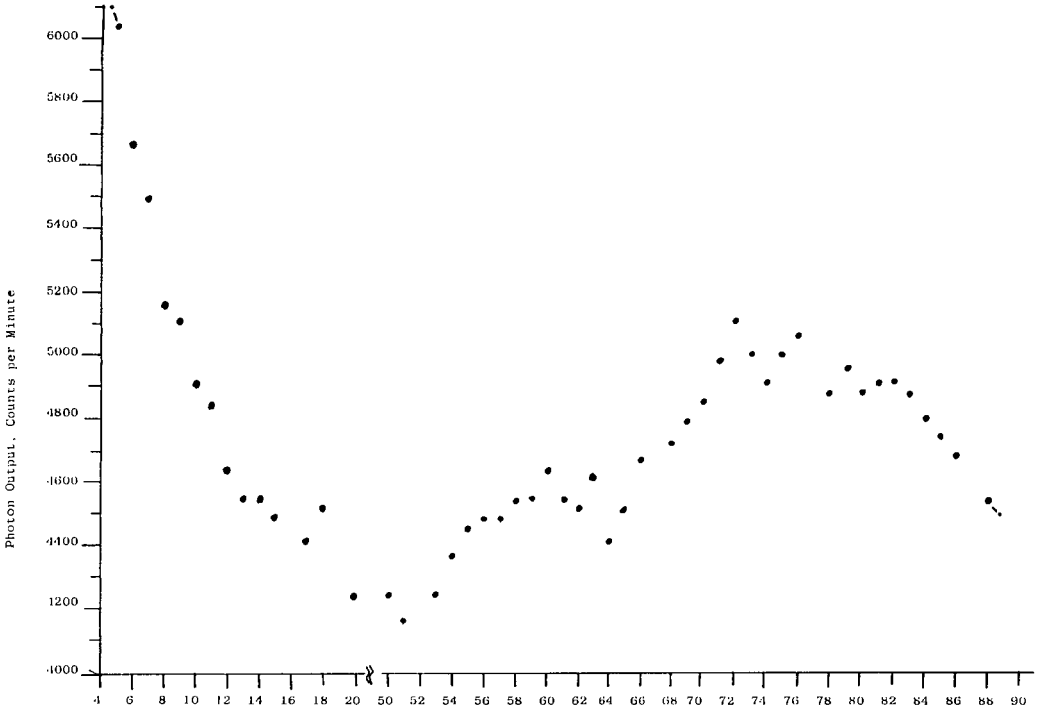

Figure 3. Photon Output on Dehydration for Coal Extraction Residue

Figure 4. Photon Output for Dehydration of Whole Coal Extract

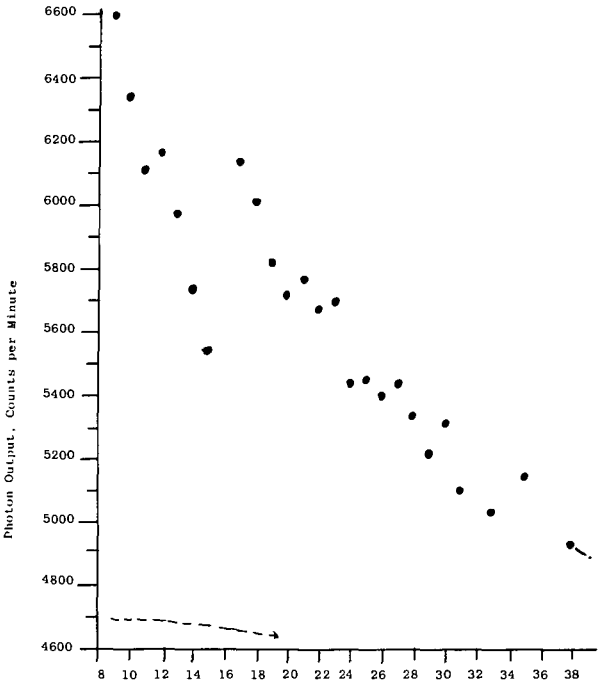

Figure 5. Photon Output for Dehydration of Recovered Coal Ash

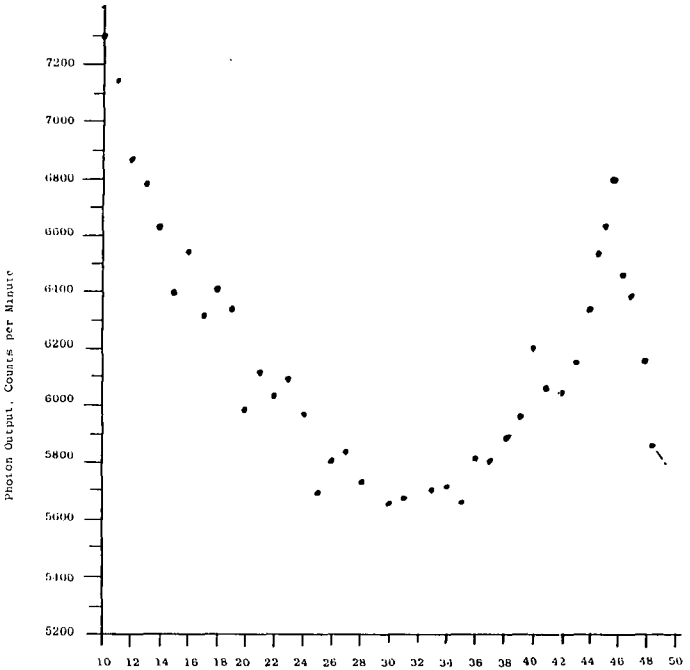

Figure 6. Photon Output for Dehydration of a Low-Iron Ash

DETERMINATION OF COMPOUND CLASS COMPOSITION OF OIL FRACTIONS OF SOME COAL LIQUIDS BY ANALYTICAL LIQUID CHROMATOGRAPHY

B. Chawla and B. H. Davis

Kentucky Energy Cabinet Laboratory
P. O. Box 13015
Lexington, KY 40512

ABSTRACT

A high-performance liquid chromatography method was developed to determine the amount of each of the compound classes (such as saturates, aromatics and polars) in the oil fraction (pentane soluble fraction) of coal liquids. The method utilizes bonded cyanosilane and aminocyanosilane columns and mixtures of benzene in n-hexane and tetrahydrofuran in methyl tert-butyl ether as mobile phases. A Tracor LC-rotating disc flame ionization detector was used to quantify the chromatographic peaks.

Oil fractions derived from different rank coals, liquefied at 385° and 445°C, were analyzed for their compound class compositions. The trends in the percentages of saturates, aromatics and polars varied with liquefaction temperature and coal rank.

INTRODUCTION

The products from coal liquefaction processes are so complex that it is almost impossible to completely analyze them. Therefore, following a practical approach widely used with petroleum, the coal liquids are divided into solubility classes such as: (i) oils - pentane soluble, (ii) asphaltenes - benzene soluble, pentane insoluble, and (iii) preasphaltenes - pyridine or tetrahydrofuran (THF) soluble, benzene insoluble.

To obtain data suitable for mechanistic considerations, it is essential that fractions or classes of compounds obtained from coal liquefaction processes be quantitatively analyzed in more detail. Such efforts have been made recently, but there remains much to be learned about the compositions of these three solubility classes of coal products. A commonly used method for separation and/or analysis of the coal liquids is based on liquid chromatographic fractionation in terms of major components such as saturates, aromatics, more polar aromatics (non-basic N, O, S - heterocyclics), monophenols, basic nitrogen heterocyclics, polyphenols, and non-eluted unidentified materials.

One method was developed in 1976 by Farcasiu (1); it has also been used recently by Winans et al. (2) to characterize materials extracted, using benzene-methanol as a solvent, from several Argonne Premium Coal Samples. To understand the liquefaction behavior of a number of coals, separations of oil, asphaltene and preasphaltene fractions of coal liquids have also been reported (3-12). However, these chromatographic techniques are laborious and time consuming. To the best of our knowledge, the high-performance liquid chromatography (HPLC) coupled with the LC-Flame Ionization Detector (FID) have not been used for characterization and/or quantitation of coal liquids.

The purpose of our investigation was to adopt an analytical HPLC technique for separation and quantitation of oil fractions (pentane-soluble) of coal liquefaction products in terms of three compound classes such as saturates, aromatics, and polars. To learn if our HPLC procedure was suitable for oil fractions of supposedly different compositions, we have analyzed the oil fractions obtained from the liquefaction of coals of different rank at two reaction temperatures (385°C and 445°C).

EXPERIMENTAL

The HPLC system consisted of two solvent delivery systems (Waters 6000A pumps), three Valco six-port valves, a Tracor 945 LC-FID and Nelson Analytical 3000 Chromatography System equipped with an ITT/XT computer and a Nelson Analytical Series 760 converter with a minimum detectable capability of 0.1 microvolt-second. Two analytical columns were used: a cyano column (Supelco 5 μm LC-CN, 25 cm x 4.6 mm i.d.) and an ammino-cyano column (Whatman 5 μm PAC, 25 cm x 4.6 i.d.). Mixtures of benzene in n-hexane and tetrahydrofuran (THF) in methyl tert-butyl ether (MTBE) were used as mobile phases. HPLC grade commercial solvents were used as received. However, the mobile phases were always degassed through a vacuum system just before their use. Of the several solvent flow rates that were tried, 1.0 to 1.5 ml/min was found to be the most suitable.

Following Pearson and Gharfeh's HPLC procedure (13) for the determination of hydrocarbon types in crude oil residues, we have used a rotating disc flame ionization detector (Tracor 945 LC-FID) developed by Tracor Inc. (14). The FID appears to be one of the few detectors among the various detectors used so far in HPLC procedures which tolerate a change from a nearly non-polar to a highly polar solvent system and can at the same time, be unaffected when the pressure drifts due to back and forth switching of the valves during a run.

In a typical run, the total column effluent is applied onto a fibrous quartz belt mounted on a rotating disc. As the disc rotates in the heated housing, the volatile solvent is vaporized and removed from the housing with the help of a vacuum pump. Non-volatile solutes remain on the fibrous belt and are carried into the flame where they are combusted and detected.

The operational logic of the HPLC system is shown in Figure I. During Step I, pump A (1.0 ml/min) with benzene solution in hexane was turned on. The switching valves were set in such a way that the mobile phase went first to the cyano column, then to an amino-cyano column and finally to the detector (see Figure I). This arrangement allowed the polar molecules to be retained by the cyano column and the aromatics to be retained by the amino-cyano column. About 3 to 4 minutes after the emergence of a saturates peak from the amino-cyano column, the system was switched to Step II. In Step II, the cyano column was isolated. Pump A was switched off and pump B with THF in methyl tert-butyl ether (MTBE), was operated at a flow rate of 1.0 ml/min. This arrangement allowed the retained aromatics to be backflushed from the amino-cyano column. Once the saturates and aromatics have been eluted, the system was switched to the final operation Step III where polars were backflushed from the cyano column using the THF/MTBE mobile phase. Upon completion of the separation, the system was brought back to its initial

conditions by reequilibriating the columns with benzene-hexane mixture. A typical chromatogram is shown in Figure II.

Liquefaction runs were made at two temperatures, 385° and 445°C, for 15 min. or 45 min. using tetralin as a solvent and a hydrogen atmosphere (800 psig, ambient). Typically 5g of dried coal and 7.5 g of tetralin were used for a run (see (15) for more experimental details). At the end of the experiment the reactor products were quantitatively removed and separated into three solubility classes through Soxhlet extractions. The oils were used for our HPLC analyses.

RESULTS AND DISCUSSION

A number of coals were used in this study (Table 1). They were selected to cover the rank range, based upon %C(daf) or vitrinite reflectance, that is present in the western Kentucky coals. A Breckinridge sample, an unusual coal that approaches the properties of a cannel coal, was also included in the study.

It was pointed out earlier that the FID detector could tolerate the solvent changes and the pressure drifts employed in the study. However, it is necessary to determine a relative response factor (ions produced/unit mass) for the various compound classes of the oil. In order to accomplish this, it was important to have aliphatics, aromatics and polars with compositions that are similar in chemical compositions as those of these components in the investigated oil fractions. The oil fractions obtained from coal liquefaction runs contained about 90-95% tetralin, the solvent used in this reactions; the preparative liquid chromatography of these samples over silica gel was not fruitful. Therefore, the oil fraction of a sample (V-1064) from the first stage reactor of the Wilsonville, Alabama coal liquefaction plant was used to carry out a larger scale separation.

The LC separation was performed using freshly activated silica gel (400°C overnight) and hexane, benzene and THF as the mobile phases. Hexane was used to elute the aliphatics from the column and 15% benzene in hexane was used to elute the aromatics. Finally, the column was backflushed with THF to obtain a polar fraction. The aliphatic, aromatic and polar fractions were tested for completeness of separation with the analytical HPLC procedure described in this report and were found to be of acceptable purity ($>$98%). A GC of the aliphatic fraction showed that it contained C_{15} - C_{37} hydrocarbons; these were mostly normal alkanes. Alkanes with a carbon number greater than C_{37} are present in very small amounts. Other components were not detected in any significant amount.

The absolute response factors for saturate, aromatic and polar fractions were obtained from the slopes of the linear plots (Figure III) of the peak areas versus their mass (over a range of concentration of 0-20 μg/μl). Their relative response factors, as area/mass, are in the ratio of 1:2.16:1.23 for saturates : aromatics : polars.

The precision and reproducibility of the data were established by making six repeated measurements on the separation of one of the oils used in this study. The maximum uncertainties in the weight percentages of saturates, aromatics and polars were determined to be within 2%, 2% and 4-5% respectively.

Finally, the oil fractions obtained from the liquefaction of eight coals at 385° and 445°C were analyzed. The results are presented in Table 2. The following observations may be made for the data in Tables 1 and 2:

(a) The relative aliphatic percentages decrease with an increase in reaction temperature for all the coals studied with the exception of Breckinridge coal sample which shows the opposite effect but this is what should be anticipated for this type of coal.

(b) The aromatic percentages remained almost constant with the increase in temperature for most of the coals including the Breckinridge sample.

(c) The polar percentages increased with an increase in temperature for all the coals except the Breckinridge sample.

(d) Aliphatic, aromatic and polar percentages do not show a systematic trend with the coal rank. However, the data at 445°C (see Table 2) show that aliphatics tend to decrease with decreasing coal rank.

(e) With the exception of the Breckinridge sample, the aliphatics, aromatics and polars are generally in the ratio of 1:2:5 (Table 2).

(f) Irrespective of the liquefaction temperature, the oil fractions from the Breckinridge coal contain extremely large amounts of aliphatics (45.8% and 55.4%) small amounts of aromatics (7.8% and 7.9%) and polars (46.4% and 36.7%) compared to those of other coals (aliphatics, 9-18%; aromatics, 19-28% and polars, 55-69%).

ACKNOWLEDGEMENT

This work was supported by the Commonwealth of Kentucky, Kentucky Energy Cabinet and by DOE Contract No. DEFC 22-85PC80009 as part of the Consortium for Fossil Fuel Liquefaction Science (administered by the University of Kentucky). The Kentucky Energy Cabinet Laboratory is administered by the University of Louisville.

REFERENCES

1. Farcasiu, M. Fuel 1977, 56, 9.

2. Xia, J. J.; Neill, P. H.; Winans, R. E. ACS Div. Fuel Preprints 1987, 32(4), 340.

3. Sternberg, H. W.; Raymond, R.; Schweighardt, F. K. Science 1975, 188, 49.

4. Given, P. H.; Cronauer, D. C.; Spackman, W.; Lovell, H. L.; Davis,A.; Biswas, B. Fuel 1975, 54, 34.

5. Given, P. H.; Cronauer, D. C.; Spackman, W.; Lovell, H. L.; Davis,A.; Viswas, B. Fuel 1975, 54, 40.

6. Liphard, K. G. Chromatographia 1980, 13(10), 603.

7. Sonnefeld, W. J.; Zoller, W. H.; May, W. E.; Wise, S. A. Anal. Chem. 1982, 54, 723.

8. Whitehurst, D. D.; Butrill, Jr. S. E.; Derbyshire, F. J.; Farcasiu, M.; Odoerfer, G. A.; Rudnick, L. R., Fuel 1982, 61, 994.

9. Lucke, R. B.; Later, D. W.; Wright, C. W.; Chess, E. K.; Weimmer, W. C. Anal. Chem. 1985, 57, 633.

10. Robbins, W. K.; McElroy, F. C. Liquid Fuel Technology 1984, 2(2), 113.

11. Allen, T. W.; Hurtubise, R. J.; Silver, H. F. Fuel 1987, 66, 1024 and references cited therein.

12. Kemp, W.; Steedman, W.; Scott, D. A.; Thomson, M. A. Fuel Process. Technol. 1987, 15, 341.

13. Pearson, D. C.; Gharfeh, S. G. Anal. Chem. 1986, 58, 307.

14. Dixon, J. B. Chimie 1984, 38, 82.

15. Chawla, B.; Keogh, R.; Davis, B. H. ACS Div. Fuel Preprints 1987, 32(3), 342.

Table 1. *Coal Analysis.*

	W. Ky. #9 71154	Breckinridge 71160	W. Ky. #9 71148	W. Ky. #9 71072
1. Ash (As-Received)	30.03	6.36	14.87	9.04
2. Volatile Matter, daf	47.83	74.28	46.10	42.90
3. Fixed Carbon, daf	52.17	25.72	53.90	57.10
4. Sulfate S, daf	0.00	0.01	0.17	0.14
5. Pyritic S, daf	1.47	1.23	1.35	0.53
6. Organic Sulfur, daf	2.27	0.55	1.70	1.91
7. Total Sulfur, daf	3.74	1.81	3.22	2.57
8. Carbon, daf	84.99	80.66	79.59	79.19
9. Hydrogen, daf	6.16	8.51	5.62	5.44
10. Nitrogen, daf	1.98	2.13	1.90	2.00
11. Oxygen, daf	3.13	6.90	9.67	10.80

	W. Ky. #11 71064	W. Ky. #11 71081	W. Ky. #11 71077	W. Ky. #9 71095
1. Ash (As-Received)	9.56	4.43	9.06	14.80
2. Volatile Matter, daf	47.47	43.23	41.74	43.73
3. Fixed Carbon, daf	52.53	56.77	58.26	56.27
4. Sulfate S, daf	0.06	0.17	0.75	0.68
5. Pyritic S, daf	1.06	0.64	2.09	4.48
6. Organic Sulfur, daf	3.11	2.21	3.35	3.27
7. Total Sulfur, daf	4.23	3.01	6.19	8.43
8. Carbon, daf	78.80	78.28	76.96	76.63
9. Hydrogen, daf	5.85	5.52	5.37	5.10
10. Nitrogen, daf	1.70	1.70	1.63	1.70
11. Oxygen, daf	9.42	11.49	9.85	8.14

Oxygen by difference.

Table 2. *HPLC Analysis of Oil Fractions at 385°C and 445°C.*

		Weight %					
		385°, 15 minutes			445°C, 15 minutes		
Coal Number	**C (daf)**	**Aliphatic**	**Aromatic**	**Polar.**	**Aliphatic**	**Aromatic**	**Polar.**
71154 (W. Ky. #9)	84.99	13.2	24.1	62.7	12.8	23.3	63.9
Breckinridge	80.66	45.8	7.8	46.4	55.4	7.9	36.7
71148 (W. Ky. #9)	79.59	15.0	20.4	64.6	11.5	20.3	68.2
71072 (W. Ky. #9)	79.19	18.4	21.6	60.0	12.1	19.7	68.2
71064 (W. Ky. #11)	78.80	13.9	19.3	66.8	10.2	20.3	69.5
71081 (W. Ky. #11)	78.28	11.0	24.3	64.7	9.7	20.5	69.8
71077 (W. Ky. #11)	76.96	12.2	25.5	62.3	9.2	24.5	66.3
71095 (W. Ky. #9)	76.63	16.6	28.2	55.2	8.8	22.0	69.2

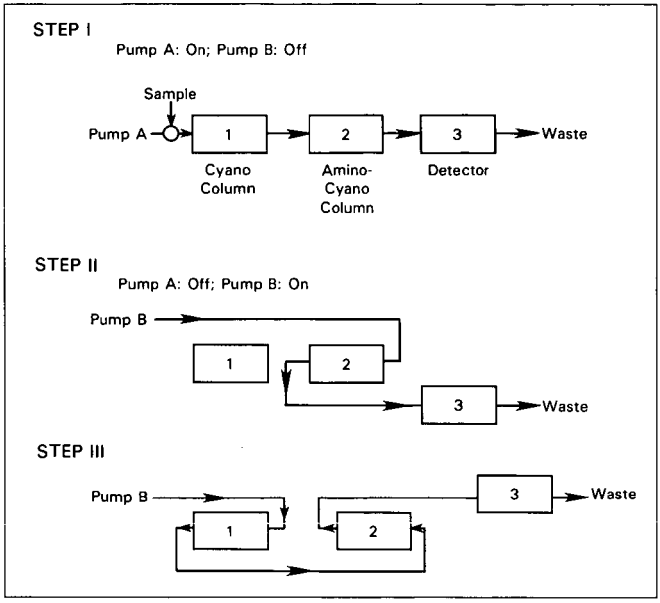

Figure I. *Operation of HPLC system.*

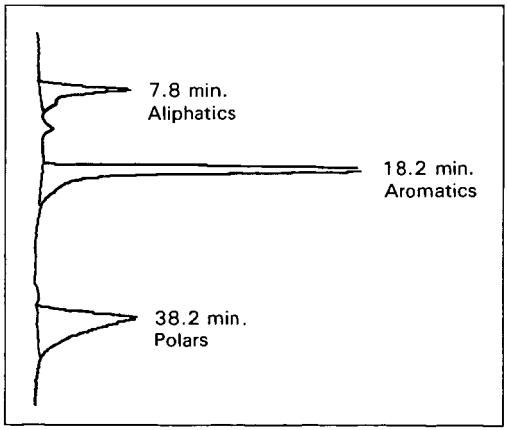

Figure II. *A typical chromatogram of an oil fraction separation.*

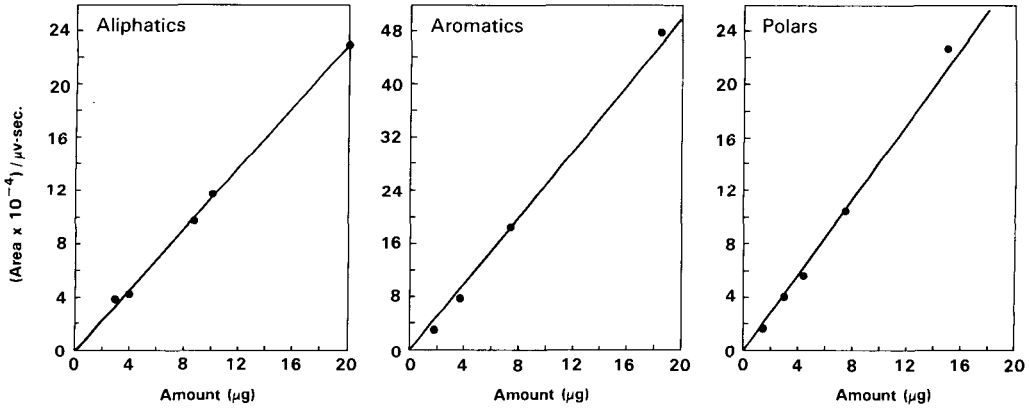

Figure III. *Calibration plots of aliphatics, aromatics, and polars.*

THE ANALYSIS OF THE ORGANIC MATTER IN CHATTANOOGA SHALE BY OXIDATION WITH PERCHLORIC ACID

Bobby J. Stanton and Chris W. McGowan

Department of Chemistry
Tennessee Technological University
Cookeville, Tennessee 38505 (USA)

ABSTRACT

A kerogen concentrate was prepared from a raw Chattanooga shale sample. The kerogen concentrate was oxidized in a stepwise fashion by varying the boiling point, and subsequent concentration and oxidizing strength of perchloric acid. The progress of the reaction was monitored with respect to the amount of undissolved material, the color of the aqueous phase, and the conversion of carbon to carbon dioxide. The dissolution of kerogen occurred between 150-180°C. The color intensity of the aqueous phase rose to a maximum, then faded to clear at 203°C. The maximum color corresponded to the dissolution of kerogen. The percentage of carbon converted to carbon dioxide was negligible when the boiling point of perchloric acid was below 150°C. Above 150°C, the carbon converted to carbon dioxide rose almost linearly. Polar unsaturated carboxylic acids were indicated as the major oxidation products.

INTRODUCTION

For some time workers have attempted to characterize the kerogen present in oil shales. Kerogen is a high molecular weight, polymeric material which is said to be insoluble in common organic solvents. In order to characterize the kerogen in oil shale, it has been necessary to destroy the kerogen by oxidative degradation of the kerogen matrix with subsequent analysis of the oxidation products. Analysis of the soluble lower molecular weight oxidation products has yielded insight into the nature of the structure of kerogen in oil shale.

Leonard (1) used 3.5 percent ozone to oxidize Chattanooga shale. Similar ether and water soluble acids were extracted from the raw shale and a kerogen concentrate prepared from the raw shale sample. The ozonization products were primarily aliphatic hydroxy acids. Ozonolysis of the kerogen of Chattanooga oil shale by Kinney and Leonard (2) yielded highly oxygenated ether and water soluble acids. Kinney and Schwartz (3) oxidized Chattanooga shale with air at 200°C for 200 hours to produce the maximum amounts of humic acids. The acids were similar to those obtained from coal, and were quinoid in nature.

This paper describes the characterization of the kerogen of Chattanooga oil shale by oxidative degradation with perchloric acid of varying boiling point. Smith (4) demonstrated that the

apparent reduction potential of perchloric acid increases sharply as the boiling point rises above 150°C and the concentration increases. A stepwise oxidation of the kerogen can be effected by increasing the boiling point and subsequent oxidizing ability of perchloric acid. This study was analogous to the work completed by McGowan and Diehl (5,6,7) on Green River Shale.

EXPERIMENTAL

A Gassaway member of the Chattanooga shale from the Eastern Highland Rim area of Tennessee was ground to -60 mesh. A kerogen concentrate was prepared from the raw shale sample by demineralization using a combination of hydrochloric and hydrofluoric acids. Samples of the kerogen concentrate were oxidized with boiling perchloric acid within a modified Bethge apparatus as described by McGowan and Diehl (5). Perchloric acid solution was added to the reaction flask of the Bethge apparatus, and the boiling point was adjusted to the desired temperature by positioning the teflon stopcock to remove reflux condensate, or by addition of water through the top of the water condenser. The boiling point was kept constant by returning the reflux condensate to the reaction vessel. The amount of perchloric acid added was varied such that approximately 50 ml of solution remained after the temperature adjustment was completed. After cooling to room temperature, three 1.00 ml aliquots were taken and titrated with 0.25 N sodium hydroxide. A 1-g sample of kerogen concentrate was added to the reaction vessel, and the system was purged for 30 minutes with nitrogen. A weighed Turner absorption bulb containing ascarite and anhydrous magnesium perchlorate was added to the reaction system. The reaction flask was heated for 1.5 hours. The stable reaction temperature was recorded. The system was repurged with nitrogen for 30 minutes at the termination of the reaction. The absorption bulb was reweighed and the percentage of carbon converted to carbon dioxide was calculated. The undissolved material was filtered and washed with 300 ml of distilled water. Upon dilution as a result of filtration, the perchloric acid solution became more aqueous, and a precipitate formed in the aqueous layer upon standing. The precipitate was filtered. The undissolved material, the aqueous layer, and the precipitate filtered from the aqueous layer were retained for the analysis of oxidation products.

The reaction time was reduced for samples KC-160 and KC-165 due to excessive foaming. Reaction KC-190 was violent. Flaming occurred on the surface of the reaction mixture. The reaction was contained in the reaction flask of the Bethge apparatus with no apparent damage to the reaction system. The sample size was reduced to 0.1 gram for KC-200 as a safety precaution. The reaction proceeded smoothly.

Each reaction was performed in a perchloric acid fume hood behind an explosion shield. The authors reccommend that extreme caution be exercised when perchloric acid alone is used to oxidize organic material.

The undissolved material was designated as KC-^{O}C-U, and the precipitate filtered from the aqueous layer was designated as KC-^{O}C-A. The undissolved material and the aqueous layer precipitate were washed free of perchloric acid with distilled water. The samples were dried and weighed.

Samples KC-110-U through KC-190-U of the undissolved material were washed with 0.25 N sodium hydroxide. The sodium hydroxide washings were acidified with 12 M hydrochloric acid. A brown precipitate formed and was filtered. The precipitate was washed with heptane into a weighed 50 ml flask. The heptane washings (KC-^{O}C-U1) were evaporated to dryness and weighed. The precipitate was then washed with benzene into a weighed 50 ml flask. The benzene washings (KC-^{O}C-U2) were evaporated to dryness and weighed. The undissolved material was washed with methanol into a weighed 50 ml flask. The methanol washings (KC-^{O}C-U3) were evaporated to dryness and weighed. The remaining precipitate (KC-^{O}C-U4) was sodium hydroxide soluble, and was retained for analysis.

Samples KC-150-A through KC-180-A of the precipitate filtered from the original aqueous layer were washed with heptane into weighed 50 ml flasks. The heptane washings (KC-^{O}C-A1) were evaporated to dryness and weighed. The precipitate was washed with benzene into a weighed 50 ml flask. The benzene washings (KC-^{O}C-A2) were evaporated to dryness and weighed. The precipitate was washed with methanol into a weighed 50 ml flask, the washings (KC-^{O}C-A3) were evaporated to dryness and weighed. Only a trace of precipitate remained after the washing of the precipitate with methanol which was sodium hydroxide soluble.

Ultraviolet spectra were recorded for all U3 and A3 samples. A portion of each sample was dissolved in methanol. A background spectrum of methanol was recorded. The spectra were recorded on a Perkin Elmer Lamda 4B UV/VIS spectrometer. Infrared spectra were obtained via a diffuse reflectance technique with a Nicolet 20 DXB FTIR spectrometer. All U3, U4, and A3 samples were esterified with methyl-8 methylating reagent. One milliliter of methyl-8 was added to 5-10 milligrams of sample. The mixture was heated for 20 minutes at 60^{O}C. The methyl esters produced from the acid oxidation products were to be analyzed by gas chromatography and gas chromatography/mass spectrometry, however, analysis was not completed at the time of the writing of this paper.

RESULTS AND DISCUSSION

The kerogen concentrate produced from the raw Chattanooga shale sample was dark brown. The kerogen concentrate was 46.53 percent carbon, 4.34 percent hydrogen, 1.37 percent nitrogen, and 19.73 percent sulfur. The atomic hydrogen to carbon ratio was 1.1 to 1.0 indicating a high degree of unsaturation for the kerogen concentrate. Scanning Electron Microscope/X-Ray Diffraction analysis of the kerogen concentrate indicated the presence of iron, sulfur, and titanium. Iron constituted 18 percent of the mineral content present in the kerogen

concentrate, determined with a Perkin Elmer Inductively Coupled Plasma Spectrometer. The kerogen concentrate was approximately 34 percent ash. The mineral content was predominantly pyrite based on the analysis of the kerogen concentrate and the percentages of iron and sulfur present.

The extent of oxidation of the organic material in Chattanooga oil shale was determined by monitoring the percentage of undissolved material, noting color changes in the aqueous phase, and calculating the percentage of carbon converted to carbon dioxide. Results from the oxidation of the kerogen concentrate are presented in Table 1.

The results presented in Table 1 for the percentage of undissolved material indicated the kerogen dissolved between 150°C and 180°C. The percentage of undissolved material decreased approximately 27 percent between 140-155°C. This was probably due to the dissolution of pyrite, which was approximately 30 percent of the kerogen concentrate. The dissolution of pyrite in boiling perchloric at 140-155°C has been demonstrated (8). Aromatic material was suspected to have dissolved between 170-180°C. It has been demonstrated by ^{13}C-NMR (9) that approximately half of the organic carbon present in Chattanooga shale is aromatic.

The color intensity of the aqueous phase rose to a maximum then faded to clear. The color changes ranged from colorless to pale yellow below 150°C, dark orange-brown between 150-180°C, dark yellow at 190°C, and clear at 203°C. The maximum color intensity corresponded to the dissolution of kerogen.

The data for the percentage of carbon converted to carbon dioxide presented in Table 1 for the kerogen concentrate indicated no significant amounts of carbon were converted to carbon dioxide when the boiling point of perchloric acid was below 150°C. The percentage of carbon converted to carbon dioxide rose in a linear fashion above 150°C. The results for the total carbon present in the kerogen concentrate at 203°C are not useful. It has been demonstrated that chlorine gas is produced by perchloric acid at 203°C (4). Thus, the calculated percentage of carbon converted to carbon dioxide at 203°C was elevated due to the absorption of chlorine onto ascarite.

The oxidation products were separated into fractions. The first type of oxidation product fractionated was the acidic fraction isolated from the undissolved material. The solid acids were separated into heptane, benzene, and methanol soluble fractions. There was no evidence that any material was extracted by heptane or benzene. Polar acids were extracted with methanol (KC-°C-U3). The remaining acids (KC-°C-U4) were sodium hydroxide soluble. The acid products KC-150-U3 through KC-170-U3 were brown in color and flaky in texture. Sample KC-180-U3 was brownish-yellow. Samples KC-150-U4 through KC-180-U4 were black. The second type of oxidation product was the precipitate which settled out of the aqueous layer. These acids were separated into heptane, benzene, and methanol soluble fractions. No acid

material was extracted with heptane or benzene. A trace of acid material remained after the methanol extraction was completed which was sodium hydroxide soluble (KC-^{o}C-A4). The methanol soluble acids (KC-^{o}C-A3) were identical in color and texture to the methanol soluble acids extracted from the undissolved material.

The infrared spectra recorded for selected U3, U4, and A3 samples were characteristic of unsaturated carboxylic acids. The spectra exhibited a broad band between 3500-3000 cm^{-1} indicative of the hydroxyl stretch of a carboxylic acid. A band between 1750-1700 cm^{-1} was typical for a carbonyl stretch of a carboxylic acid. The presence of aldehydes and ketones can not be ruled out. A peak from 1610 cm^{-1} to 1590 cm^{-1} was the typical region for carbon-carbon double bonds. The bands between 1200-1300 cm^{-1} and 1400-1440 cm^{-1} were typical for the C-O stretching and O-H bending of a carboxylic acid.

The ultraviolet spectra were recorded for all U3 and A3 samples. Each spectra contained one broad peak which was essentially identical for each sample. The maximum absorbance occurred between 206-211 nm. This was the characteristic region for unsaturated carboxylic acids which were also indicated by infrared analysis. Each peak exhibited a shoulder peak in the 230 nm to 255 nm region which was suspected to have arisen from the presence of aromatic material in the oxidation products.

CONCLUSION

A stepwise oxidation of the kerogen of Chattanooga oil shale was effected by oxidative degradation with perchloric acid. The dissolution of the kerogen occurred between 150-180^{o}C. The atomic hydrogen to carbon ratio indicated a high degree of unsaturation. Highly polar unsaturated carboxylic acids were indicated as the primary oxidation products. Gas chromatography and gas chromatography/mass spectrometry analysis of the oxidation products were not completed at the time of the writing of this paper. No suitable technique has been developed to separate organic oxidation products from perchloric acid solution. Work will be continued in this area utilizing XAD resins. The GC/MS data and the data obtained from the oxidation of model compounds will be used to propose a model for the structure of the kerogen of Chattanooga oil shale.

ACKNOWLEDGEMENTS

This work was funded through an American Chemical Society - Petroleum Research Fund grant-in-aid # 19461-B2, and a Faculty Research Grant from Tennessee Technological University. The authors would like to thank Dr. Wayne Leimer of the Geology Department at Tennessee Technological University, Glenn Norton from the Ames Laboratory at Iowa State University, and Karen R. Merkley from Fleetguard Inc. for technical assistance.

REFERENCES

1. Leonard, J.T., Univ. Microfilms (Ann Harbor), L.C. Card No: Mic 59-2987: 1288, (1959).

2. Kinney, C.R. and Leonard, J.T., J. Chem. Eng. Data, 6: 474 (1961).

3. Kinney, C.R. and Schwartz, D., Ind. Eng. Chem., 49: 1125 (1957).

4. Smith, G.F., Analyst, 80: 16, (1955).

5. McGowan, C.W. and Diehl, H., Fuel Process. Technol., 10: 169, (1985).

6. McGowan, C.W. and Diehl, H., Fuel Process. Technol., 10: 181, (1985).

7. McGowan, C.W. and Diehl, H., Fuel Process. Technol., 10: 195, (1985).

8. McGowan, C.W. and Markuszewski, R., Fuel. Process. Technol., 17: 29, (1987).

9. Minkis, F.P. and Smith, J.W., Org. Geochem., 5: 193, (1984).

TABLE 1

Results obtained from the oxidation of the Kerogen Concentrate

Sample	Normality $HClO_4$	Boiling point $HClO_4$ (^oC)	Reaction temp (^oC)	Reaction time (hour)	Total Carbon (percent of sample)	Undissolved material (percent of sample)
KC-111	2.07	111	106	1.5	0.63	97.80
KC-120	4.26	120	112	1.5	0.49	98.11
KC-132	6.30	132	123-4	1.5	0.47	96.62
KC-141	6.77	141	129-30	1.5	0.17	89.91
KC-151	8.02	151	139-40	1.5	3.08	72.27
KC-156	8.42	156	145-48	1.5	10.96	62.37
KC-162	8.52	162	149-52	1.2	12.00	56.37
KC-166	8.63	166	152-60	1.3	14.70	47.65
KC-171	9.26	171	163-68	1.5	16.26	38.74
KC-181	9.73	181	169-74	1.5	27.45	13.53
KC-190	10.46	190	175-83	1.5	54.06	0.27
KC-203	11.67	203	202	1.5	119.04	0.00

RAPID EVALUATION OF REACTION CONDITIONS ON COAL PYROLYZATES USING COUPLED PYROLYSIS GC/MS

David J. Miller, Steven B. Hawthorne, and Ronald C. Timpe

University of North Dakota Energy and Minerals Research Center
Box 8213 University Station
Grand Forks, North Dakota 58202

ABSTRACT

The optimization of processes using coal as a carbon source for reaction with steam to produce hydrogen requires an understanding of the composition of the volatile components released during the charring process. A coupled pyrolysis GC/MS method has been developed to rapidly evaluate the effect of reaction conditions, including catalysts used to accelerate the char-steam reaction on the composition of the coal pyrolyzate. Four samples (one uncatalyzed and three catalyzed with 10 wt% $CaCO_3$, K_2CO_3, and Na_2CO_3, respectively) of a North Dakota (Velva) lignite were pyrolyzed under helium at 700 °C for ten minutes. The volatile products (primarily benzene and alkylbenzenes, phenol and alkylphenols, dihydroxybenzenes, and methoxyphenols) were swept from the pyrolysis chamber directly into a capillary gas chromatographic column and cryogenically trapped prior to GC/MS analysis. While simulated distillation plots for the uncatalyzed Velva and three catalyzed samples were similar, dramatic reductions in the amounts of catechols and guaiacols were observed in the K_2CO_3 and Na_2CO_3 catalyzed samples.

INTRODUCTION

Pyrolysis gas chromatography/mass spectrometry has become increasingly popular for the analysis of solid fuel and fuel related materials. In recent papers, pyrolysis-GC/MS has been applied to hydronaphthalenes to determine degradation pathways (1), asphaltenes (2), oil shale (3), kerogens (2), buried wood (4), coalified logs (4), and coal (5,6). Ekstrom and Callaghan have used pyrolysis coupled directly to the ion source of a mass spectrometer to study pyrolysis kinetics of oil shale (7). In general, pyrolysis probes utilizing 5 to 100 µg of samples are used for pyrolysis GC/MS. Our technique utilizes a larger sample size (2-4 mg) and split injection to obtain a more representative sample for GC/MS analysis. Pyrolysis products are introduced into a split injector and are cryogenically trapped at the head of a fused-silica capillary gas chromatographic column.

Timpe and co-workers have shown that the addition of alkali carbonates to low-rank coals prior to charring has increased the rate of hydrogen production from the char-steam reaction (8). We have used pyrolysis GC/MS to determine the effect of three alkaline carbonate catalysts, $CaCO_3$, K_2CO_3, and Na_2CO_3, on the composition of pyrolysis products produced at 700 °C.

EXPERIMENTAL

Samples

North Dakota (Velva) lignite was ground to -200 mesh and dried in a vacuum desiccator for 48 hours prior to pyrolysis. Three additional samples containing catalysts were prepared from the same North Dakota Lignite. Ten weight percent of dry $CaCO_3$, K_2CO_3, or Na_2CO_3 (Trona - a naturally occurring Na_2CO_3 mineral) was mixed with the North Dakota lignite and dried in the same manner as the uncatalyzed sample.

Pyrolysis Gas Chromatography/Mass Spectrometry

GC/MS analysis of the pyrolysis products was performed with a Hewlett-Packard 5985B using a 60 m x 0.25 mm i.d. (0.25 µm film thickness) DB-5 fused silica capillary column (J & W Scientific, Folsum, CA). Electron impact (EI) mass spectra were generated at 70 eV with a scan range of 50-400 amu. Helium was used as the carrier gas at an approximate linear flow rate of 50 cm/sec.

Figure 1 shows a schematic diagram of the pyrolysis apparatus. Approximately 2-4 mg of coal was placed in a 30 cm x 4 mm i.d. quartz tube. The sample was positioned approximately 5 cm from the outlet of the quartz tube with a plug of quartz wool. 1-chloronaphthalene was added as an internal standard for each analysis by injecting 1 µl of a 1.47 µg/µl solution into the quartz plug and allowing the solvent to evaporate for 15 minutes prior to pyrolysis. The outlet of the tube was attached to a 1/4" x 1/16" stainless steel union fitted with a 2 in. x 0.20 mm i.d. needle. The upper end of the sample tube was then placed in a brass heater block (preheated to 700 °C) but the sample was maintained at ambient temperature. A helium purge line was attached to the upper end of the sample tube. During the pyrolysis step, the helium flow was diverted from the injection port to sweep the pyrolysis products out of the pyrolysis chamber and into the injection port, the needle was inserted into the split/splitless injection port, and the block heater was dropped down around the sample (this resulted in a temperature of 650 °C in 30 seconds and 700 °C in one minute). The pyrolyzates were swept into the split injection port and were cryogenically trapped on the head of a fused-silica capillary chromatographic column by holding the oven temperature a 0 °C during the 10 minute pyrolysis. Upon completion of the pyrolysis, the sample tube injection needle was removed from the injection port, the helium flow switched back to the injection port, the column oven was heated rapidly to 50 °C, followed by temperature programming at 8 °C/min to 320 °C.

RESULTS AND DISCUSSION

Figures 2, 3, 4, and 5 show the total ion current chromatograms resulting from the pyrolysis of uncatalyzed Velva lignite, Velva with 10 wt% $CaCO_3$, Velva with 10 wt% K_2CO_3, and Velva with 10 wt% Trona. The numbered peaks in Figures 2, 3, 4, and 5 are identified in Table 1. Good chromatographic peak shapes were obtained with cryotrapping at 0 °C. The major species detected were benzene, toluene, and C_2-C_4 benzenes; phenol and C_1-C_3 phenols, catechol and C_1 catechols; and guaiacol and C_1 guaiacols. Also present were normal alkanes in the range from C_6 to C_{26}.

The boiling points of the normal alkanes found in the pyrolysis product of each sample were used to generate the simulated distillation plots shown in Figure 6. Cumulative integrated areas of the total ion current chromatograms (normalized to the internal standard) of the species eluting between the between n-alkanes (starting with C_6) were used to generate the plots shown in Figure 6. Each pyrolyzate showed similar simulated distillation plots with approximately one-half of the volatile species having boiling points of less than 250 °C. The slight variation in the plot for the Velva with 10 wt% K_2CO_3 as a catalyst may be due to the relatively small amount of catechol present and the absence of C_1 catechols in the pyrolyzate for this sample.

Figure 7 shows a plot of the molecular ion areas normalized to the area of the internal standard for several of the most abundant compound classes found in each of the pyrolyzates. Components 1 thru 4 are benzene and C_1-C_3 benzenes. All four samples contained similar amounts of these components with the $CaCO_3$ catalyzed sample having slightly lower amounts of benzene and toluene. Phenol, C_1 phenols, and C_2 phenols, (components 5, 6, and 7, respectively) generally decreased with added catalyst. An exception to this trend was the higher amount of phenol present in the Velva sample catalyzed with K_2CO_3.

Dramatic differences in the amounts of catechol, C_1 catechols, guaiacol, and C_1 guaiacols (components 8, 9, 10, and 11) were observed. Both the K_2CO_3 and the Trona catalyzed samples showed a large reduction in catechol (>90%) and C_1 catechols (>80%) compared to the uncatalyzed sample while pyrolysis with $CaCO_3$ showed little reduction. Catalysis with K_2CO_3 showed a larger reduction in guaiacol and C_1 guaiacols than the other catalysts. The mechanism for this process is not known and will require additional investigation using model compounds.

CONCLUSIONS

Coupled pyrolysis gas chromatography/mass spectrometry with split injection can be a valuable tool for studying the effect of catalysts on the composition of pyrolyzates. The use of an internal standard allows direct comparison of pyrolyzates and can be used to estimate liquid yields and liquid quality. The addition of catalysts to the Velva lignite had minor effects on pyrolyzate yield. However, catalysis with K_2CO_3 and Trona showed large reductions in catechols and guaiacols.

CREDIT

The authors would like to thank the U.S. Department of Energy for support for this work under contract number DE-FG22-86PC90911.

REFERENCES

1. Bredael, P., and Vinh, T. H., Fuel, 58, 211-214 (1979).

2. Solli, H., and Leplat, P., Org. Geochem., 10, 313-329 (1986).

3. Suuberg, E., Sherman, J., Lilly, W. D., Preprints, Div. of Petroleum Chem., ACS, 32(1), 138-142 (1987).

4. Hatcher, P. G., Lerch, H. E., Kotra, R. K., and Verheyen, T. V., Preprints, Div. of Fuel Chem., ACS, 32(1), 85-93 (1987).

5. Siskin, M. and Aczel, T., Fuel, 62, 1321-1326 (1983).

6. Miller, D. J., and Hawthorne, S. B., Preprints, Div. of Fuel Chem., ACS, 32(4), 10-17 (1987).

7. Ekstrom, A., and Callaghan, G., Fuel, 66, 331-337 (1987).

8. Timpe, R. C., Sears, R. E., and Montgomery, G. G., Div. of Fuel Chem., ACS, 32(4), 1-9 (1987).

TABLE I. Identification of Numbered Peaks from Figures 2, 3, 4, and 5.

Peak Number	Species
1	1-hexene
2	hexane
3,5	C_6H_8 isomer
4,6	C_6H_{10} isomer
7	benzene
8	thiophene
9,11,12	C_7H_{14} isomer
10	C_7H_{16} isomer
13	toluene
14	C_7H_{10} isomer
15	C_8H_{16} isomer
16	C_8H_{18} isomer
17,18	C_2 benzene
19	C_9H_{18} isomer
20	cyclooctatetraene
21	C_2 benzene
22	C_9H_{20} isomer
23,24,25	C_3 benzene
26	phenol
27	$C_{10}H_{22}$ isomer
28,29	C_3 benzene
30	C_4 benzene
31,32	C_1 phenol
33	guaiacol
34	$C_{11}H_{24}$ isomer
35,36,37,38	C_2 phenol
39	catechol
40	C_2 benzofuran
41	C_3 phenol
42,43	C_1 catechol
44	C_1 naphthalene
45,46	C_1 guaiacol
47	1-chloronaphthalene (IS)
48	C_2 naphthalene
49	$C_{15}H_{32}$ isomer
50,51,52	M=206 sesquiterpene isomer
53	$C_{16}H_{34}$ isomer
54	C_3 naphthalene
55	$C_{17}H_{36}$ isomer
56	M=266 biological marker
57	$C_{18}H_{38}$ isomer
58	$C_{19}H_{40}$ isomer
59	$C_{20}H_{42}$ isomer
60	$C_{21}H_{44}$ isomer
61	$C_{22}H_{46}$ isomer
62	$C_{23}H_{48}$ isomer
63	$C_{24}H_{50}$ isomer
64	$C_{25}H_{52}$ isomer
65	$C_{26}H_{54}$ isomer

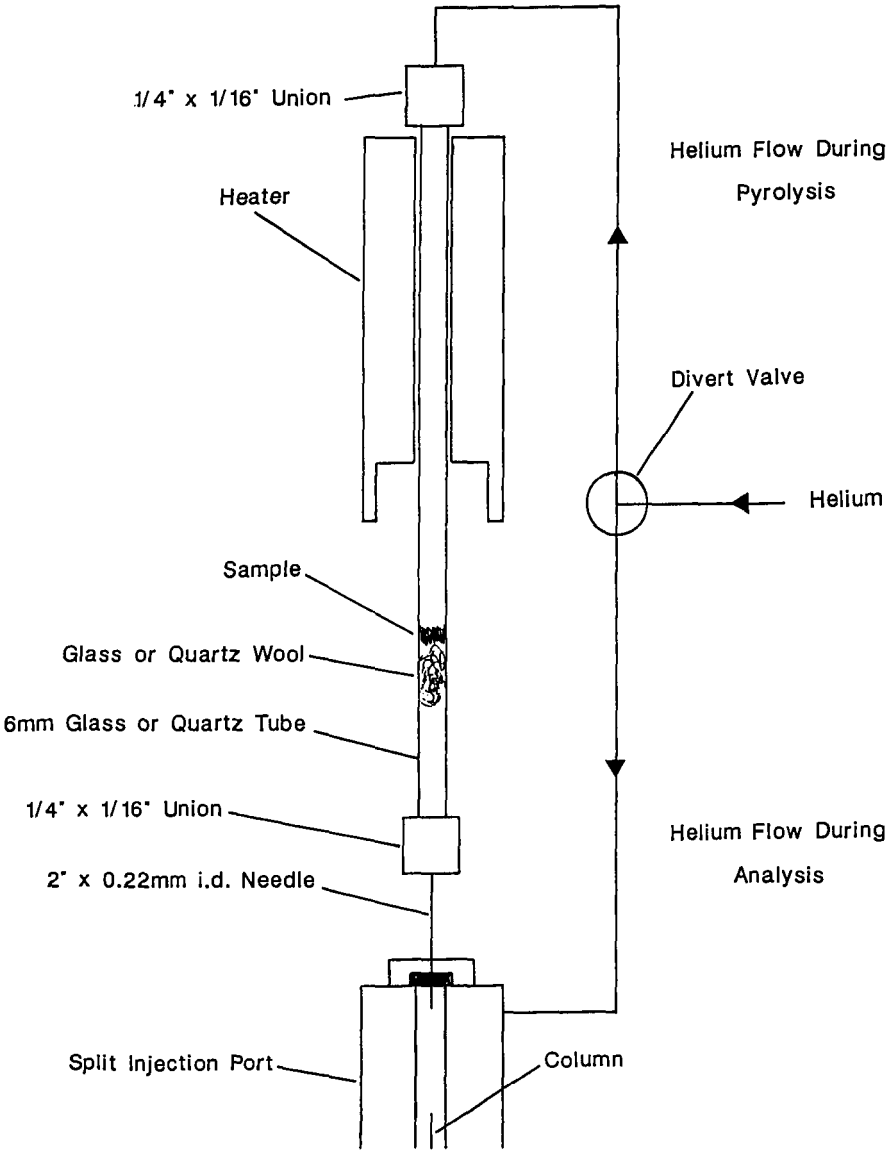

Figure 1. Pyrolysis Apparatus.

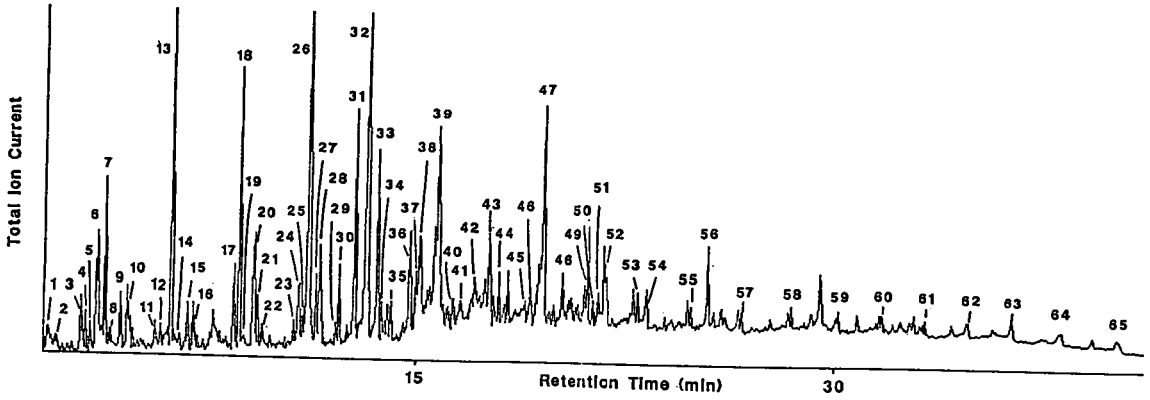

Figure 2. Pyrolysis TIC trace from uncatalyzed Velva lignite.

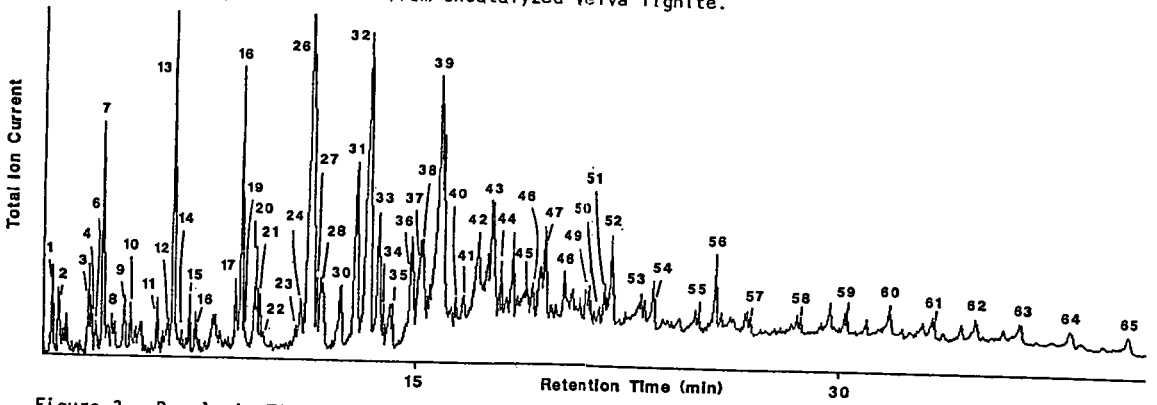

Figure 3. Pyrolysis TIC trace from $CaCO_3$ catalyzed Velva lignite.

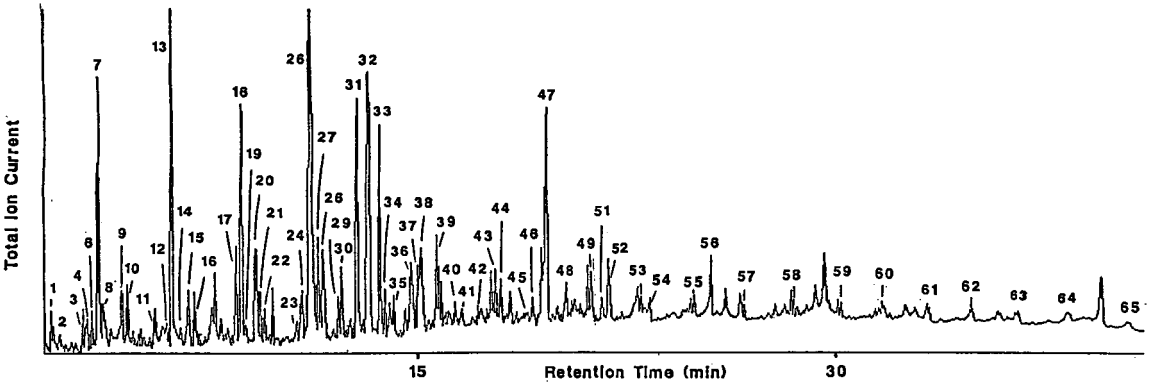

Figure 4. Pyrolysis TIC trace from K_2CO_3 catalyzed Velva lignite.

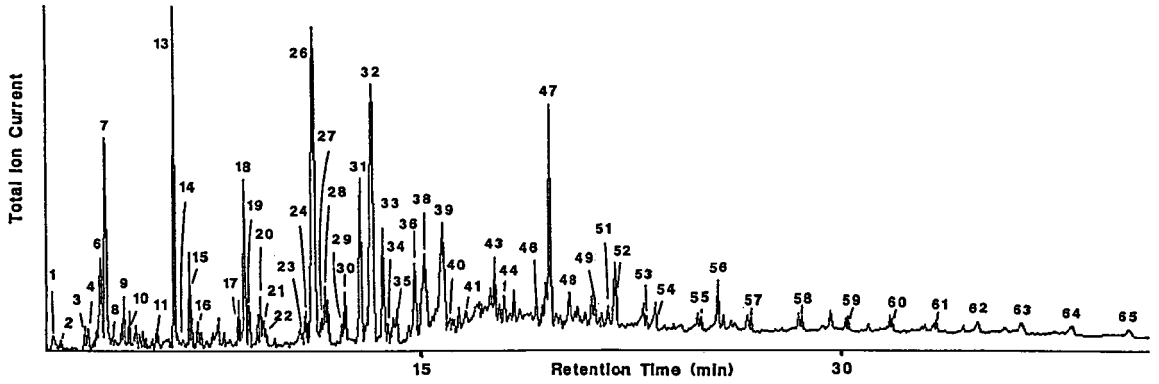

Figure 5. Pyrolysis TIC trace from Na_2CO_3 catalyzed Velva lignite.

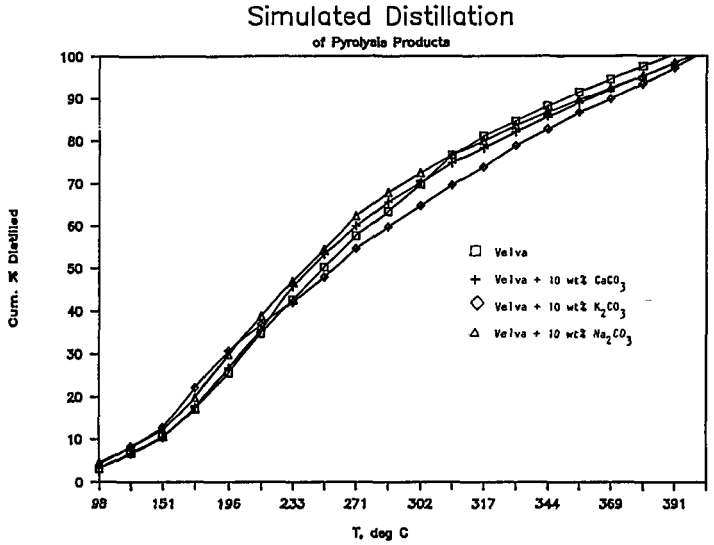

Figure 6. Simulated distillation plots for Velva lignite with and without catalyst.

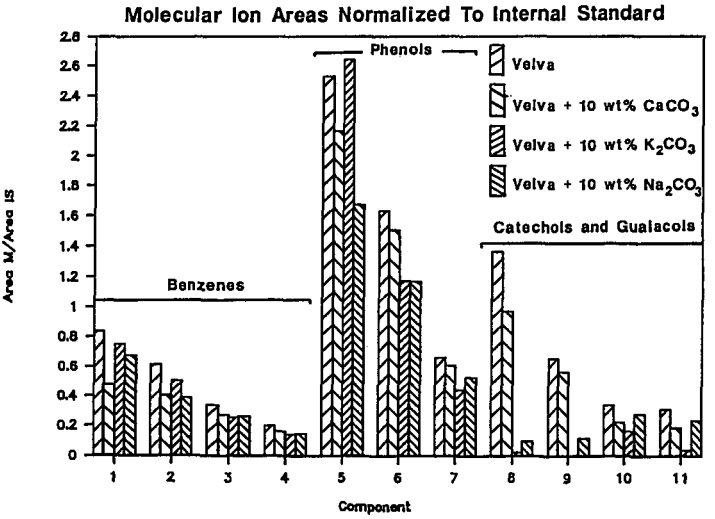

Figure 7. Comparison of the most abundant compound classes in the pyrolysis products of Velva lignite with and without catalyst. Components: 1-benzene, 2-toluene, 3-C_2 benzenes, 4-C_3 benzenes, 5-phenol, 6-C_1 phenols, 7-C_2 phenols, 8-catechol, 9-C_1 catechols, 10-guaiacol, 11-C_1 guaiacols.